



National Library
of Canada

Bibliothèque nationale
du Canada

Canadian Theses Service

Service des thèses canadiennes

Ottawa, Canada
K1A 0N4

NOTICE

The quality of this microform is heavily dependent upon the quality of the original thesis submitted for microfilming. Every effort has been made to ensure the highest quality of reproduction possible.

If pages are missing, contact the university which granted the degree.

Some pages may have indistinct print especially if the original pages were typed with a poor typewriter ribbon or if the university sent us an inferior photocopy.

Reproduction in full or in part of this microform is governed by the Canadian Copyright Act, R.S.C. 1970, c. C-30, and subsequent amendments.

AVIS

La qualité de cette microforme dépend grandement de la qualité de la thèse soumise au microfilmage. Nous avons tout fait pour assurer une qualité supérieure de reproduction.

S'il manque des pages, veuillez communiquer avec l'université qui a conféré le grade.

La qualité d'impression de certaines pages peut laisser à désirer, surtout si les pages originales ont été dactylographiées à l'aide d'un ruban usé ou si l'université nous a fait parvenir une photocopie de qualité inférieure.

La reproduction, même partielle, de cette microforme est soumise à la Loi canadienne sur le droit d'auteur, SRC 1970, c. C-30, et ses amendements subséquents.

UNIVERSITY OF ALBERTA

**DEMONSTRATION OF A NOVEL CODE DIVISION
MULTIPLE ACCESS SYSTEM AT 800 MCHIPS/S**

BY

NIRANJAN VETHANAYAGAM



A THESIS

SUBMITTED TO THE FACULTY OF GRADUATE STUDIES AND RESEARCH
IN PARTIAL FULFILMENT OF THE REQUIREMENTS FOR THE DEGREE OF
MASTER OF SCIENCE.

DEPARTMENT OF ELECTRICAL ENGINEERING

EDMONTON, ALBERTA

SPRING 1991



National Library
of Canada

Bibliothèque nationale
du Canada

Canadian Theses Service Service des thèses canadiennes

Ottawa, Canada
K1A 0N4

The author has granted an irrevocable non-exclusive licence allowing the National Library of Canada to reproduce, loan, distribute or sell copies of his/her thesis by any means and in any form or format, making this thesis available to interested persons.

The author retains ownership of the copyright in his/her thesis. Neither the thesis nor substantial extracts from it may be printed or otherwise reproduced without his/her permission.

L'auteur a accordé une licence irrévocable et non exclusive permettant à la Bibliothèque nationale du Canada de reproduire, prêter, distribuer ou vendre des copies de sa thèse de quelque manière et sous quelque forme que ce soit pour mettre des exemplaires de cette thèse à la disposition des personnes intéressées.

L'auteur conserve la propriété du droit d'auteur qui protège sa thèse. Ni la thèse ni des extraits substantiels de celle-ci ne doivent être imprimés ou autrement reproduits sans son autorisation.

ISBN 0-315-66571-8

Canada

UNIVERSITY OF ALBERTA

RELEASE FORM

NAME OF AUTHOR : **NIRANJAN VETHANAYAGAM**

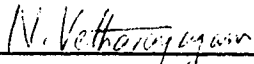
TITLE OF THESIS: **DEMONSTRATION OF A NOVEL CODE
DIVISION MULTIPLE ACCESS SYSTEM
AT 800 MCHIPS/S**

DEGREE: **MASTER OF SCIENCE**

YEAR THIS DEGREE GRANTED: **SPRING 1991**

Permission is hereby granted to the UNIVERSITY OF ALBERTA LIBRARY to reproduce single copies of this thesis and to lend or sell such copies for private, scholarly or scientific purposes only.

The author reserves other publication rights, and neither the thesis nor extensive extracts from it may be printed or otherwise reproduced without the author's written permission.



(Niranjan Vethanayagam)

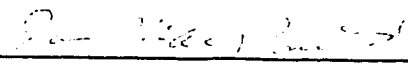
#129, 10633 - 31 Avenue
Edmonton, Alberta
T6J 4N4

Date : December 18, 1990

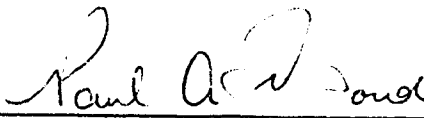
THE UNIVERSITY OF ALBERTA

FACULTY OF GRADUATE STUDIES AND RESEARCH

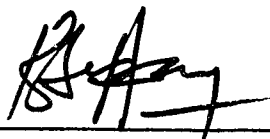
The undersigned certify that they have read , and recommended to the Faculty of Graduate Studies and Research for acceptance, a thesis entitled **DEMONSTRATION OF A NOVEL CODE DIVISION MULTIPLE ACCESS SYSTEM AT 800 MCHIPS/S** submitted by **Niranjan Vethanayagam** in partial fulfilment of the requirements for the degree of **Master of Science.**



Dr. R. I. MacDonald, Supervisor



Dr. P. A. Goud, Internal Examiner



Dr. A. Sesay, External Examiner

Date : November 23, 1990

ABSTRACT

The object of this thesis is to demonstrate a novel high speed Code Division Multiple Access (CDMA) system for optical communications using Alberta codes and complementary correlation detection. Such a system has been demonstrated with two users at 800 MChips/s. The basic data rate is 50 Mbits/s. The receiver can be switched easily to receive transmissions from any transmitter in the system. Complementary correlation detection is performed optoelectronically by an array of Metal-Semiconductor-Metal photodetectors fabricated especially for this project.

Results of Bit Error Rate (BER) measurements carried out on the system indicate that the BER performance is nominally independent of the number of interfering users in the system. This provides proof for the claim that the Alberta codes, when taken together with complementary correlation detection, are truly orthogonal. Bit error rates of the order of 10^{-7} were achieved in the presence and absence of the interfering transmitter.

The responsivity of the photodetectors was the factor limiting the performance of the system. Since the BER curves gave no indication of an error floor, it is anticipated that bit error rates better than 10^{-9} can be achieved with available photodetectors. Possible areas of application of such a system include high speed high capacity trunk multiplexing and the distribution of wideband digital signals as in high definition television.

ACKNOWLEDGEMENTS

I would like to express my sincere thanks to Dr. R. I. MacDonald, upon whose idea this thesis is based, for his capable supervision, support and encouragement. I am also greatly indebted to Darrell Barabash for his many excellent suggestions and guidance through the wilderness of RF design.

I have appreciated the help and assistance given to me by the staff and students at the Alberta Telecommunications Research Centre. In particular, I wish to thank my colleagues Ashutosh Pande and Marc Veilleux for their suggestions and helpful discussions. I would also like to acknowledge Graham McKinnon at the Alberta Microelectronics Centre for his assistance with the wire bonding and the Communications Research Centre, Department of Communications for fabricating the photodetectors for this project.

For financial assistance I am indebted to the Alberta Telecommunications Research Centre for their Graduate Scholarship and to my supervisor Dr. R. I. MacDonald.

Last but not least I thank my parents and my brother for their support and encouragement over the years.

TABLE OF CONTENTS

Chapter		Page
1	INTRODUCTION.....	1
1.1	Spread spectrum communications.....	2
1.2	Direct sequence modulation.....	4
1.3	Coding schemes for CDMA	8
1.3.1	Maximal length codes.....	11
1.3.2	Gold codes.....	12
1.4	Coding schemes for optical CDMA	14
1.4.1	Prime codes.....	17
1.4.2	Optical orthogonal codes	17
1.5	Thesis objectives and organisation.....	20
1.5.1	Thesis objectives	20
1.5.2	Thesis organisation.....	21
2	THE ALBERTA CODES AND COMPLEMENTARY CORRELATION	22
2.1	Orthogonality in optical systems	22
2.2	The complementary correlator	25
2.3	The Alberta code.....	29
2.4	Operation of the Alberta code - complementary correlator	32
2.5	Properties of the Alberta code - complementary correlator	35
2.6	Performance analysis of a FO-CDMA system using Alberta codes and complementary correlation	40
2.6.1	Assumptions	40
2.6.2	Binary FO-CDMA system.....	41
2.6.3	Probability density function for the interference signal I_1	47
2.6.4	Probability of error	50
2.7	Summary.....	54

Chapter	Page
3	SYSTEM DESIGN.....55
3.1	The experimental setup.....55
3.1.1	Power budget requirements56
3.2	Transmitter design constraints57
3.2.1	The choice of laser57
3.2.2	Passive optical vs passive electrical encoding58
3.3	Transmitter design.....60
3.3.1	The pulse generator.....61
3.3.2	The modulator63
3.3.3	The encoder.....66
3.3.4	The laser driver circuit.....69
3.4	Receiver design constraints.....73
3.4.1	Photodetector requirements73
3.4.2	Choice of photodetector74
3.5	Receiver design79
3.5.1	The complementary correlator detector.....80
3.5.2	The clipping circuit.....86
3.5.3	The gain circuits.....90
3.5.4	The data regenerator circuit.....92
3.6	System construction.....94
3.6.1	The transmitter.....94
3.6.2	The receiver.....96
3.7	Summary.....100
4	EXPERIMENTAL RESULTS.....102
4.1	Transmitter performance103
4.2.1	The pulse generator.....103
4.2.2	The modulator circuit.....104
4.2.3	The encoder circuit.....106
4.2.4	The laser driver circuit.....107
4.2	The passive optical multiplexer.....110

Chapter	Page
4.3 Receiver performance.....	112
4.3.1 The complementary correlator detector plus gain stage cascade.....	112
4.3.2 The clipping circuit.....	118
4.3.3 The data regenerator circuit.....	120
4.4 Bit error rate (BER) performance.....	123
4.5 Power spectrum measurements	128
4.6 Summary.....	131
 5 DISCUSSION AND CONCLUSION	 132
 REFERENCES	 137
 APPENDIX A SPICE SIMULATION PROGRAMS FOR THE VARIOUS TRANSMITTER MODULES	 142
 APPENDIX B SPICE SIMULATION PROGRAM FOR THE COMPLEMENTARY CORRELATOR DETECTOR.....	 150
 APPENDIX C DEVICE DATA SHEETS	 156
 APPENDIX D PRINTED CIRCUIT BOARDS	 174

LIST OF FIGURES

Figure		Page
1.1	Direct sequence spread spectrum signal 180 degree PSK modulated by a 5 MChips/s code.....	5
1.2	Direct sequence bi-phase modulator.....	5
1.3	Overall direct sequence modulation system showing waveforms.....	6
1.4	Spread spectrum correlation process [5].....	8
1.5	Possible configuration of a CDMA network.....	8
1.6	CDMA coding (a) Un-encoded data (b) Encoded data.....	9
1.7	Illustration of a m-sequence code generator of length $N = 15$	11
1.8	Gold code generator.....	12
1.9	Conceptual block diagram of a correlator for either optical or electrical correlation.....	15
2.1	Non-periodic correlation operation to generate truly orthogonal functions [19].....	24
2.2	Complementary optoelectronic correlator detector for an Alberta code of length $N = 8$ and weight $w = 4$ Receiver code: 0000111100000000.....	26
2.3	Overall FO-CDMA system showing waveforms.....	33
2.4	Representation of the complementary correlation operation.....	34
2.5	Output waveforms from the complementary correlator (a) Auto-correlation (b) Cross-correlation (c) Sum of auto- and cross-correlation waveforms.....	36
2.6	Output of the complementary correlator for (a) five users in the network (b) one user in the network.....	37
2.7	Computer simulation of the complementary correlator detector for Alberta codes [17].....	38
2.8	Plot of Bandwidth expansion factor vs the Code weight factor for Alberta codes of weight 4 and 6 with those for Prime codes shown for comparison [17].....	39

Figure		Page
2.9	Possible relative chip positions for the chip synchronous case.....	45
2.10	Possible relative chip positions for the chip asynchronous case	46
2.11	Plot of Probability of error (PE) vs Number of interfering users for Alberta codes of weight 4 and 6.....	52
3.1	Configuration of the experimental system to demonstrate an FO-CDMA system using Alberta codes and complementary correlation detection.....	55
3.2	Three possible passive optical encoder configurations.....	59
3.3	Block diagrams of transmitters 1 and 2.....	60
3.4	Pulse generator circuit used to generate the 500 ps wide electrical pulses.....	61
3.5	(a) The modulator circuit (b) Timing diagram showing the timing of the data and the pulse streams.....	64
3.6	SPICE simulation of the modulator circuit showing the output for a data bit '1'.	65
3.7	Configuration of the encoder circuit for Transmitter 1 Address: 0000111100000000	67
3.8	SPICE simulation of the encoder circuit. The data bit '1' is encoded with the address of transmitter 1	68
3.9	Laser driver circuit showing the positive and negative biasing supplies.....	70
3.10	SPICE simulation of the laser driver circuit.....	72
3.11	Structure of the Metal-Semiconductor-Metal photodiode.....	75
3.12	Frequency response characteristics of the MSM photodetector for varying levels of optical power (500, 400, 300, 200 and 100 μ W).....	76
3.13	Structure of the surface depleted photoconductor	77
3.14	Frequency response curves for the surface depleted photoconductors for varying levels of optical power (500, 400, 300, 200 and 100 μ W).....	77

Figure	Page
3.15	Block diagram of the receiver that can be switched to receive transmissions from either transmitter 1 or 2.....79
3.16	Schematic diagram of the complementary correlator detector for an Alberta code set of length $2N = 16$ and weight $w = 4$81
3.17	(a) SPICE model of the MSM photodiode/Surface depleted photoconductor [36].....82
	(b) Simulated pulse response of the Surface depleted photoconductor82
3.18	Simulated output from the complementary correlator detector for an input data stream of 010.....84
3.19	Responsivity vs Optical power curves for the MSM photodetector for different frequency ranges.....85
3.20	Simulated base voltage vs Collector current characteristics of the Avantek AT42085 bi-polar transistor.....87
3.21	Clipping circuit used to recover the auto-correlation peak from the bi-polar signal at the output of the complementary correlator detector array88
3.22	Simulation results for the clipping circuit showing (a) the voltage waveform input to the circuit (b) the current waveform at the output.....89
3.23	Configuration of the gain circuit cascade.....91
3.24	Regenerator circuit used to regenerate the NRZ data from the recovered auto-correlation peaks.....92
3.25	Photograph of transmitters 1 and 2 showing the two stages of each transmitter, the co-axial delay lines and the laser diodes mounted on the casing of stage 2 of each transmitter.....95
3.26	Photograph showing the optical delay lines.....96
3.27	Part of the monolithically intergrated array of 16 MSM photodetectors with 16 independent bias lines and one common output.....97

Figure	Page
3.28	Cross section of the complementary correlator detector module showing the position of the de-coupling capacitors and the dc bias lines98
3.29	Configuration of the complementary correlator detector showing the 16 fibres, the 'V' groove and the 'V' groove holder setup.....100
4.1	Configuration of the experimental FO-CDMA system.....102
4.2	Output pulse from the pulse generator circuit with pulse width 439.5 ps (at the base) and amplitude 3.4 V103
4.3	(a) Pulse stream at the output of the pulse generator with repetition frequency 50 MHz (b) 1010 data pattern produced by the HP3730A pattern generator/BER tester.....104
4.4	Output of the modulator circuit for a 1010 data pattern.....105
4.5	Output of the passive encoder circuit for the transmitter 1 code of 0000111100000000.....105
4.6	Current waveform going to the laser measured with the sampling head of a high speed storage oscilloscope107
4.7	Optical output from transmitter 1 for a data bit '1' detected with a single MSM photodiode.....108
4.8	Output from transmitter 1 for two adjacent data bit 1's.....109
4.9	Optical output from transmitter 2 for adjacent data bit 1's110
4.10	Multiplexed optical output from the passive optical multiplexer for a data '1' from both transmitters 1 and 2.....111
4.11	Frequency response of the complementary correlator detector - INA 03170 cascade with a single detector illuminated with 0.1 mW of optical power.....112
4.12	Group delay measurement of the complementary correlator detector - INA-03170 cascade113
4.13	Frequency response of the MSA-0885 gain stage with feedback.....114
4.14	Frequency response of the complementary correlator detector- INA03170 - MSA 0885 cascade115

Figure	Page
4.15	Amplified output from the complementary correlator detector for the transmitted PRBS data sequence.....116
4.16	Amplified output from the complementary correlator detector for a PRBS pattern117
4.17	Output of the clipping circuit showing a recovered auto-correlation peak for a PRBS pattern of length 2^9-1119
4.18	Output of the clipping circuit for a PRBS = 2^9-1 data pattern obtained with an oscilloscope with a 1 GHz bandwidth.....119
4.19	(a) PRBS = 2^9-1 data pattern transmitted by transmitter 1 (b) Waveform at the output of the second differential amplifier.....121
4.20	(a) PRBS = 2^9-1 data pattern transmitted by transmitter 1 (b) Regenerated data at the output of the ECL D flip-flop122
4.21	(a) PRBS = 2^9-1 data pattern transmitted by transmitter 1 (b) Output of the ECL to TTL translator123
4.22	Plot of BER vs average received optical power per detector per chip (a) No interfering users (b) Transmitter 2 interfering124
4.23	Plot of BER vs average received optical power per detector per chip (a) No interfering users (b) Transmitter 1 interfering125
4.24	Spectrum of the PRBS data pattern of length 2^9-1 at 50 Mbits/s.....129
4.25	Spectrum of the encoded data at the output of the passive electrical encoder circuit.....129
4.26	Spectrum of the signal at the output of the complementary correlator detector.....130
4.27	Spectrum of the regenerated data at the output of the receiver.....130

LIST OF TABLES

Table		Page
2.0	Optical correlation [19].....	23
2.1	Correlations required [19].....	23
3.1	Truth table for the operation of the modulator	63

LIST OF ABBREVIATIONS

AC	Alternating Current
AM	Amplitude Modulation
AMC	Alberta Microelectronics Centre
ATM	Asynchronous Transfer Mode
ATRC	Alberta Telecommunications Research Centre
BER	Bit Error Rate
BPF	Band Pass Filter
CDMA	Code Division Multiple Access
C/NL	Non-Linear Circuit Analysis Program
CRC	Communications Research Centre
dB	Decibel
DC	Direct Current
DIP	Dual Inline Package
ECL	Emitter Coupled Logic
FB	Ferrite Bead
FET	Field Effect Transistor
FM	Frequency Modulation
FO-CDMA	Fibre Optic Code Division Multiple Access
FWHM	Full Width Half Maximum
GaAs	Gallium Arsenide
GHz	Giga Hertz
ISDN	Intergrated Services Digital Network
mA	Milliamperes
μ A	Microamperes
MESFET	Metal Semiconductor Field Effect Transistor
MHz	Megahertz
MMIC	Monolithic Microwave Intergrated Circuit
MSM	Metal - Semiconductor - Metal
μ W	Microwatts
mW	Milliwatts
NRZ	Non Return to Zero
ns	Nanoseconds
Op-Amp	Operational Amplifier

PCB	Printed Circuit Board
PE	Probability of Error
PN	Pseudo Noise
PRBS	Pseudo Random Bit Sequence
PRF	Pulse Repetition Frequency
ps	Pico seconds
PSK	Phase Shift Keying
RL	Resistor Inductor
RZ	Return to Zero
SNR	Signal to Noise Ratio
SPICE	Simulation Program with Intergrated Circuit Emphasis
SRD	Step Recovery Diode
TTL	Transistor Transisitor Logic
UV	Ultra Violet

LIST OF SYMBOLS

a	Stored sequence
a'	Complement of the stored sequence
$A(t)$	Bi-polar output of the complementary correlator detector
$A_j^{(u)}$	u^{th} periodic sequence of binary optical pulses (0, +1)
$b_u(t)$	Binary data signal at the u^{th} transmitter
$b_k^{(u)}$	Value of the data sequence of the u^{th} user or transmitter
$b_0^{(1)}$	Amplitude of the zero th data bit of the 1 st transmitters (users) signal
C	Channel capacity
$DP_u(t)$	u^{th} user's Alberta code
$DP_1(t)$	1 st user's Alberta code
$I_u^{(1)}$	Interference at receiver 1 due to the u^{th} transmitter in the system
I_1	Sum of the interference signals at the 1 st receiver due to the U-1 transmitters in the system
M_{I_1}	Mean of the interference signal I_1
$M_{I_u^{(1)}}$	Mean of each interference signal $I_u^{(1)}$ at receiver 1 due to the u^{th} transmitter in the system
$2N$	Length of the Alberta codes, i.e., no of chips in the code
p	Probability that $I_u = 0$
$P_{I_u^{(1)}}^{(1)}$	Probability density function of the signal from the u^{th} transmitter in the system received at receiver 1
$P_T(t)$	Amplitude of a data bit
$P_{T_c}(t)$	Amplitude of a chip
q	Probability that $I_u = 0$
r	Probability that $I_u = -1$
$r(t)$	Optical intensity modulated signal at the receiver

S_u	Intensity of the optical signal transmitted by the u^{th} transmitter
$S_u(t)$	Baseband signal at the output of the u^{th} transmitter
T	Time period of a data bit
T_c	Time period of a chip
U	Total number of users (transmitters/receivers) in the system
u	Number of users in the system
w	Hamming weight of the Alberta code
λ_a	Value of the auto-correlation function
λ_c	Value of the cross-correlation function
$\delta(x)$	Dirac delta function
$\sigma_{I_1}^2$	Variance of the total interference signal I_1
$\sigma_{I_u}^2$	Variance of the interference signal I_u at receiver 1 due to the u^{th} transmitter in the system
τ_u	Time delay associated with the distance of the u^{th} receiving station from the transmitters

CHAPTER 1

INTRODUCTION

The use of optical fibre for carrying information in telecommunication systems allows for the creation of a number of new services, for example wideband ISDN, which would be difficult to support in an existing metallic cable environment. This is possible because optical fibres have much larger bandwidths and lower losses than their metallic cable counterparts. Due to the lack of a mature integrated optical component technology at the present time (optical amplifiers, optical detectors etc), many key signal processing functions such as multiplexing and demultiplexing are performed electronically for the most part. Therefore, the stream of optical pulses in the fibre must first be converted to electrical signals before any signal processing can be carried out and then converted back to optical signals and transported by fibre to the next destination. This technique of optical-to-electrical and electrical-to-optical conversion for signal processing limits the fibre bandwidth that can be used, by the speed limitations of the electronic signal processors. It is believed that the optical components, once fully developed and integrated, would allow much higher speeds to be attained.

There are a number of other advantages to introducing higher speed wideband signal processing. Such a capability would be of use in high speed high capacity optical trunk lines. The wideband capability would be useful for such applications as the distribution of high resolution digital television signals. Furthermore, the ability to carry out high speed optical signal processing would help to reduce the growing electronic and software complexity that exists in today's communication networks and in turn allow for more flexible networks.

Therefore, from an economic point of view, the access cost for customers would be reduced.

One technique which would allow the utilisation of the available fibre bandwidth beyond the limits of electronics is Fibre Optic Code Division Multiple Access (FO-CDMA). FO-CDMA is a subset of Code Division Multiple Access (CDMA) which is in turn a subset of Direct Sequence Spread Spectrum communications. This scheme takes advantage of the excess bandwidth in fibre to map the low information rate optical or electrical signals into very high rate optical pulse sequences for the purpose of achieving multiple access communication. In addition, this technique is well suited to allow passive optical multiplexing and demultiplexing for improved network simplicity.

1.1 SPREAD SPECTRUM COMMUNICATIONS

An important parameter which is used to determine the performance of a communication system is the signal-to-noise ratio. Since many telecommunication systems must operate with low signal-to-noise ratios, considerable effort has been expended over the years to find techniques that would allow communication systems to operate under such conditions with a high degree of accuracy of information transmission. One such technique is spread spectrum, which has been used quite extensively in the context of satellite [1] and mobile radio [2] communications.

Channels are characterised by their channel capacity [3] :

$$C = W \log_2 \left(1 + \frac{S}{N} \right) \quad (1.1)$$

Where C = Capacity in bits per second W = Bandwidth in Hz
 N = Noise power S = Signal power

The expression for the channel capacity shows the relationship between the ability of a channel to transfer error-free information, the signal-to-noise ratio existing in the channel and the bandwidth used to transmit the information.

If C is the desired information rate, then changing bases and using logarithmic expansion, it can be shown that:

$$\frac{C}{W} = 1.44 \frac{S}{N} \quad (1.2)$$

Rearranging,

$$\frac{N}{S} = \frac{1.44W}{C} \approx \frac{W}{C} \quad (1.3)$$

and

$$W = \frac{NC}{S} \quad (1.4)$$

Therefore, it is apparent from equation (1.4) that, for any given signal-to-noise ratio, a low information rate can be achieved by increasing the bandwidth used to transfer that information. This is the basis of spread spectrum communications.

Spread spectrum techniques may be classified into three general areas [4]:

1. Direct Sequence Modulation: the carrier is modulated by a code sequence whose bit rate is much higher than the information signal bandwidth.

2. Frequency Hopping : the carrier frequency shifts in discrete increments in a pattern dictated by a code sequence. The transmitter jumps from frequency to frequency within some predetermined set ; the order of the frequency usage being determined by the code sequence.
3. Pulsed FM or "Chirp " Modulation: the carrier is swept over a wide band during a given pulse interval.

1.2 DIRECT SEQUENCE MODULATION

Direct sequence modulation (or, to be more exact, directly carrier - modulated, code sequence modulation) is the modulation of a carrier sequence by a code sequence. In a very general case, the format may be amplitude modulation (pulse), frequency modulation or any other amplitude or angle modulation form. 180 degree bi-phase phase-shift keying is the most popular. The basic form of a direct sequence signal is that produced by a simple biphase modulated (PSK) carrier. A typical spectrum for this signalling format is shown in Figure 1.1 below. The main lobe bandwidth (null-to-null) of the signal shown is twice the clock rate of the code sequence used as the modulating signal. Each of the sidelobes has a bandwidth from null - to - null that is equal to the clock rate; that is, if the code sequence being used as the modulating waveform has a 5 MChips/s operating rate, the main lobe bandwidth will be 10 MHz and each sidelobe will be 5 MHz wide. This is exactly the case in Figure 1.1. Generally, the direct sequence biphase modulator has the form shown in Figure 1.2 [4].

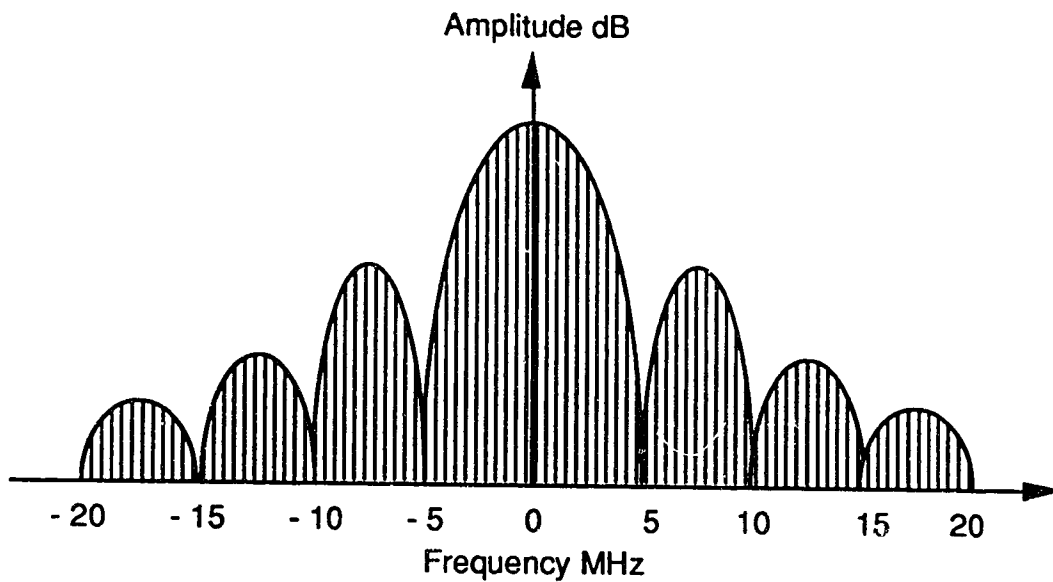


Figure 1.1 Direct sequence spread spectrum signal 180 degrees PSK modulated by a 5MChips/s code

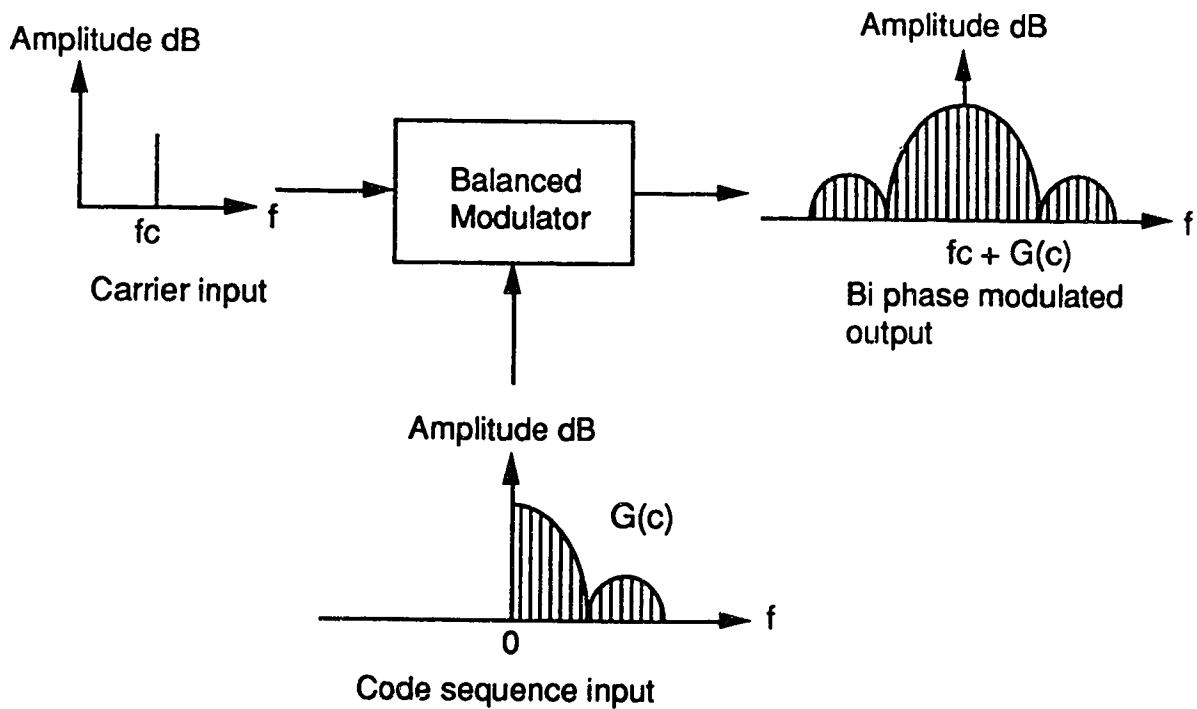
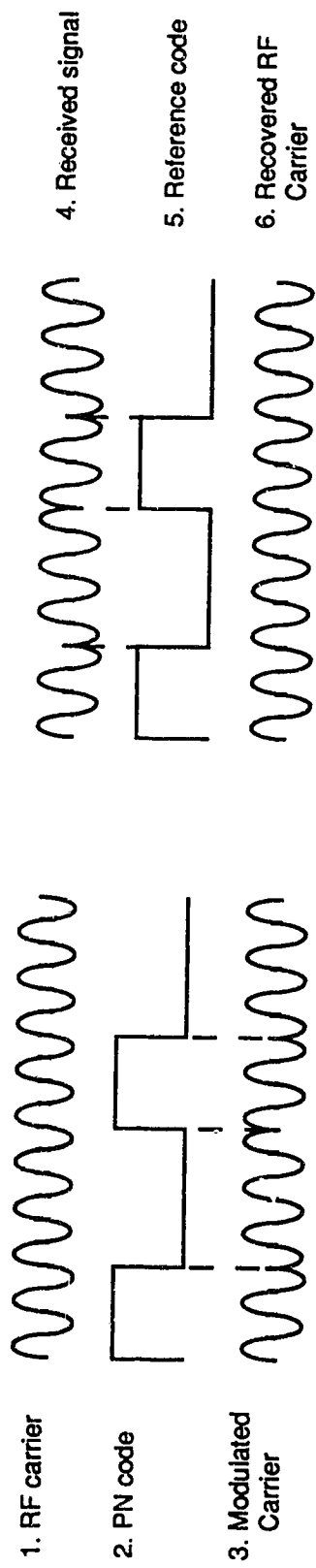
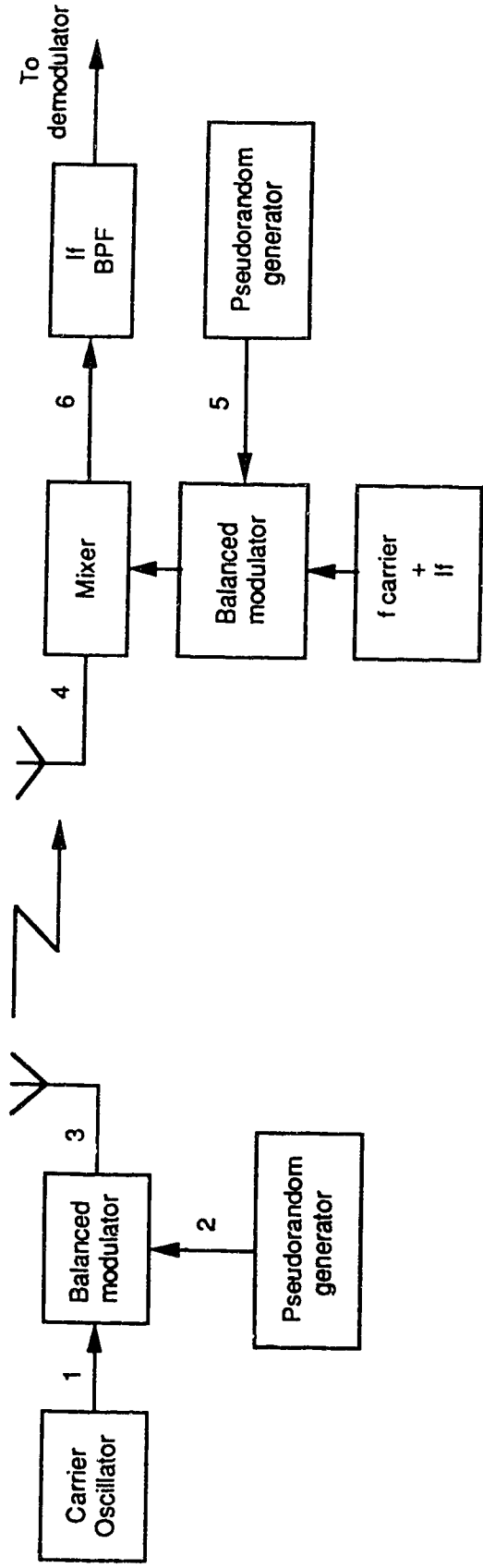


Figure 1.2 Direct sequence bi-phase modulator (adapted from [4])



PN = Pseudo Noise

Note: Assume that the transmitter and receiver pseudorandom code generators have already been synchronised by the transmission of a synchronisation preamble

Figure 1.3 Overall Direct Sequence Modulation System showing waveforms , adapted from [4]

In the time domain the biphase modulated carrier looks like waveform 3 shown in Figure 1.3. The carrier is transmitted with one phase when the code sequence is a "one" and with a 180 degree phase shift when the code sequence is a "zero". The simplified block diagram in Figure 1.3 shows a typical direct sequence communications link. It can be seen that the direct sequence system is similar to a conventional AM or FM communications link with the code modulation overlaid on the carrier. In actual practice however, the carrier is not usually modulated by the baseband information. The baseband information is usually in digital form and is added to the code sequence.

At the receiver, the received signal will consist of the transmitted signal, additive uncorrelated interference and noise. This is shown in Figure 1.4 (a). The mixture of received signals is correlated, i.e., multiplied with a replica of the same code used to spread the wanted message signal. This correlation process removes the coding from the wanted signal, leaving only the narrowband message signal, but since the unwanted signals are uncorrelated with the receiver code, they are still spread over a wide band by the code. This is seen clearly in Figure 1.4 (b). When the signal at the output is passed through a narrowband filter, only that portion of the unwanted signal falling within the bandwidth of the filter will cause interference to the wanted signal. When the codes are chosen properly for low cross-correlation, minimum interference occurs between users, and receivers set to use different codes are reached only by the transmitters sending that code. Therefore more than one signal can be transmitted without ambiguity in the same band and at the same time; selective addressing and code division multiplexing are implemented by the coded modulation format.

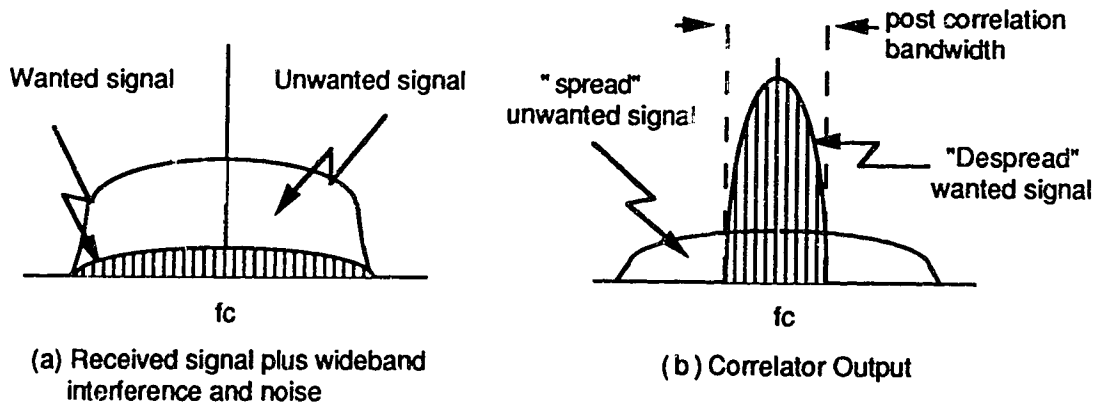


**Figure 1.4 Spread spectrum correlation process
(adapted from [5])**

1.3 CODING SCHEMES FOR CDMA

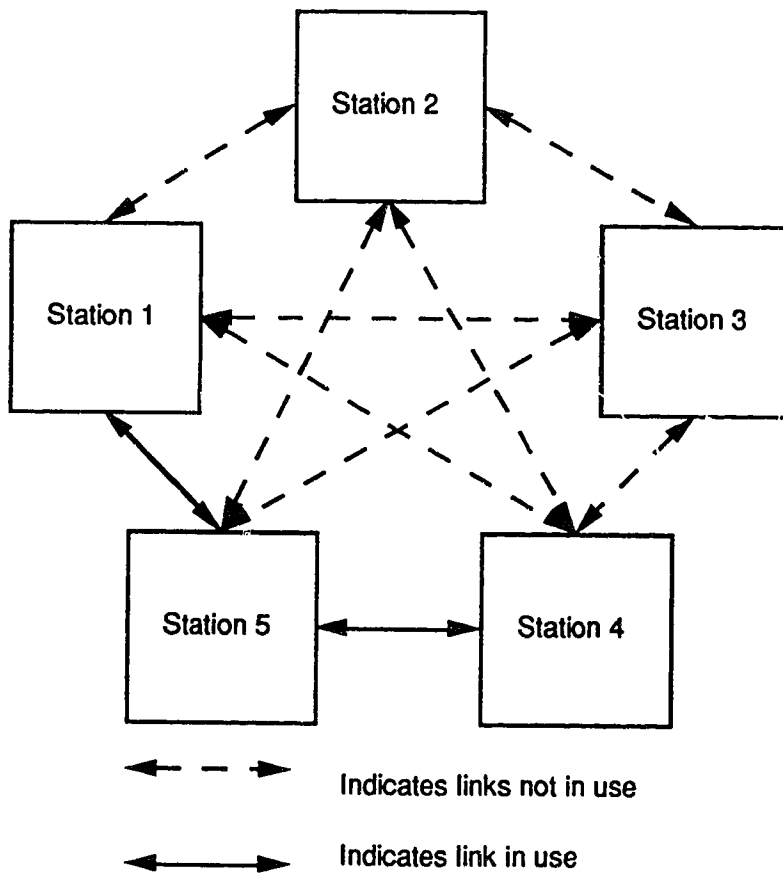


Figure 1.5 Possible configuration of a CDMA network

In CDMA, which is a more restricted case of direct sequence modulation discussed above, the same analysis applies except that the information to be sent is in digital form. For a CDMA network consisting of 5 stations for example (Figure 1.5), each station in the network is assigned a fixed code sequence which serves as its address. Any station wishing to transmit data encodes each data bit with the code sequence or address of the intended receiver station. For the network shown above, if station 1 wishes to transmit to station 5, and the address of station 5 is 1-1-11-111-1, for example, then a data bit "one" leaving station 1 will be of the form shown in Figure 1.6 (b), where Figure 1.6 (a) represents the data bit "one" before encoding.

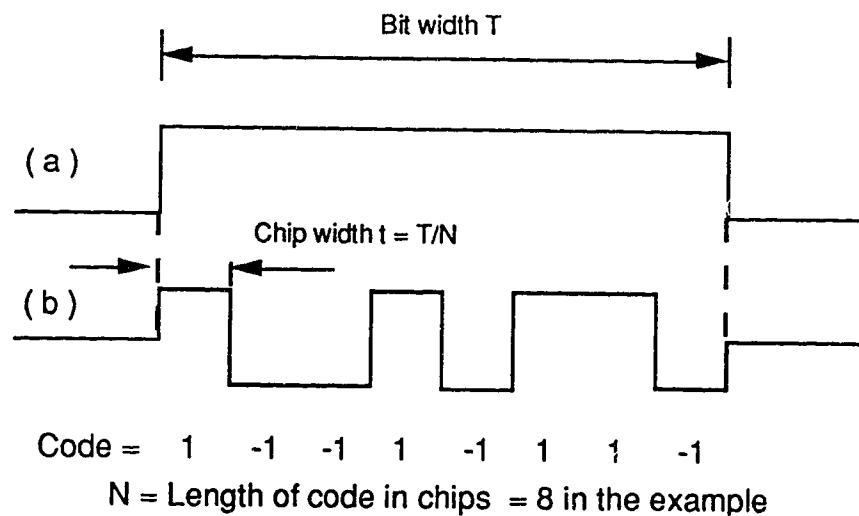


Figure 1.6 CDMA coding (a) Un-encoded data (b) encoded data

Now, whenever there are a large number of users who wish to use the same communications channel simultaneously, it is desirable that the code sequences that identify each of those users be distinguishable from time shifted versions of themselves and also be distinguishable from (possible time shifted versions of) each other. This can be approximately achieved by choosing those code

sequences that are orthogonal or uncorrelated (in statistical terms orthogonal means uncorrelated).

A good measure of distinguishability is the correlation process, which can be defined mathematically in term of the auto- and cross-correlation functions:

(1) Auto - correlation property : for any periodic sequence $x = (x_n)$ with length N and weight W in the set

$$|z_{xx}^{(l)}| = \sum_{n=0}^{N-1} x_n x_{n+l} = \begin{cases} W & \text{for } l = 0 \\ \lambda_a & \text{for } 1 \leq l \leq N - 1 \end{cases} \quad (1.5)$$

(2) Cross - correlation property : for each pair of periodic sequences $x = (x_n)$ and $y = (y_n)$ with length N and weight W

$$|z_{xy}^{(l)}| = \sum_{n=0}^{N-1} x_n y_{n+l} \leq \lambda_c \quad \text{for } 0 \leq l \leq N - 1 \quad (1.6)$$

Now, strict orthogonality or complete uncorrelation would require $\lambda_a = \lambda_c = 0$. No coding schemes that has been presented so far have precise orthogonality over a single sequence, the closest approach to orthogonality is obtained by optical Barker sequences [7]. Therefore, it has been found that by making $\lambda_a = \lambda_c$ to be equal to their minimum value, reasonable results can be achieved.

In the network with 5 stations (Figure 1.5), if station 1 is transmitting to station 5 , then equation (1.5) would apply. If on the other hand both stations 1 and 2 are transmitting, but station 5 is not the intended receiver of station 2, then equation (1.6) would apply to station 5 for the signal from station 2 (i.e., the signal from station 2 would be the interfering signal for the receiver at station 5). Therefore, at each receiver, in order to maximise the discrimination between the correct signal and the interference, the auto - correlation function must be maximised

and the cross - correlation function minimised. This can be achieved by choosing the address code sequences carefully. Two such orthogonal code sequences are the maximal length codes (m - codes) and Gold codes, both of which have been used quite extensively in spread spectrum communications [4].

1.3.1 MAXIMAL LENGTH CODES

Maximal length codes are, by definition, the longest codes that can be generated by a given shift register or delay line element of a given length. For example, the maximum length sequence that can be generated by an "n" stage shift register is $N = 2^n - 1$ chips.

A shift register sequence generator consists of a shift register working in conjunction with the appropriate logic, which feeds back a logical combination of the state of two or more of its stages to its input. The output of a sequence generator and the contents of its n-stages at any sample clock time is a function of the outputs of the stages fed back at the preceding sample time. Feedback connections have been tabulated for maximal length code generators from 3 to 100 stages, so that sequences of any length from 7 through 2^{36} are readily available [4]. Figure 1.7 below illustrates a m-sequence generation of a code of length 15.

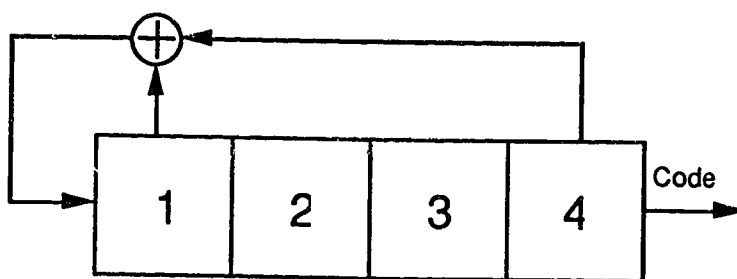


Figure 1.7 Illustration of a m-sequence code generator of length $N = 15$

A characteristic of the maximal length code is its two valued discrete auto-correlation function given by [6]:

$$r(t) = \begin{cases} N & \text{for } t = 0 \\ -1 & \text{for } t = \frac{iT}{N} \end{cases} \quad (1.7)$$

where, $T =$ data bit width

This characteristic makes the maximal length code sequence easy to distinguish from time shifted versions of itself. But, the peak of the cross-correlation function is not less than $-1 + 2^{-(n+1)/2}$. This means that certain maximal length code sequences will interfere very strongly with one another. Those code sequences that exhibit the minimum possible cross-correlation peak (i.e., equal to $-1 + 2^{-(n+1)/2}$) are referred to as preferred maximal length code sequences. Now, the set of preferred maximal length code sequences are limited in number [6], which means that the maximal length codes are not suited to conventional CDMA where a large number of assignable addresses are required.

1.3.2 GOLD CODES

Gold codes are of considerable interest in CDMA due to the existence of a large number of orthogonal sequences. Gold codes are generated by modulo-2 addition of a pair of maximal linear sequences as shown in Figure 1.8 below.

The code sequences are added chip-by-chip by synchronous clocking. The codes themselves are of the same length. Therefore, the two code generators maintain the same phase relationship and the codes generated have the same length as the two base codes, which are added together but are non-maximal.

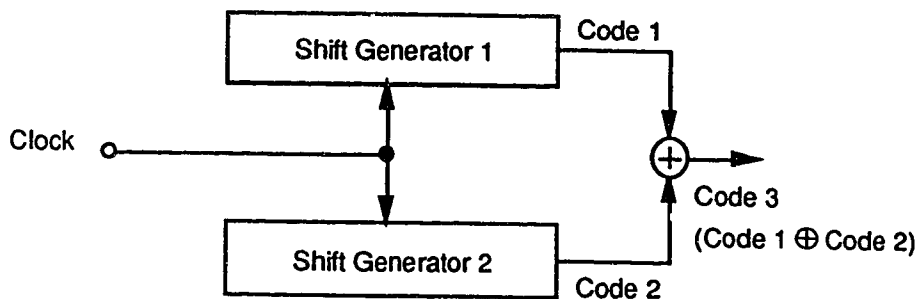


Figure 1.8 Gold Code Generator

A Gold code is therefore a set of $N+2$ code sequences given by $\{a, b, a+b, a+\tau.b, \dots, a+\tau^{N-1}b\}$ where $\{a,b\}$ is the preferred maximal length code sequence pair, and τ^i represents an operator that shifts a sequence cyclically i chip intervals to the left. The auto-correlation function of a Gold code sequence exhibits side lobes which depend on the pair of code sequences considered. The cross-correlation function on the other hand is bounded. Therefore Gold codes are attractive for applications in which a number of code division multiplexed signals are to be used. The same guarantee of bounded cross-correlation is not possible for maximal length sequences of the same length.

A method has been presented [8] for choosing the linear maximal codes used as components to generate the Gold code sequences that gives a set of sequences, each of whose members has cross-correlation and auto-correlation side lobes bounded by

$$r(t) \leq 2^{\frac{(n+1)}{2}} + 1 \quad \text{for } n = \text{odd}$$

$$r(t) \leq 2^{\frac{(n+1)}{2}} - 1 \quad \text{for } n = \text{even} \quad (1.8)$$

The signal-to-noise ratio (SNR) is represented as the ratio of the square of the peak of the autocorrelation function to the variance of the amplitude of the interference. Assuming synchronisation between the transmitter and receiver, and considering the interference due to the other users to be the dominant source of noise in the system, the SNR for Gold codes has been shown to be [9]:

$$\text{SNR} = 4 \left[\frac{N^3}{(U - 1)(N^2 + N - 1)} \right] \quad (1.9)$$

Now, the variance of the amplitude of the cross-correlation function (the denominator of the SNR) increases with both the number of users U and the number of chips, N , which is also the length of the code. It has been shown [12] that the performance of the system degrades as the number of users increases, as would be expected. A conventional CDMA system using Gold codes, electronic processing and transmission over an optical channel has been reported [9]. Although the system did multiplex the signals from the various users optically, it was nevertheless limited by the processing speed of the electronics.

1.4 CODING SCHEMES FOR OPTICAL CDMA

To fully realize the potential of CDMA, wide band signal processing is required at the receiver. This wideband signal requirement is due to the fact that the signals reaching the CDMA are extremely wide band and as explained in Section 1.2 only at the output of the correlator does the signal bandwidth reduce to its original narrow bandwidth. Therefore, the correlator itself needs to have a wide bandwidth in order for the correlation to take place correctly. Correlation is performed quite easily in optics using tapped fibre delay lines

and an optical summer [10]. But there is a fundamental difference between electrical and optical correlation. Conventional delay lines combine tapped signals coherently. Optical fibre delay lines, on the other hand, combine the tapped signals incoherently in the case of an incoherent optical system. This results simply in the summation of the optical power. This difference between electrical and optical correlation is shown quite clearly in Figure 1.9.

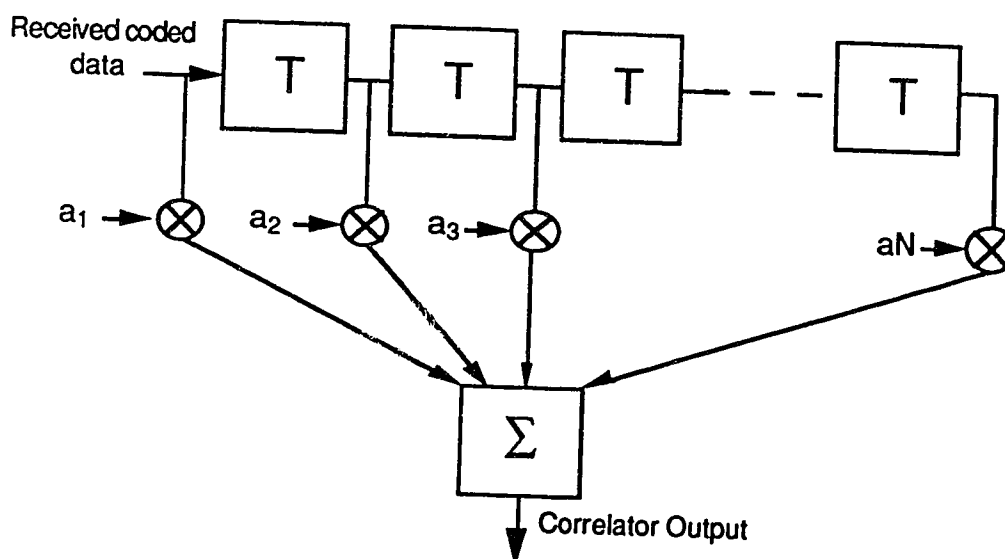


Figure 1.9 Conceptual block diagram of a correlator for either optical or electrical correlation

The taps on the delay lines equal the code sequence that corresponds to the appropriate destination address. The taps equal +1 or -1 for electrical processing and +1 or 0 for optical processing. Although coherent optical processing is possible in principle, it is not practical at the present time, due to the high frequency of the optical carrier.

Using incoherent optical processing, the levels of the transmitted optical code sequence would correspond to light 'ON' or light 'OFF'. The taps on the optical correlator shown in Figure 1.9 are set to zero at positions corresponding to light

'OFF' in the correct code sequence, and set to a one at positions corresponding to light 'ON' in the correct code sequence. For this form of correlator, the peak of the auto-correlation function will be equal to the number of one's in the code sequence. The peak of the cross-correlation function will be equal to the number of coincidences of one's in all the shifted versions of the two code sequences. In the case of Gold codes, the number of one's in the code will vary depending on the code and as a result, so will the peak of the auto-correlation function. Also, the number of coincidences of one's in the shifted versions of the two codes can be large and therefore the peak of the cross-correlation function could be large as well. As a result, the difference between the auto and cross correlation functions may not be large enough to be detectable in the presence of noise and other sources of interference. Gold codes are therefore not well suited for incoherent optical communication although dynamic detection techniques may be used to extract the auto-correlation peak. This would lead to increased complexity in the receiver design and therefore to slower processing speeds.

For these and other reasons, a number of coding schemes designed specifically for optical systems have been proposed. These include (1) Prime codes of length $N = P^2$ which are derived from prime sequences of length P obtained from a Galois field $GF(P)$, where P is a prime number [11] and (2) Optical Orthogonal Codes [14] which are orthogonal (0,1) sequences intended specifically for "unipolar" systems (i.e., systems which lack negative components).

1.4.1 PRIME CODES

As noted previously, the prime code set in question is a set of prime codes of length $N = P^2$ derived from prime sequences of length P obtained from a Galois field $GF(P)$, where P is a prime number [11].

The code is generated as follows: starting with $GF(P) = \{ 0, 1, 2, \dots, j, \dots, P-1 \}$, a prime sequence $S_x = \{S_{x0}, S_{x1}, \dots, S_{xy}, \dots, S_{x(P-1)}\}$ is constructed by multiplying every element of $GF(P)$ by an element x of $GF(P)$ modulo P . Therefore, P number of distinct prime sequences can be obtained. For prime codes, the number of coincidences of one's for all shifted versions of any two code sequences has been found to be either 1 or 2. The peak of the cross-correlation function is therefore at most two, which is much less than that for the optically processed Gold codes. But, the number of ones in a code sequence and the auto-correlation are both equal to P , which is much less than that for Gold codes. Since, the cross-correlation peak is at most equal to two, the threshold level of the decision circuit can be set just above two. This is not possible for Gold codes with optical processing where, depending on the choice of coding sequences chosen, the value of the cross-correlation peak will vary.

A FO-CDMA system using prime codes and optical processing has been demonstrated at 100 MChips/s (data rate of 3.125 Mbits/s) [12][13].

1.4.2 OPTICAL ORTHOGONAL CODES

For a code division multiple access system to be successful, the choice of the coding scheme upon which the information data bits of the different users are

mapped is important. The correlation function, which is the basis for determining a good sequence is given by equations (1.5) and (1.6).

Considering equations (1.5) and (1.6), strict orthogonality would require that $\lambda_a = \lambda_c = 0$. But, for the purpose of generating these codes, a sequence is considered to be orthogonal to a shifted version of itself if λ_a takes on its minimum value and two sequences are considered to be orthogonal if λ_c takes on its minimum value.

Based on the two conditions given above, it has been shown [14], that for a given number of chips N and weight W , where $W(W - 1) \leq (N - 1)$, and $\lambda_a = \lambda_c = 1$, at most U number of optical orthogonal codes can be generated. i.e.,

$$U \leq \left\lfloor \frac{N-1}{W(W-1)} \right\rfloor \quad (1.10)$$

where $\lfloor x \rfloor$ represents the integer portion of the real value x .

Using the constraints given above, a number of techniques have been proposed to generate the optical orthogonal codes [15][16]. Projective geometry, greedy algorithm, iterative construction and algebraic coding theory are some of the techniques that have been proposed.

A set of optical orthogonal codes have been generated using the Greedy algorithm technique and a CDMA system using optical orthogonal codes, optical processing and passive optical multiplexing has been demonstrated at 125 MChips/s [16].

The two optical coding schemes mentioned above achieve multiple access capability and also allow low information data rates to be mapped into high rate

address codes. But, they have a number of limitations. One such limitation is the large bandwidth expansion per channel, which is defined as the number of chips per bit normalised to the number of channels or users carried. For example, a prime code sequence set capable of carrying 5 channels has a bandwidth expansion per channel of 5 [17], while an optical orthogonal code sequence set for the same number of users or channels has a bandwidth expansion per channel of 200. Although the capacity of the optical channel is high, such wasteful use of bandwidth would not be acceptable in a number of applications.

It is apparent from the brief review of the state of the art that, most of the research in the area of fibre optic code division multiple access has taken the form of new coding techniques for some minimum level of cross-talk. As a result a single detector was used to detect the optically summed signals [12] [13] [16]. The disadvantage with the optical correlation/ single detector scheme is that optical summation requires fairly precise fibre delay lines. Optical summation is also wasteful of power since it involves the splitting and recombination of optical signals. Also, the minimum level of cross-talk condition is a limitation imposed by the optical summation process which is unipolar in nature. An alternative approach is to invent different detection techniques, which in combination with a new code sequence would result in significant improvement of the system performance. A correct choice of code sequence and correlation technique should therefore allow zero cross-talk to be achieved, in principle.

The Alberta codes introduced in this thesis overcome a number of limitations including high bandwidth expansion factors and high cross-talk levels. In addition, the structure of the codes allow the use of complementary correlation

methods [17] to demultiplex and decode the received optical pulse train containing the transmitted data.

1.5 THESIS OBJECTIVES AND ORGANISATION

1.5.1 Thesis Objectives

This thesis involved the design, construction and characterisation of a two channel Code Division Multiple Access system using Alberta codes [17] and complementary correlation detection methods.

The objective of this project was to demonstrate :

1. A code division multiplex system using Alberta codes and complementary correlation at high chip rates using low speed electronics and passive optical signal processing.
2. That the Alberta code - complementary correlation combination allows zero cross-talk to be achieved, when the system is working synchronously.
3. That the receiver code can be switched easily to receive transmissions from different transmitters, using the optoelectronic correlator. This concept could be of use in the distribution of wideband digital signals such as high definition television.
4. That the bit error rate performance of a synchronous FO-CDMA system using Alberta codes and complementary correlation is independent of the number of interfering users, i.e., the Alberta codes taken together with complementary correlation are truly orthogonal.

5. That the performance of an asynchronous system using the Alberta code - complementary correlation combination improves with increasing number of users. This claim is in direct contrast to conventional systems where the system performance degrades with an increasing number of users.

In order to achieve these objectives, a code division multiplex system using Alberta codes and optoelectronic complementary correlation detection is demonstrated at 800 MChips/s. To the authors knowledge, this is the fastest direct detection code division multiple access system demonstrated at the present time. The results of this demonstration provide conclusive proof of concepts 2, 3 and 4. The thesis also provides some theoretical evidence to support objective 5. Complementary correlation was implemented optoelectronically with Metal-Semiconductor-Metal photodiodes [18].

1.5.2 THESIS ORGANISATION

The thesis is divided into five chapters. Chapter 1 gave a brief overview of spread spectrum communications and the concept of CDMA/ FO-CDMA. Chapter 2 introduces the Alberta code ; its generation and characteristics. A derivation for the performance of the Alberta code when applied to an asynchronous FO-CDMA system is also presented. Chapter 3 discusses in detail, the design and construction of the FO-CDMA system and consists of two large sections, namely, the transmitter and receiver. Simulation results are presented, where necessary, to justify the designs adopted. Chapter 4 presents experimental results for single and two channel transmission. Chapter 5 , which is the concluding chapter, discusses the results obtained and also suggests some areas for future investigation.

CHAPTER 2

THE ALBERTA CODE AND COMPLEMENTARY CORRELATION

As mentioned in Chapter 1, the coding sequences proposed for fibre-optic code division multiple access (FO-CDMA) systems hitherto have had a number of limitations which include high bandwidth expansion factors and cross-talk due to the optical processing and detection techniques currently used. A need exists for coding schemes and detection techniques that will allow better bandwidth efficiencies and lower cross-talk limits to be achieved.

2.1 ORTHOGONALITY IN OPTICAL SYSTEMS

Perfect orthogonality between members of a code set would require that the auto-correlation wings and cross-correlation peaks be equal to zero. With optical systems, which are uni-polar, this is difficult to achieve because optical signals are normally intensity - modulated signals, and intensities cannot be combined subtractively.

A technique has been proposed [19] whereby a sequence of code operations can be performed on the received uni-polar optical signals to create a truly orthogonal correlation. The logical operations desired as a result of the optical correlation can be summarised by the truth table in Table 2.0.

The output is the summation of all the individually stored code-word bit correlations. Table 2.0 shows that the operation required is basically a 'logical AND' or an alignment of 1's between the stored and detected bits.

Table 2.0 Optical Correlation (adapted from [19])

Stored Bit	Detected Bit	Correlation Value
0	0	0
0	1	0
1	0	0
1	1	1

The sidelobes of the auto-correlation function are then reduced by subtracting the cross-correlation between the stored complement of the transmitted sequence and the detected sequence from the auto-correlation sequence formed from the incoming signal. This operation is summarised in Table 2.1.

Table 2.1 Correlation Required (adapted from [19])

Stored Bit	Detected Bit	Correlation
a a'	b	ab - a'b
0 1	0	0
0 1	1	-1
1 0	0	0
1 0	1	+1

The final output from the correlator is therefore the difference between the 1's alignment correlation value of the stored sequence and the complement of the stored sequence with the detected signal.

With reference to maximal or m - sequences, the non-periodic auto-correlation, aa , has a general shape of the form shown in Figure 2.1(a), where, a is the stored sequence (it is the same as the transmitted sequence). The non-periodic cross-correlation, $a'a$, has the general form shown in Figure 2.1(b), where, a' is

the complement of the stored sequence. The required operation is $aa - a'a$ and the general shape of this correlation is shown in Figure 2.1(c).

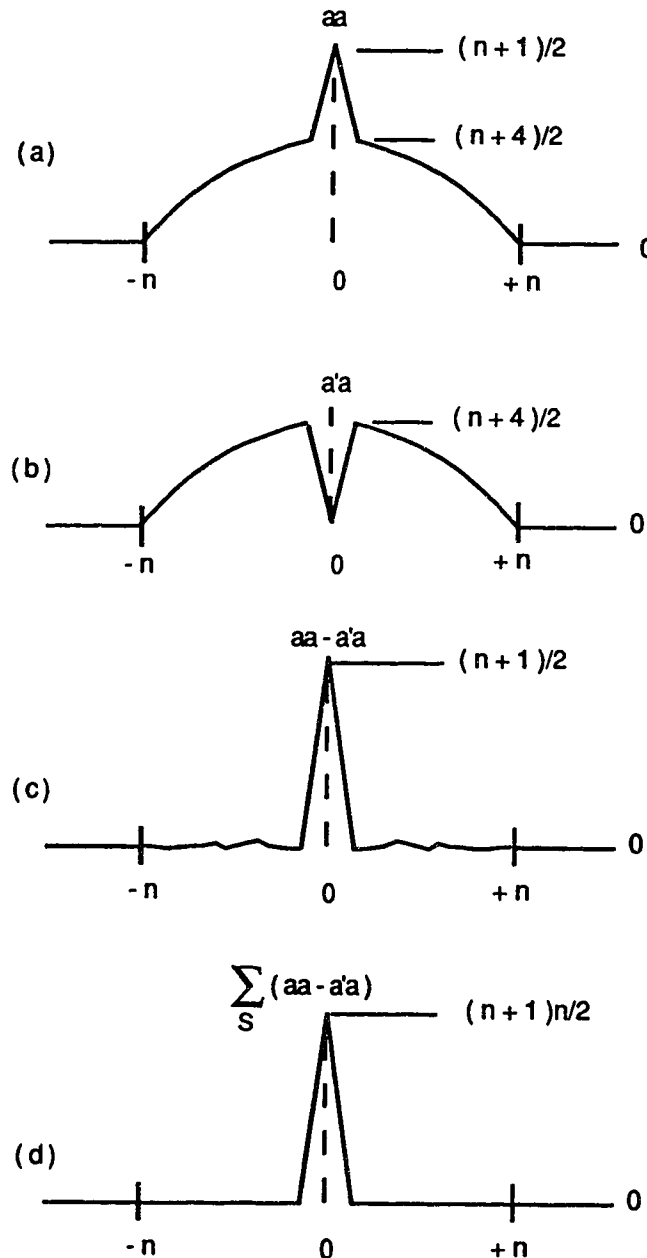


Figure 2.1 Non-periodic correlation operations to generate truly orthogonal functions (adapted from [19])

By considering all possible cyclic shifts of the m-sequence in question and by summing the resulting correlation functions, the result shown in Figure 2.1(d) is obtained. As can be observed, the actual correlation peaks add linearly to form a large correlation value while the side-lobes sum to zero. This process is the basis of complementary correlation.

This technique cannot be applied directly to FO-CDMA due to the fact that it does not provide a means of identifying the different channels and also because the digital signal processing operations required do not allow real time reception. However, it can be applied to FO-CDMA with some modification.

2.2 THE COMPLEMENTARY CORRELATOR

The operation of correlating a received optical signal with some sequence and with its complement, and the subtraction of the two (hence the name complementary correlation) can be performed with relative ease using optoelectronics. The resultant signal obtained will be bi-polar. Code sequences can be designed such that only the auto-correlation peak is positive. Since, the correlations are performed in real time and the operation of summing over all the codewords is eliminated, this method is directly applicable to FO-CDMA transmission systems.

Figure 2.2 shows the configuration of an optoelectronic correlator which will perform the complementary correlation and generate a bi-polar signal at the output.

The optoelectronic complementary correlator consists of an array of photodetectors, one per chip, in the chip sequence that represents each bit. Each detector is fed a portion of the signal through a fibre delay line.

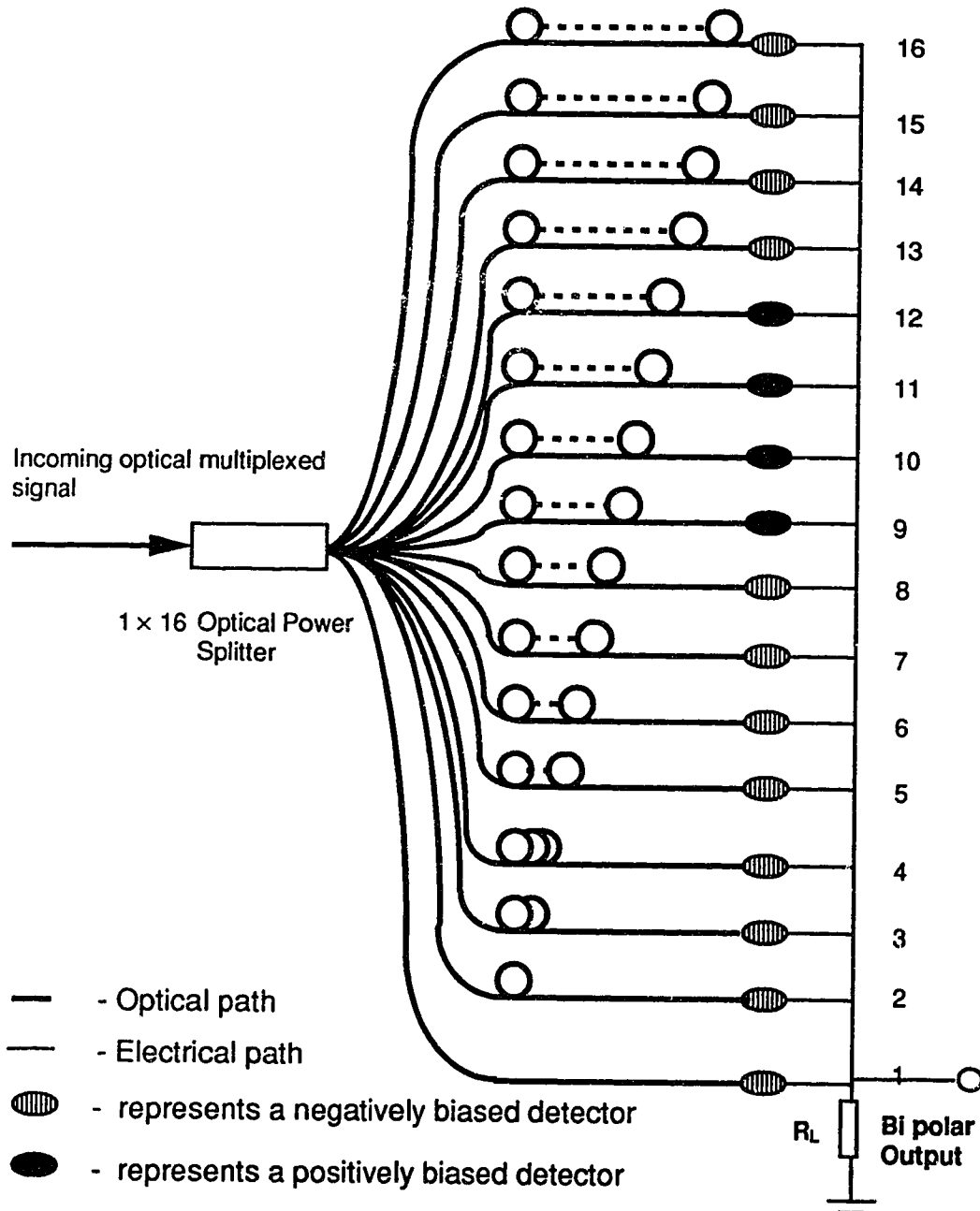


**Figure 2.2 Complementary Optoelectronic Correlator
Detector for an Alberta Code of length $N = 8$ and
weight $w = 4$.
Receiver code: 0000111100000000**

The lengths of the fibre delay lines increase progressively by one chip interval going from detectors 1 to N for a N chip code. The outputs of the photodetectors are all connected to a common load so that the output electrical signal will be the summation of the various delayed input optical signals. The summation of photocurrents from switched photodetectors is the basis of optoelectronic matrix switching [20] [21], and this principle has been demonstrated with a number of different types of detectors.

For this particular application, symmetrical devices with zero-bias off states such as photoconductors or metal-semiconductor-metal photodiodes would be required. This is to obtain the simultaneous subtraction of the correlation of the incoming signal with the receiver address code and with its complement.

Since the detection and decoding operations take place within the detector array, the necessity for electronic logic to decode the detected signals (as is currently the case) is eliminated. Thus the speed of operation will only be limited by the speed of the detectors and very fast processing can be achieved by the correct choice of detector [32][49]. Also, since the signal processing electronics is eliminated, the complexity of the receiver is greatly reduced.

The receiver address is introduced as follows: If the receiver address code sequence is 11110000, then the complement of the receiver address code would be 00001111. A positive bias is applied to those detectors that correspond to a '1' in the receiver address code sequence. A negative bias is applied to those detectors which correspond to a '1' in the complement of the receiver address code sequence. No detectors are assigned to a '0' in either the receiver address code sequence or the complement of the receiver address code sequence. The application of a negative bias to those detectors that

correspond to a '1' in the complement of the receiver address code sequence allows for the subtraction operation to take place. The resulting output current from the complementary correlator will correspond to the correlation of the received signal with the receiver address code sequence minus the correlation of the received signal with the complement of the receiver address code sequence.

The complementary correlation operation at the receiver may be represented by:

$$A(t) = \sum_{n=0}^N S(t + nT) \{ T(nT) - [U(nT) - T(nT)] \} \quad (2.1)$$

where,

T = Chip interval

N = Length of the receiver code sequence

$S(t)$ = Chip pattern of the received signal

$T(nT)$ = Chip pattern of the receiver address code sequence
It has a value of either '1' or '0' at each chip

$$U(nT) = \begin{cases} 1, & 0 < n < N \\ 0, & \text{otherwise} \end{cases}$$

The non-periodic correlation of the received signal with the receiver address code is :

$$R(t) = \sum_{n=0}^N S(t + nT) \cdot T(nT) \quad (2.2a)$$

and the non-periodic correlation of the received signal with the window $U(nT)$ is:

$$W(t) = \sum_{n=0}^N S(t + nT) \cdot U(nT) \quad (2.2b)$$

Equation (2.1) can thus be rewritten as:

$$A(t) = 2R(t) - W(t) \quad (2.3)$$

It is therefore apparent that, for a given set of code sequences with the same weight, the result of the detection process is a positive going signal corresponding to the correlation of the received signal sequence with the receiver address code sequence, shifted in the negative direction by an amount equal to the code weight $w = W(0)$.

2.3 THE ALBERTA CODE

As noted in Section 2.2, the output of the complementary correlator is a positive going signal corresponding to the correlation of the received signal sequence with the receiver address code sequence, shifted in the negative direction by an amount equal to the code weight $w = W(0)$.

For the auto-correlation peak to be extracted from the bi-polar signal at the output of the complementary correlator and for the complementary correlation to work correctly at all times, the code sequences used to encode the transmitted bits should satisfy the condition that the correlation function must have a magnitude less than or equal to $w/2$ for $0 < n < N - 1$, (where N is the length of the code sequence used to encode a data bit '1') and be equal to $2w$ at $n = N$ (the chip at which the correlation peak occurs).

The auto- and cross-correlation constraints for the above mentioned conditions may thus be stated as:

(1) For any sequence $x = (x_n)$ in the set, the auto-correlation function is :

$$|Z_{xx}^{(n)}| = \begin{cases} 2w & \text{for } n = N \\ \lambda_a \leq \frac{w}{2} & \text{for } 0 \leq n \leq N - 1 \end{cases} \quad (2.4)$$

(2) For any pair of sequences $x = (x_n)$ and $y = (y_n)$, the cross-correlation function is:

$$|Z_{xy}^{(n)}| = \lambda_c \leq \frac{w}{2} \quad \text{for } 0 \leq n \leq N - 1 \quad (2.5)$$

Therefore, for the purpose of defining such codes, a code sequence will be considered to be orthogonal with respect to a shifted version of itself if λ_a takes on a value $\leq w/2$ and two sequences in a set will be considered to be orthogonal if λ_c takes on a value $\leq w/2$, where w is the Hamming weight of the code sequence block.

It has been found that modifying the codes and the complementary correlator slightly ensures that the auto-correlation wings and cross-correlation peaks do not exceed $w/2$. This allows a 'zero - level' to be defined for the bipolar output from the complementary correlator and thus for the auto-correlation peak to be extracted relatively easily. The modification consists of extending the code sequence with $N/2$ additional zero's at each end of the code (the code length is therefore $2N$). $N/2$ additional detectors are also added to either end of the detector array in the complementary correlator detector. This is shown in Figure 2.2 where detectors 1 to 4 and 13 to 16 are the additional negatively biased detectors mentioned above. The additional zeroes and the negatively biased detectors ensure a negative shift of $R(t)$ (equation 2.2a). With such a modification, the codes in question have a correlation less than or equal to $w/2$ at all times ($0 < n < N-1$) other than at $n = 2N$, where the correlation will have a value of w , the Hamming weight of the code. Code sequences which satisfy the above conditions are defined as Alberta or A codes.

A number of methods exist for the generation of codes with tools from projective geometry, the greedy algorithm, iterative construction, algebraic coding theory, block design and a number of other combinatorial techniques [15].

The operation of the greedy algorithm is as follows: Originally the code set is empty. For a $(0, 1)$ code sequence of length N and weight w , $\binom{N}{w}$ possible codewords exist (i.e., there are $\binom{N}{w}$ ways in which w ones can be located in a code of length N chips). Therefore, the algorithm examines all the $\binom{N}{w}$ codewords, one at a time. If a codeword satisfies the auto-correlation property (equation 2.4) and it also satisfies the cross-correlation property (equation 2.5) with every codeword already included, it is added to the group of Alberta codes of length N and weight w ; otherwise it is discarded.

The main disadvantage with this code generation technique is that it is extremely time consuming and is basically a brute force method, especially when applied to fairly large code lengths. For example, there are 8008 possible ways in which 6 one's can be arranged in a codeword of length 16. To generate the 7 Alberta codes of length 16 and weight 6 that exist, processing time equivalent to 12 days was required by a Sun workstation. This is the longest Alberta code known at the present time.

As a result of the time consuming nature of the code generation method adopted, it has not been possible to investigate the Alberta codes to the maximum possible extent. For example, it has not been possible to find the maximum length of the code set that can be generated without losing chip or user efficiency. More efficient algorithms for Alberta code generation were not attempted in this thesis as the purpose was primarily to demonstrate their operation. This is one possible area for future work on Alberta codes.

2.4 OPERATION OF THE ALBERTA CODE - COMPLEMENTARY CORRELATOR

With reference to Figure 2.3, the operation of the complementary correlator is as follows: Consider, for example, a possible FO-CDMA network consisting of five transmitting and receiving stations using Alberta codes and complementary correlation. Assume bit synchronous operation (i.e., where all the transmitting stations are synchronised on a bit-by-bit basis, relative to each other). A possible application of such a network could be in high speed trunk multiplexing. The address codes of transmitting stations 1,2,3,4 and 5 are as shown in Figure 2.3 and the address codes of the 5 receiving stations are the same as those of the corresponding transmitters.

The individual channel rate is 44.736 Mbits/s. If for example only the first three stations, out of the possible five, are transmitting and the data sequences are 101, 111 and 010 respectively, then the coded data leaving stations 1,2 and 3 will be of the form shown at points 1,2 and 3 of Figure 2.3. Since the system is synchronised, the coded data reaching node 4 will all arrive at the same time and the intensity modulated signals will thus add. The multiplexed signal leaving node 4 will be of the form shown in Figure 2.3. Since this is a spread spectrum system, all the receiving stations in the system will receive transmissions from all the transmitting stations. Therefore the signal reaching receiving station 1 will be the same as that reaching receiving stations 2,3,4 and 5 and will consist of the expected signal (i.e., the data stream from transmitting station 1) plus the interfering signals from transmitting stations 2 and 3. The address code sequence of receiving station 1 is 0000111100000000.

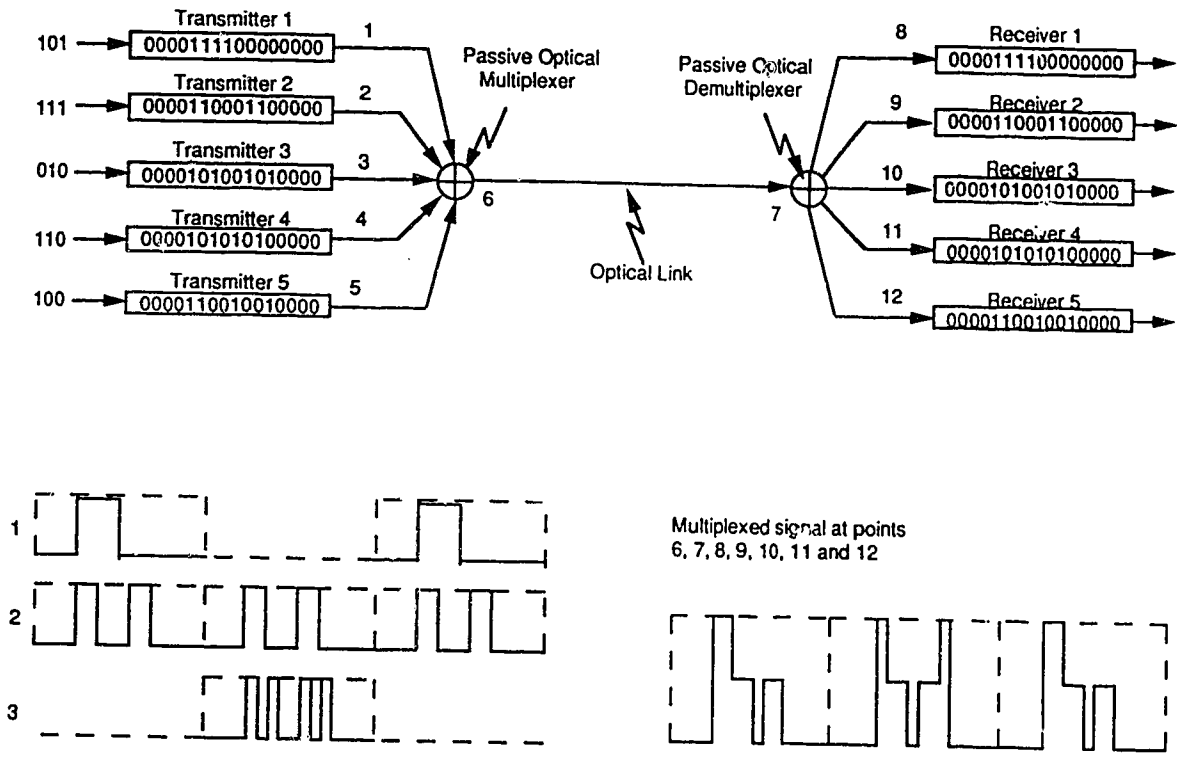


Figure 2.3 Overall FO-CDMA system showing waveforms

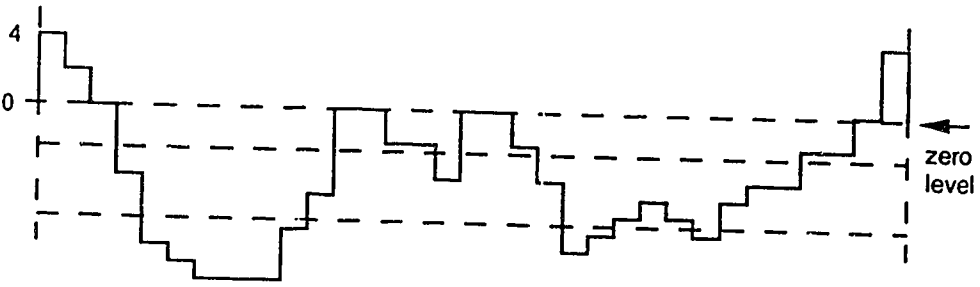
The correlation operations taking place at the complementary correlator may be represented by the diagram in Figure 2.4 (a). Using the complementary correlator detector (Figure 2.2) with $2N = 16$ detectors, for a code of length $N = 8$, the coded data stream reaching each detector is delayed by one chip interval relative to the data stream reaching the previous detector. The data stream reaching detector 2, for example, is delayed by one chip interval relative to the data stream reaching detector 1. This process is repeated for all 16 detectors in the correlator, and is seen quite clearly in Figure 2.4 (a).

Since the detectors are all connected to a common output, the detected electrical data streams sum at the output of the array and the resulting signal will be of the form shown in Figure 2.4 (b). As expected, the output signal is bi-

polar with only the auto-correlation peak being positive. By setting the zero level to be as shown in Figure 2.4 (b), the auto-correlation peak can be extracted with relative ease. As can be seen from Figure 2.4(b), the recovered auto-correlation peaks correspond to the data pattern 101. This is the data pattern that was input to the system at transmitting station 1 (see Figure 2.3).

Delayed Data Stream	Detector Bias
0 0 0 0 0 -1 -1 -2 0 0 -1 -1 -2 0 0 0 0 0 0 0 0 0 -1 -1 0 -1 -1 -2 -2 0 0 0 0	-ve
0 0 0 0 0 0 -1 -1 -2 0 0 -1 -1 -2 0 0 0 0 0 0 0 0 0 0 -1 -1 0 -1 -1 -2 -2 0 0 0	-ve
0 0 0 0 0 0 0 -1 -1 -2 0 0 -1 -1 -2 0 0 0 0 0 0 0 0 0 0 -1 -1 0 -1 -1 -2 -2 0 0	-ve
0 0 0 0 0 0 0 0 -1 -1 -2 0 0 -1 -1 -2 0 0 0 0 0 0 0 0 0 0 -1 -1 0 -1 -1 -2 -2 0	-ve
2 0 0 0 0 0 0 0 0 1 1 2 0 0 1 1 2 0 0 0 0 0 0 0 0 0 0 1 1 0 1 1 2 2	+ve
2 2 0 0 0 0 0 0 0 0 1 1 2 0 0 1 1 2 0 0 0 0 0 0 0 0 0 0 1 1 0 1 1 2	+ve
1 2 2 0 0 0 0 0 0 0 0 1 1 2 0 0 1 1 2 0 0 0 0 0 0 0 0 0 0 1 1 0 1 1 2	+ve
1 1 2 2 0 0 0 0 0 0 0 0 1 1 2 0 0 1 1 2 0 0 0 0 0 0 0 0 0 0 1 1 0 1 1	+ve
0 -1 -1 -2 -2 0 0 0 0 0 0 0 0 -1 -1 -2 0 0 -1 -1 -2 0 0 0 0 0 0 0 0 0 0 1 1 0 1	+ve
-1 0 -1 -1 -2 -2 0 0 0 0 0 0 0 0 -1 -1 -2 0 0 -1 -1 -2 0 0 0 0 0 0 0 0 0 -1 -1 0	-ve
-1 -1 0 -1 -1 -2 -2 0 0 0 0 0 0 0 0 -1 -1 -2 0 0 -1 -1 -2 0 0 0 0 0 0 0 0 0 -1 -1	-ve
0 -1 -1 0 -1 -1 -2 -2 0 0 0 0 0 0 0 0 -1 -1 -2 0 0 -1 -1 -2 0 0 0 0 0 0 0 0 -1	-ve
0 0 -1 -1 0 -1 -1 -2 -2 0 0 0 0 0 0 0 0 -1 -1 -2 0 0 -1 -1 -2 0 0 0 0 0 0 0 0	-ve
0 0 0 -1 -1 0 -1 -1 -2 -2 0 0 0 0 0 0 0 0 -1 -1 -2 0 0 -1 -1 -2 0 0 0 0 0 0	-ve
0 0 0 0 -1 -1 0 -1 -1 -2 -2 0 0 0 0 0 0 0 0 -1 -1 -2 0 0 -1 -1 -2 0 0 0 0 0	-ve
0 0 0 0 0 -1 -1 0 -1 -1 -2 -2 0 0 0 0 0 0 0 0 -1 -1 -2 0 0 -1 -1 -2 0 0 0 0	-ve
0 0 0 0 0 -1 -1 0 -1 -1 -2 -2 0 0 0 0 0 0 0 0 -1 -1 -2 0 0 -1 -1 -2 0 0 0 0	-ve

(a) Correlation Process



(b) Output from Correlator

Figure 2.4 Representation of the Complementary Correlation operation: (a) Correlation process (b) Output of the complementary correlator detector.

The recovered auto-correlation peak will be basically a return to zero (RZ) data pattern with a 6.25% duty cycle. This is due to the fact that each data bit is encoded with a 16 chip code and the auto-correlation peak is one chip wide.

Therefore, the data recovered from the complementary correlator can be considered to be RZ data with a duty cycle of 6.26% (i.e., 1/16 of the bit width). The RZ data is easily converted to the non-return to zero (NRZ) format to match the data input to the system.

2.5 PROPERTIES OF THE ALBERTA CODE - COMPLEMENTARY CORRELATOR

The properties of the Alberta code - complementary correlator combination are discussed in this subsection.

Figure 2.5 (a) shows the output waveform from the complementary correlator for the case where the transmitted code sequence is 0000111100000000 and the signal is received at the correct receiver (i.e., the receiver address code is 0000111100000000). Considering all amplitudes relative to the 'zero level' shown in Figure 2.5, the correlated output has a peak of height 4 (which is the weight, w , as expected) and auto-correlation wings have magnitudes no greater than 2 (i.e., $w/2$ as expected). If the receiver address code sequence is still 0000111100000000 but the received code sequence is now 0000110011000000 (i.e., an interfering station), then the cross-correlation waveform at the output of the complementary correlator will be of the form shown in Figure 2.5 (b). With the Alberta code - complementary correlation detection combination, the maximum value of the cross-correlation function does not exceed 'zero', with reference to the 'zero level' as defined in Figure 2.5. Also, the general shape of the cross-correlation waveform does not vary significantly from that shown in Figure 2.5(b)

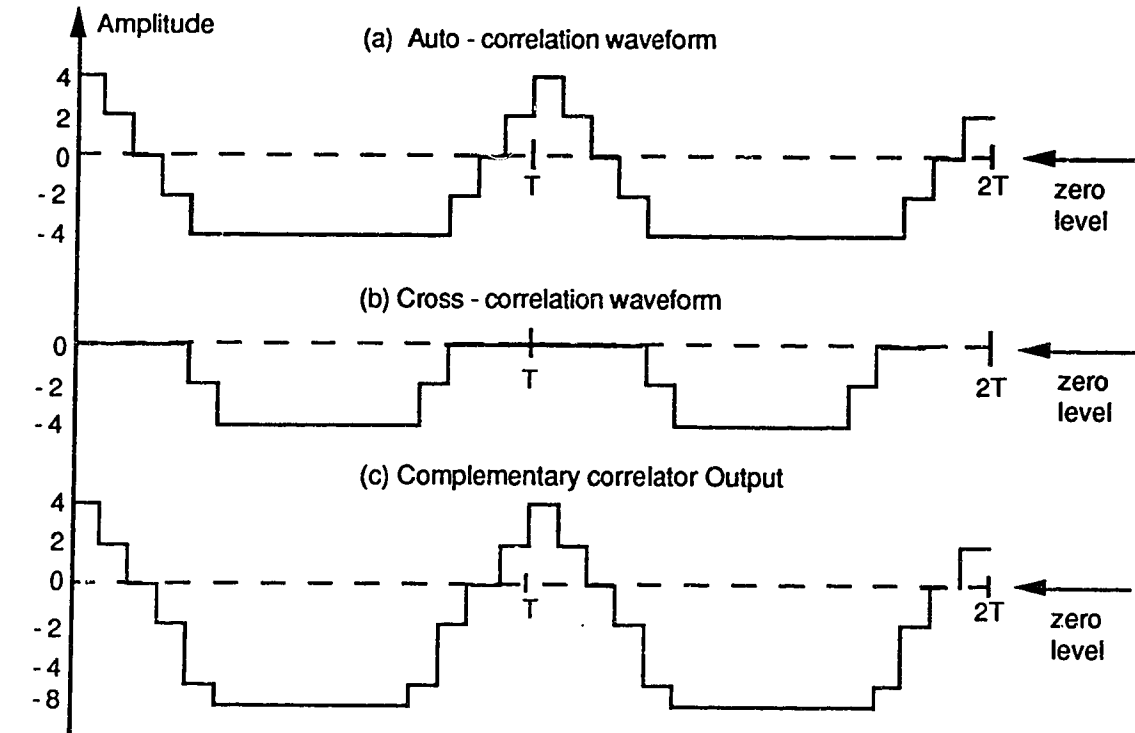
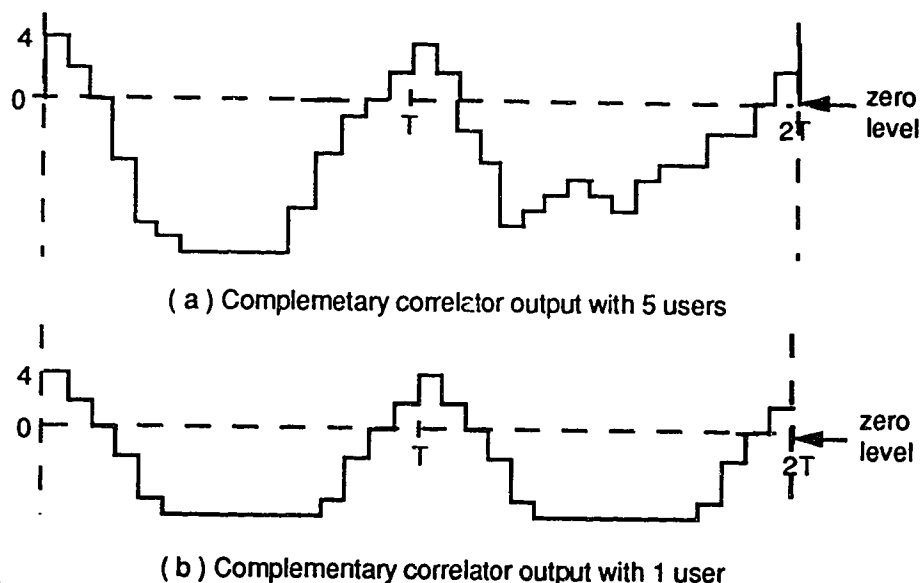


Figure 2.5 Output waveforms from the Complementary Correlator
(a) Auto-correlation (b) Cross-correlation (c) Sum
of auto plus cross correlation waveforms

If the encoded data streams corresponding to the correlated outputs in Figure 2.5 (a) and (b) occur at the same time, as would be the case in a synchronous (bit as well as chip) FO-CDMA system with two users, then the output from the complementary correlator of the receiving station would be equal to the sum of the two waveforms in Figure 2.5 (a) and (b) and is shown in Figure 2.5(c). Comparing the three waveforms, it can be seen that the 'zero' part of the cross-correlation function occurs in the same time frame as the auto-correlation peak. Since only the auto-correlation peak is of interest, it can be seen from Figure 2.5(c) that the cross-correlation function has no effect on the auto-correlation peak at the complementary correlator output. As mentioned before, the cross-correlation functions have the same general wave shape for a given code set.

Therefore, the sum of say five cross-correlation functions will still have a value of zero in the region of interest. Thus, the auto-correlation peak will be unaffected by the cross-correlation, irrespective of the number of interfering stations.



**Figure 2.6 Output of Complementary Correlator
for (a) five users in the network
(b) one user in the network**

Referring to Figure 2.6 which shows the output from a complementary correlator with (a) five stations transmitting and (b) with one station transmitting, it can be seen that even though the waveform in (a) contains a greater negative content, the region of interest, namely the auto-correlation peak, is unaffected by the number of interfering stations. Therefore, ideally, in the absence of noise and other forms of interference (e.g., inter-symbol-interference) a bit synchronous FO-CDMA system using Alberta codes and complementary correlation detection should have no errors. In the more realistic case where noise is

present, the Bit Error Rate (BER) performance of the system should be independent of the number of interfering stations although one would expect a small amount of degradation due to increased detector noise. Such a property would be particularly useful in high capacity high bit rate trunk multiplexing systems.

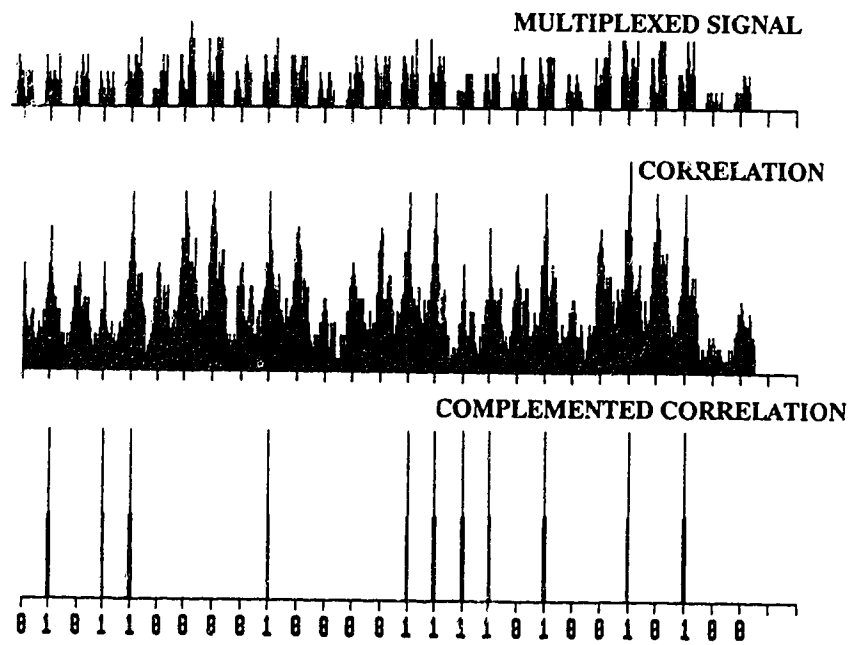


Figure 2.7 Computer Simulation of the complementary correlator detector for Alberta codes (adapted from [17])

Figure 2.7 shows the results of a computer simulation for the Alberta code - complementary correlator combination. The signal received at the receiver, Figure 2.7 (a), consists of 7 channels multiplexed using an Alberta code of length $N = 13$ and weight $w = 6$. Figure 2.7(b) shows the correlated output if a conventional correlator is used. As can be seen, it would be impossible to recover any useful information from such a correlator. This reinforces the

concept that the Alberta codes and complementary correlator must be used together for any useful result to be achieved. The rectified output of the complementary correlator is shown in Figure 2.7 (c). It is clearly evident that zero cross-talk can be achieved, in principle, if the system is operated with all the transmitting stations in the network synchronised at the individual channel bit rate.

Figure 2.8 shows a plot of the bandwidth expansion factor normalised to the number of channels carried as a function of the code weight factor. The code weight factor is defined as the ratio of the code weight, w , to the code length, N . Curves for Alberta codes with Hamming weights 4 and 6 are shown with those for Prime codes shown for comparison. The number of channels carried by each code is indicated at each point.

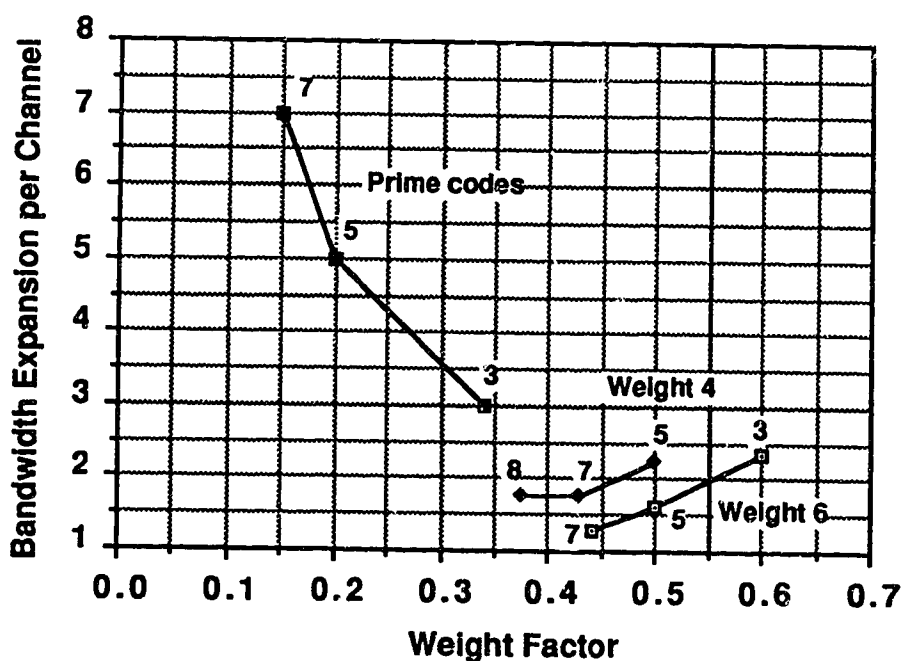


Figure 2.8 Plot of Bandwidth expansion per channel vs the Code weight factor for Alberta codes of weight 4 and 6 with those for Prime codes shown for comparison

It is apparent from these graphs that the Alberta codes have very low bandwidth expansion factors which in fact get even lower as the number of users increases. It is felt that this property of the Alberta codes will allow for much more efficient use of the bandwidth available in fibre. This aspect of the Alberta codes could be exploited for the distribution of wideband digital signals as for example in the distribution of high definition television channels.

2.6 PERFORMANCE ANALYSIS OF A FO-CDMA SYSTEM USING ALBERTA CODES AND COMPLEMENTARY CORRELATION

The original design of the Alberta code - Complementary correlator [17] was based on the assumption that the system operated bit synchronously (i.e., the transmissions from all the stations were perfectly synchronised on a bit by bit basis). Therefore in the absence of any form of interference or noise (i.e., an ideal system), the probability of error, PE, would be equal to zero for the bit-synchronous system. The technique is thus suitable for multiplex transmission. This section looks at the more general case of an asynchronous system with no network control (which could be used for multiple access) and attempts to determine the performance of a system using Alberta codes and complementary correlation when operating asynchronously.

2.6.1 ASSUMPTIONS [15]

1. There is no probability of error if all the stations in the system are perfectly synchronised. The performance of the system degrades only if there is a loss of synchronisation among the stations in the system.
2. A perfect electrical - to - optical and conversely optical - to - electrical signal conversion takes place.

3. The effects of thermal and quantum noise are ignored.
4. All light sources are perfectly incoherent. Therefore, the optical light intensity of multiple stations occurring at the same time would sum.
5. All the stations in the system have the same average optical power at any station. Therefore a station cannot overwhelm any other. This is in effect an idealisation which applies an upper bound on the performance of the system.
6. All the stations have identical bit rates and signalling formats.
7. There is no overall network time reference. Therefore, all the relative bit times among the users are asynchronous. Also, the system codes are used asynchronously, i.e., the relative positions of all the stations' codes are mutually random.

2.6.2 BINARY FO-CDMA SYSTEM

Consider a generalised FO-CDMA network (of the form shown in Figure 2.3) consisting of U transmitter and receiver pairs (i.e., U stations). For analysis purposes, assume that the communication between each of the u^{th} (for $1 \leq u \leq U$) transmitter and receiver pairs is continuous.

Therefore, the u^{th} baseband signal, $S_u(t)$, at the output of the u^{th} encoder, is given by:

$$S_u(t) = S_u \cdot b_u(t) \cdot DP_u(t) \quad (2.6)$$

Where, $S_u = u^{\text{th}}$ station's transmitted optical intensity
 $b_u(t) =$ binary data signal to the u^{th} transmitter

$DP_u(t) = u^{\text{th}}$ station's Alberta code

The u^{th} station's binary data signal, $b_u(t)$, for continuous communication, is given by:

$$b_u(t) = \sum_{k=-\infty}^{\infty} b_k^{(u)} \cdot P_T(t + kT) \quad (2.7)$$

Where, $b^{(u)} = (b_k^{(u)})$ is the u^{th} data sequence that takes on a value 0 or 1 for each value of k with equal probability and $P_T(t)$ is the rectangular pulse of duration T which starts at $t = 0$.

$DP_u(t)$, the u^{th} user's Alberta code is given by:

$$DP_u(t) = \sum_{j=-\infty}^{\infty} A_j^{(u)} \cdot PT_c(t + jT_c) \quad (2.8)$$

Where, $A^{(u)} = (A_j^{(u)})$ is the u^{th} periodic sequence of binary optical pulses (0, +1) with period $2N$, ie., $2N = T/T_c$, $A_j^{(u)} + 2N = A_j^{(u)}$ and weight w .

Also,
$$PT_c(t) = \begin{cases} 1 & 0 \leq t \leq T_c \\ 0 & \text{elsewhere} \end{cases} \quad (2.9)$$

Where, $PT_c(t)$ represents the amplitude of one chip.

Now, ideally the transmitters will be synchronised so that all the transmitted signals reach the passive multiplexer at the same time. But the time at which the incoherently summed signals arrive at any of the receiving stations will vary from one receiving station to another.

Therefore, at any receiving station, the incident optical intensity modulated signal can be represented by:

$$r(t) = \sum_{u=1}^U S_u(t + \tau_u) \quad (2.10)$$

where, τ_u = Time delay associated with the distance of the u^{th} receiving station from the transmitters.

Replacing $r(t)$ by its constituent terms

$$r(t) = \sum_{u=1}^U S_u \cdot b_u(t + \tau_u) \cdot DP_u(t + \tau_u) \quad (2.11)$$

It can be assumed that $S_u = 1$ for $1 \leq u \leq U$ (based on the equal amplitude assumption). Considering only relative time delays for the purpose of this analysis, one can assume that $\tau_u = 0$ when analysing the receiver station that is matched to the u^{th} signal.

For ease of notation, assume that the desired station's signal is denoted by $u = 1$. Therefore, $A^u(t) = A^1(t)$. $A^1(t)$ is written simply as $A(t)$.

Now, the complementary correlation and detection operation is represented by the following equation, where $A(t)$ is the bipolar output of the complementary correlator detector:

$$A(t) = \sum_{n=0}^{2N} r(t + nT_c) \{DP_1(nT_c) - [U(nT_c) - DP_1(nT_c)]\} \quad (2.12)$$

Where, $DP_1(nT_c) = 1^{\text{st}}$ station's Alberta code

$$U(nT_c) = \begin{cases} 1 & 0 \leq n \leq N \\ 0 & \text{elsewhere} \end{cases} \quad (2.13)$$

$2N$ = Length of the codeword, taking into account the $N/2$ zero's added to either end of a codeword of length N .

Therefore,

$$A(t) = \sum_{n=0}^{2N} r(t + nT_c) [2DP_1(nT_c) - 1] \quad (2.14)$$

$$A(t) = \sum_{n=0}^{2N} \left[\sum_{u=1}^U b_u(t + nT_c).DP_u(t + nT_c) \right] [2DP_1(nT_c) - 1]$$

$$A(t) = \sum_{n=0}^{2N} b_1(t + nT_c).DP_1(t + nT_c)[2DP_1(nT_c) - 1]$$

$$+ \sum_{u=2}^U \sum_{n=0}^{2N} b_u(t + nT_c).DP_u(t + nT_c)[2DP_1(nT_c) - 1] \quad (2.15)$$

$$A(t) = b_0^{(1)}.w + \sum_{u=2}^U I_u \quad (2.16)$$

$$A(t) = b_0^{(1)}.w + I_1 \quad (2.17)$$

Where, $b_0^{(1)}.w$ = Desired signal

I_1 = Undesired signal

$b_0^{(1)}$ is the amplitude of the zeroth data of the first user's signal and can take on two values, 0 or 1, with equal probability. The undesired signal I_1 is composed of $(U - 1)$ interference signals $I_u^{(1)}$, where each $I_u^{(1)}$ is a random variable with mean $M_{I_u^{(1)}}$ and variance $\sigma_{I_u^{(1)}}^2$.

Now, each of the I_u in equation (2.16) are independent and identically distributed random variables. Therefore, the mean and variance of the total interference signal I_1 can be expressed as :

$$M_{I_1} = (U - 1).M \quad (2.18)$$

$$\sigma_{I_1}^2 = (U - 1).\sigma^2 \quad (2.19)$$

Where, $M = M_{I_u^{(1)}}$ and $\sigma^2 = \sigma_{I_u^{(1)}}^2$ for $2 \leq u \leq U$.

In the ideal case, the transmitters of all the transmitting stations would be perfectly synchronised i.e., the transmitters are synchronised on a bit by bit

basis. For such a system, in the ideal case (i.e., no noise or interference), the probability of error, PE, will be 0.

If there is no synchronisation between the transmitting stations of the FO-CDMA network (i.e., as in a true multiple access system with effectively zero access delay), then the position of a chip from any transmitting station will be completely random relative to a chip from any other transmitting station in the network. Thus, two possible conditions can be considered:

1. The shift between any two chips of two transmitting stations is a multiple of a chip width. This is referred to as the chip synchronous case and can be represented as shown in Figure 2.9.

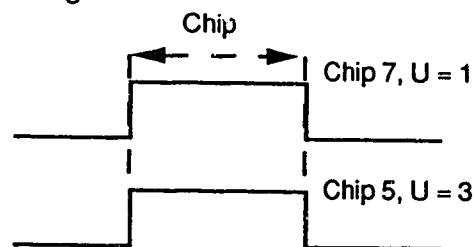


Figure 2.9 Possible relative chip positions for the synchronous case

This is an idealised case with a low probability of occurrence and is considered here only for the purpose of analysis.

2. The shift between any chips of two transmitting stations is a fraction of a chip width. This is referred to as the chip asynchronous case and can be represented by Figure 2.10 below.

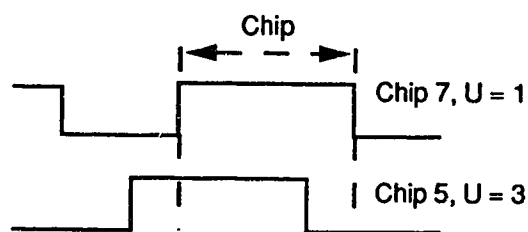


Figure 2.10 Possible relative chip positions for the chip asynchronous case

The chip synchronous case may be considered to be a specific condition of the more general chip asynchronous case. It is considered for the purposes of analysis as it provides the worst case interference to the signal of interest.

Referring to equations (2.15) and (2.17), the interference due to the $U - 1$ interfering transmitting stations is given by:

$$I_1 = \sum_{u=2}^U \sum_{n=0}^{2N} b_u(t + nT_c) \cdot DP_u(t + nT_c) [2DP_1(nT_c) - 1] \quad (2.20)$$

where, equation (2.20) takes into account the complementary correlation operations and:

$$b_u(t + nT_c) = \begin{cases} 1 \\ 0 \end{cases} \quad \begin{array}{l} \text{with probability : } 1/2 \\ \text{with probability : } 1/2 \end{array} \quad (2.21)$$

$$DP_u(t + nT_c) = \begin{cases} 1 \\ 0 \end{cases} \quad \begin{array}{l} \text{with probability: } w/2N \\ \text{with probability: } (2N - w)/2N \end{array} \quad (2.22)$$

$$[2DP_1(nT_c) - 1] = \begin{cases} 1 \\ -1 \end{cases} \quad \begin{array}{l} \text{with probability : } w/2N \\ \text{with probability : } (2N - w)/2N \end{array} \quad (2.23)$$

Therefore, the probability density function for the generalised interference between any one interfering transmitting station and the receiving station address code can be written as:

1. *Synchronous case*

$$[P_{I_u}(I_u)] = p\delta(I_u - 1) + q\delta(I_u) + (1 - p - q)\delta(I_u + 1) \quad (2.24)$$

Where, p is the probability that $I_u = 1$, q is the probability that $I_u = 0$ and $(1-p-q)$ is the probability that $I_u = -1$. It must be noted that I_u in this case can take on values of either 1, 0 or -1, due to the complementary correlation.

2. Asynchronous case

$$[P_{I_u}(I_u)] = p\delta(I_u - 1) + q\delta(I_u) + r\delta(I_u + 1) + s(I_u) + (1 - p - q - r - s)(I_u) \quad (2.25)$$

Where again, p is the probability that $I_u = 1$, q is the probability that $I_u = 0$ and r is the probability that $I_u = -1$.

$$\text{Also, } (\dot{x}) = \begin{cases} 1 & 0 \leq x \leq 1 \\ 0 & \text{elsewhere} \end{cases} \quad (2.26)$$

$$(\dot{x}) = \begin{cases} -1 & -1 \leq x \leq 0 \\ 0 & \text{elsewhere} \end{cases} \quad (2.27)$$

2.6.3 PROBABILITY DENSITY FUNCTION FOR THE INTERFERENCE SIGNAL I_1

In evaluating the probability density function for the interference signal I_1 , two possible cases (1) Chip synchronous and (2) Chip asynchronous are considered. The evaluation of the exact probability density function for I_1 would require knowledge of the probability density functions associated with each of the interfering sources $I_u(1)$ for $2 \leq u \leq U$. For a system with U users in an FDDMA network, the interference I_j at the output of the j th receiver, for $1 \leq j \leq U$, will contain $(U - 1)$ interfering terms and therefore a total knowledge of $U(U-1)/2$ probability density functions is required. The process of evaluating the $U(U-1)/2$ probability density functions would be extremely tedious, especially for large values of U . Therefore, the two extreme cases presented in Figures 2.9 and 2.10 will be considered for the analysis of the interfering signals.

The variance of a random variable (in this case, the variance of the interfering signals) is a measure of its strength and it can be proved [16] that the interference in the chip synchronous case corresponds to a pessimistic approximation to the actual interference and the chip asynchronous case corresponds to an optimistic approximation, i.e.,

$$[P_{I_u}(I_u)]_{\text{Case 2}} \leq \text{Actual Prob. Density Funct.} \leq [P_{I_u}(I_u)]_{\text{Case 1}} \quad (2.28)$$

Therefore, the two cases effectively form the upper and lower bounds to the actual probability density function. Since the purpose of this analysis was to investigate the applicability of Alberta codes and complementary correlation detection to an asynchronous FO-CDMA system, it was felt that determining the upper bound would be sufficient.

A complete analysis for the asynchronous case (case 2) would be long and involved and is especially complicated by the bi-polar nature of the output from the complementary correlator. The synchronous case (i.e., case 1) is thus considered in greater detail.

From equations (2.15) and (2.16),

$$I_u^{(1)} = \sum_{n=0}^{2N} b_u(t + nT_c) \cdot DP_u(t + nT_c) [2DP_1(nT_c) - 1] \quad (2.29)$$

Where, $I_u^{(1)}$ represents the interference at receiving station 1 due to any one of the transmitting stations. Taking into account the probability of occurrence of b_u , DP_u and DP_1 from equations (2.21), (2.22) and (2.23) and substituting in equation (2.24), the probability density function of the interference signal due to any transmitting station is given by:

$$P_{I_u}^{(1)}(I_u) = \frac{w^2}{2(2N)^2} \cdot \delta(I_u - 1) + \frac{w(2N - w)}{2(2N)^2} \cdot \delta(I_u + 1) + \left[1 - \frac{w^2}{2(2N)^2} - \frac{w(2N - w)}{2(2N)^2} \right] \cdot \delta(I_u)$$

(2.30)

Also,

$$I_1 = \sum_{u=2}^U I_u^{(1)}$$

(2.31)

where, I_1 is the sum of $(U - 1)$ independent identically distributed random variables, $I_u^{(1)}$, with probability density function defined as in equation (2.30).

The statement that each I_u is an identically distributed independent random variable may or may not be true depending on the application. In the case of a trunk multiplexing application this statement is not strictly true due to the fact that every time a code word in a given code set is used, the same codeword cannot be used at the same time by another transmitter or receiver. Therefore the probability of a code word in a given code set being picked is dependent on the previous history of the code set. Thus, the assumption that each I_u is an independent random variable simply results in an upper bound to the true probability density function of I_u . In the case of a broadcast application however, the statement that each I_u is an identically distributed independent random variable is perfectly true since in such an application more than one receiver can be switched to a given transmitter at any one time, i.e., all the code words in a given code set are equi-probable at all times. Thus for the purpose of this analysis, which is not a rigorous one, it is assumed that each I_u is an independent identically distributed random variable.

Therefore, the probability density function of I_1 , $P_{I_1}(I_1)$, is given by the convolution of the probability density functions of the random variables $I_u^{(1)}$ for $2 \leq u \leq U$.

Therefore,

$$P_{I_1}(I_1) = \sum_{u=0}^U \sum_{j=0}^u \binom{U-1}{u} \binom{U-1-u}{j} \left[\frac{w^2}{2(2N)^2} \right]^u \left[\frac{w(2N-w)}{2(2N)^2} \right]^j \times \left[1 - \frac{w^2}{2(2N)^2} - \frac{w(2N-w)}{2(2N)^2} \right]^{U-1-u-j} \cdot \delta(I_1 - u - j) \quad (2.32)$$

2.6 4 PROBABILITY OF ERROR

As a result of the relationship of the variances [16] and the probability density functions, equation (2.28), the probability of error derived from case 1, PE_{case1} , would be an upper bound on the exact probability of error, $PE(\text{exact})$, and the probability of error derived from case 2, PE_{case2} , would be the lower bound on the exact probability of error, i.e.,

$$PE_{\text{case2}} \leq PE(\text{exact}) \leq PE_{\text{case1}} \quad (2.33)$$

The exact probability of error, $PE(\text{exact})$, is defined as:

$$PE(\text{exact}) = \Pr(A(t) \geq 0 \mid b_0^{(1)} = 0) \cdot \Pr(b_0^{(1)} = 0) + \Pr(A(t) < 0 \mid b_0^{(1)} = 1) \cdot \Pr(b_0^{(1)} = 1) \quad (2.34)$$

It must be noted that the threshold level has been set at zero.

Considering the second term of equation (2.43), for $0 \leq Th \leq w$,

$$\Pr(A(t) < Th \mid b_0^{(1)} = 1) = \Pr(w - Th + I_1 < 0)$$

$$= \Pr(\eta < 0) \quad (2.35)$$

$$\text{Where, } \eta = w - T_h + I_1 \quad (2.36)$$

Now, depending on the number of chip shifts that may have occurred for each of the interfering transmitting stations, η could be a negative number. Therefore,

$$\begin{aligned} \text{PE(exact)} &= \frac{1}{2} \Pr\left(\sum_{u=2}^U I_u^{(1)} \geq 0 \right) + \frac{1}{2} \Pr\left(\sum_{u=2}^U I_u^{(1)} \geq w \right) \\ &= \frac{1}{2} \Pr(I_1 \geq 0) + \frac{1}{2} \Pr(I_1 \geq w) \end{aligned} \quad (2.37)$$

$$= \frac{1}{2} \int_0^{\infty} P_{I_1}(I_1) dI_1 + \frac{1}{2} \int_w^{\infty} P_{I_1}(I_1) dI_1 \quad (2.38)$$

The integrals in equation (2.38) above can be replaced by summations, to a very good approximation. This is due to the fact that the probability density functions are in fact delta functions.

Therefore,

$$\text{PE(exact)} < \text{PE(approximation)} \quad (2.39)$$

And,

$$\begin{aligned} \text{PE} &= \frac{1}{2} \sum_{u=0}^{U-1} \sum_{j=0}^u \binom{U-1}{u} \binom{U-1-u}{j} \left[\frac{w^2}{2(2N)^2} \right]^u \left[\frac{w(2N-w)}{2(2N)^2} \right]^j \left[1 - \frac{w^2}{2(2N)^2} - \frac{w(2N-w)}{2(2N)^2} \right]^{U-1-u-j} \\ &+ \frac{1}{2} \sum_{i=w}^{U-1} \sum_{j=0}^i \binom{U-1}{i} \binom{U-1-i}{j} \left[\frac{w^2}{2(2N)^2} \right]^i \left[\frac{w(2N-w)}{2(2N)^2} \right]^j \left[1 - \frac{w^2}{2(2N)^2} - \frac{w(2N-w)}{2(2N)^2} \right]^{U-1-i-j} \end{aligned} \quad (2.40)$$

Thus, equation (2.40) above gives the upper bound on the probability of error, PE, of an asynchronous FO-CDMA system using Alberta codes and complementary correlation and detection techniques.

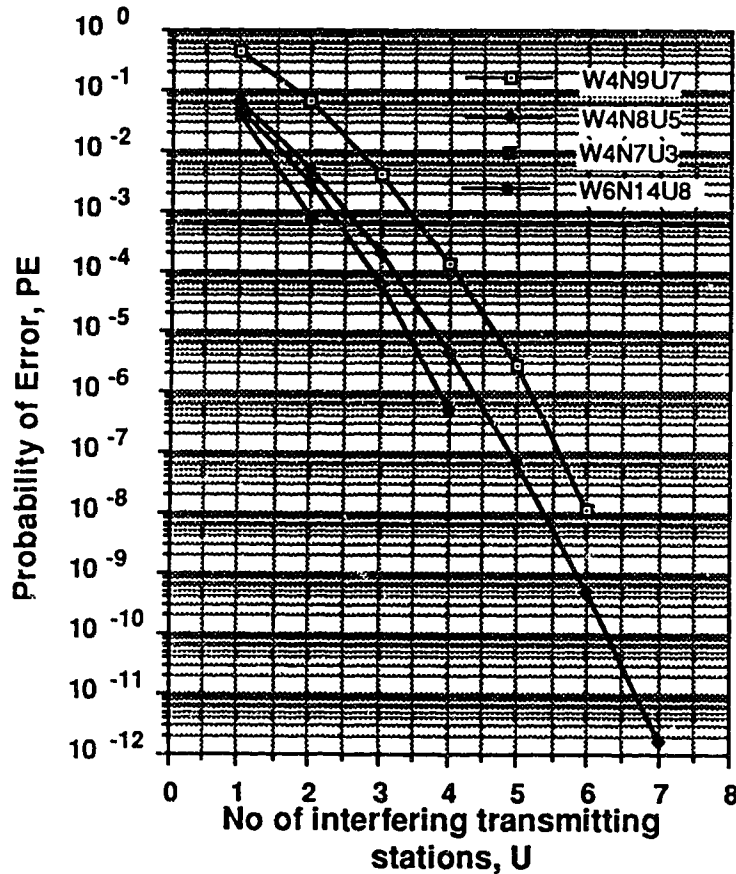


Figure 2.11 Plot of Probability of Error (PE) vs Number of Interfering Users for Alberta Codes of weight 4 and 6

Figure 2.11 shows the plot of the Probability of error, PE, (i.e., equation (2.40)), as a function of the number of interfering transmitting stations for Alberta codes of weight 4 and 6.

Referring to Figure 2.11, it can be seen that the Bit Error Rate (BER) performance of an asynchronous FO-CDMA network using Alberta codes and

complementary correlation improves with the number of increasing users, in the absence of noise and other forms of interference (e.g inter-symbol interference). This concept is in direct opposition to that in conventional systems, where the performance of a system degrades as the number of users increases. This property is a direct consequence of the Alberta code - complementary correlation combination. This peculiarity can be explained as follows: By the definition of Alberta codes, the cross-correlation functions never exceed zero (Section 2.3). The only effect of additional users in the system is an increase in the negative content of the signal at the output of the complementary correlator detector (see Figure 2.6). Thus as the negative content increases, the probability of mistaking a '1' for a '0' and vice versa decreases since the auto-correlation peak is unaffected by the number of interfering users present in the system. The probability of error performance thus improves as the number of users increases.

It can also be observed from Figure 2.11 that the system performance is dependent on the length of the Alberta code set, i.e., the longer the length of the code set, the better the BER performance.

As noted previously, the above analysis is only an upper bound on the probability of error and as such depicts a worst case scenario. A more rigorous analysis of the system performance should yield even better performance results. The results of this analysis indicate that although designed primarily for synchronous operation, the Alberta code-complementary correlation combination can be used in an asynchronous environment with no network control, i.e., a true multiple access situation. This is another possible area for future investigation.

2.7 SUMMARY

The Alberta codes and the concept of complementary correlation have been presented. A technique for generating these codes has also been discussed. The performance of a network using Alberta codes and complementary correlation has been analysed with respect to asynchronous operation and the results obtained indicate that the performance of an asynchronous system using Alberta codes and complementary correlation improves as the number of users in the network increases.

CHAPTER 3
SYSTEM DESIGN

3.1 THE EXPERIMENTAL SETUP

Figure 3.1 shows the configuration of the experimental system to demonstrate an FO-CDMA network using Alberta codes and complementary correlation detection. The FO-CDMA network consists of two transmitters, a 3x1 passive optical power combiner and a receiver that can be switched to receive transmissions from either transmitter. The complementary correlator detector configuration used in the receiver is that shown in Figure 2.2.

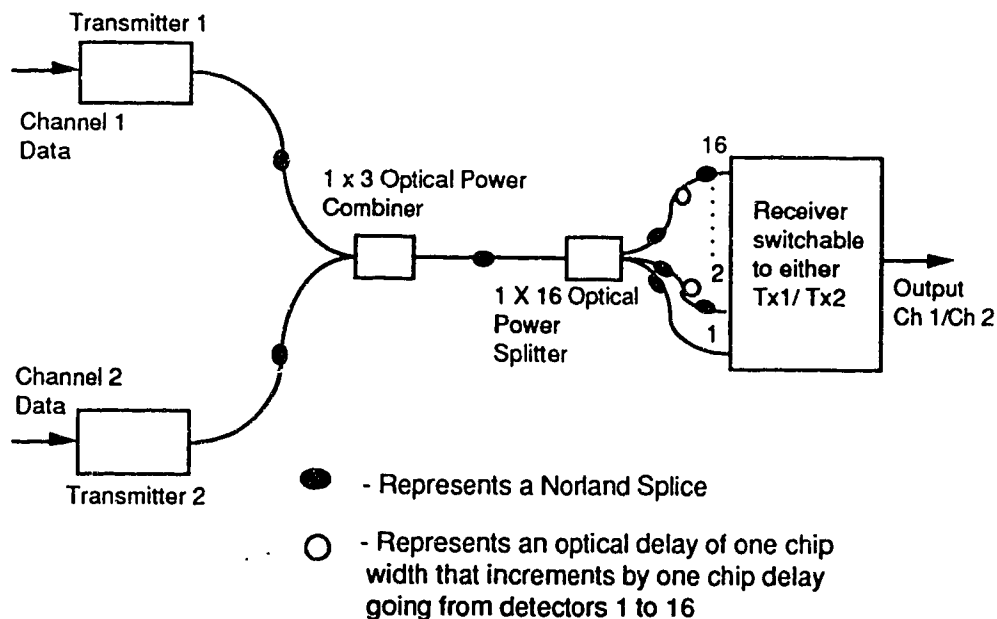


Figure 3.1 Configuration of the experimental system to demonstrate an FO-CDMA system using Alberta codes and complementary correlation detection

The Alberta code set that will be used in the demonstration is of length $2N = 16$ and weight $w = 4$. This code set is capable of carrying 5 users (i.e., 5 Alberta codes of length $2N = 16$ and weight $w = 4$ have been found).

An individual channel rate of 50 Mbits/s is adopted as this is the number closest to the DS3 rate of 44.736 Mbits/s which when multiplied by a code of length 16 allows a round figure to be achieved for the chip rate. This in turn allows for a reasonable value to be obtained for the chip width. The system chip rate is therefore $50 \text{ Mbits/s} \times 16 = 800 \text{ MChips/s}$, since each bit '1' is encoded with the 16 chip address. It must be noted that no information is transmitted for a data bit '0'. At 50 Mbits/s, the bit width, T , corresponds to 20 ns (for NRZ data). Therefore, the chip width $t = T/2N = 20 \text{ ns}/16 = 1.25 \text{ ns}$. In this demonstration, pulses are used to represent chips and therefore the widths of the pulses used to encode the data must be at most 1.25 ns to avoid inter-symbol interference between two adjacent chips.

3.1.1 POWER BUDGET REQUIREMENTS

Referring to the system configuration in Figure 3.1, there are four fibre splices in the optical path from each transmitter to each of the 16 detectors in the receiver. The optical splices used throughout the experiment are of the Norland type. Tests carried out indicate that the splicing losses are of the order of 0.5 dB/splice for 50/125 μm multimode fibre. Therefore, the total splicing loss in the system will be 2.0 dB.

The experimental system contains a 1x3 optical power combiner (used as a passive optical multiplexer) and a 1x16 optical power splitter within the receiver. The excess plus splitting (or combining) losses of the 1x3 combiner and 1x16 splitter are given by the manufacturers to be 3.8 dB and 14.8 dB respectively. (The data sheets for the 1x3 power combiner and 1x16 power splitter are given in Appendix C). Therefore, the total system loss is 20.6 dB.

Based on measurements carried out on surface depleted photoconductors [22] and Metal-Semiconductor-Metal photodiodes [18], the two types of detectors most likely to be used in the receiver [17] (refer to Section 3.4.2 for the choice of photodetector), at least $80 \mu\text{W}$ (-41 dB) of peak optical pulsed power would be required at the detector array per pulse for correlation to take place. Taking into account the system loss of 20.6 dB, peak optical power of 9.2 mW (-20.37 dB) would be required at the transmitter per pulse.

3.2. TRANSMITTER DESIGN CONSTRAINTS

3.2.1 THE CHOICE OF LASER

Since Gallium Arsenide (GaAs) detectors, which operate in the 800nm wavelength region, were chosen for the demonstration (as discussed in the Section 3.4.2), the lasers that could be used were limited to the GaAlAs type that also operate in the 800 nm region. These lasers, while not being ideal for long distance transmission, are excellent for transmissions over short lengths and for demonstration purposes.

Tests carried out at the Alberta Telecommunications Research Centre (ATRC) on short wavelength lasers designed for use in compact disc players, high speed laser printers and optical disc memories indicate that they are well detected by GaAs detectors of the type mentioned above [23]. These short wavelength lasers are also becoming progressively cheaper, making them most attractive for use in optical transmitters. One such laser is the Mitsubishi ML 6411C [24]. The frequency response of such a device has been found to be flat to within 3 dB for the range 300 kHz to 3 GHz [23]. Acceptable pulse response characteristics, i.e., optical pulses with widths of the order of 800 ps to 1.2 ns,

were obtained depending on the bias point of the laser. The Mitsubishi ML 6411C laser diodes were thus chosen not only because they satisfied the pulsed response requirements but also because of their relatively low cost and the ease of availability of a commercially pigtailed device.

3.2.2 PASSIVE OPTICAL VS PASSIVE ELECTRICAL ENCODING

Two methods of passive encoding (i.e., the coding of each data bit '1' with the address of the receiver) exist : optical and electrical.

Figure 3.2 shows three possible configurations of a passive optical encoder. The encoder shown in Figure 3.2 (a) consists of a single laser diode, a 1x4 optical power splitter, four optical fibre delay lines [10], the lengths of which would depend on the address of the encoder, and a 4x1 optical power combiner. As can be observed from Figure 3.2(a), there will be four splices in this configuration. The 4x1 optical power combiners/ splitters have a splitting/ combining plus excess loss of 8.0 dB. The total loss in the encoder will thus be 18.0 dB. If the laser is pulsed at peak power (i.e., 10 mW) then the encoded output from the encoder would have a peak pulsed power of 160 μ W. Referring to the configuration shown in Figure 3.2(b), there will be 8 dB less loss as compared to the configuration in Figure 3.2(a). The encoder loss is therefore 9.5 dB and thus the encoded output will have a pulsed peak power of 1.12 mW per pulse. Considering Figure 3.2(c), there will be a loss of 6 dB per 1x2 optical power splitter. The total loss is 19.0 dB and therefore the encoded output will have a peak pulsed power of 126 μ W. Comparing the peak pulsed optical power available from the optical encoders discussed above with the power budget requirement (Section 3.1.1), it is apparent that optical encoding cannot be used due to power constraints. The other alternative would have been to use

higher power lasers but, due to cost constraints this alternative was not adopted. Passive electrical encoding was therefore used. This method of encoding is discussed in Section 3.3.2 .

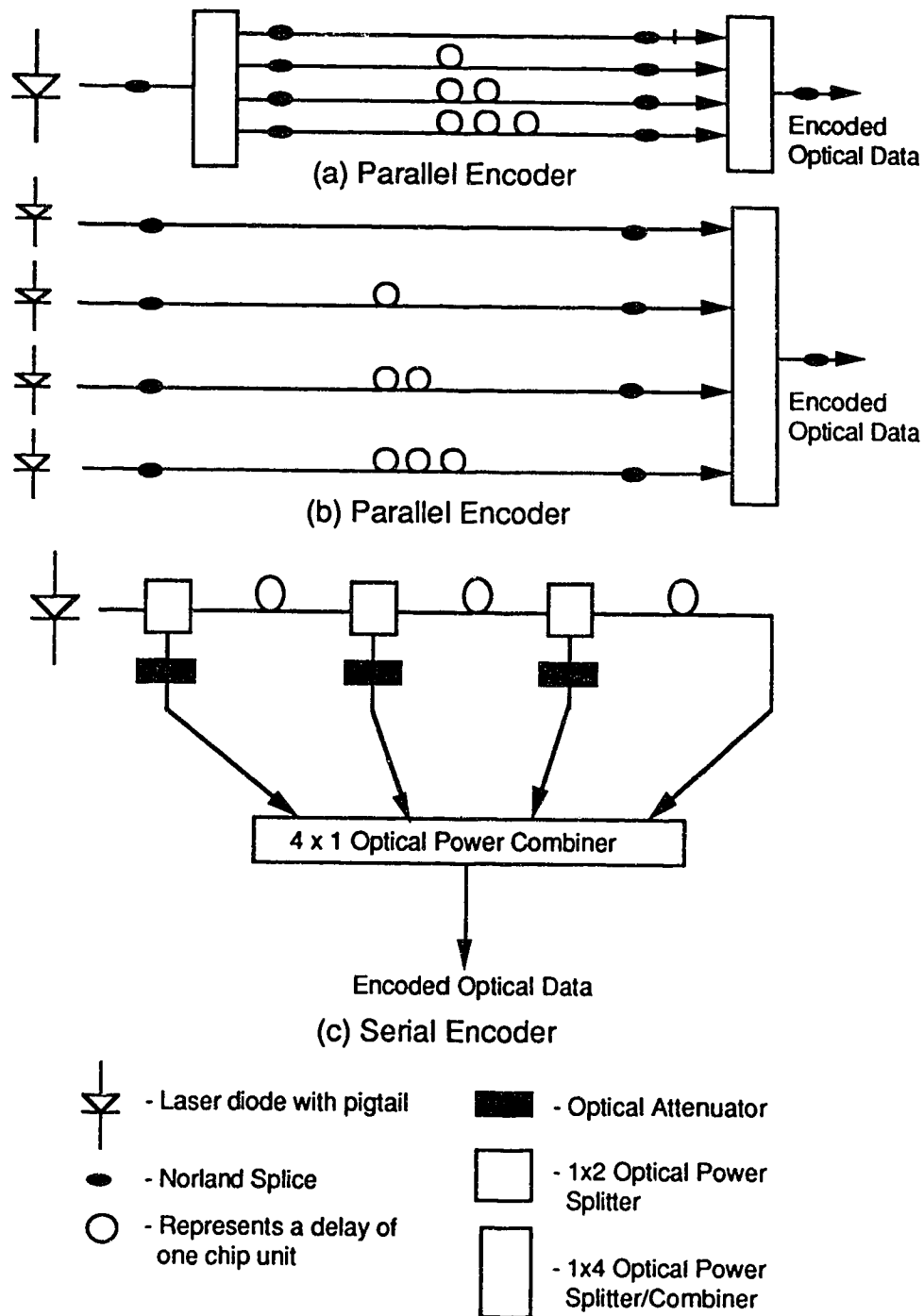


Figure 3.2 Three possible passive optical encoder configurations

3.3 TRANSMITTER DESIGN

Figure 3.3 shows the block diagram of transmitters 1 and 2. Each transmitter consists of the following stages: a pulse generator (which is common to both transmitters), a modulator for modulating the data with the pulse stream to generate the RZ data with duty cycle 6.25%, a passive electrical encoder to encode the modulated data stream with the address of the transmitter in question and a laser driver circuit to perform the electrical to optical conversion. A 50 MHz sine wave is used as the master clock for both the transmitters and the receiver.

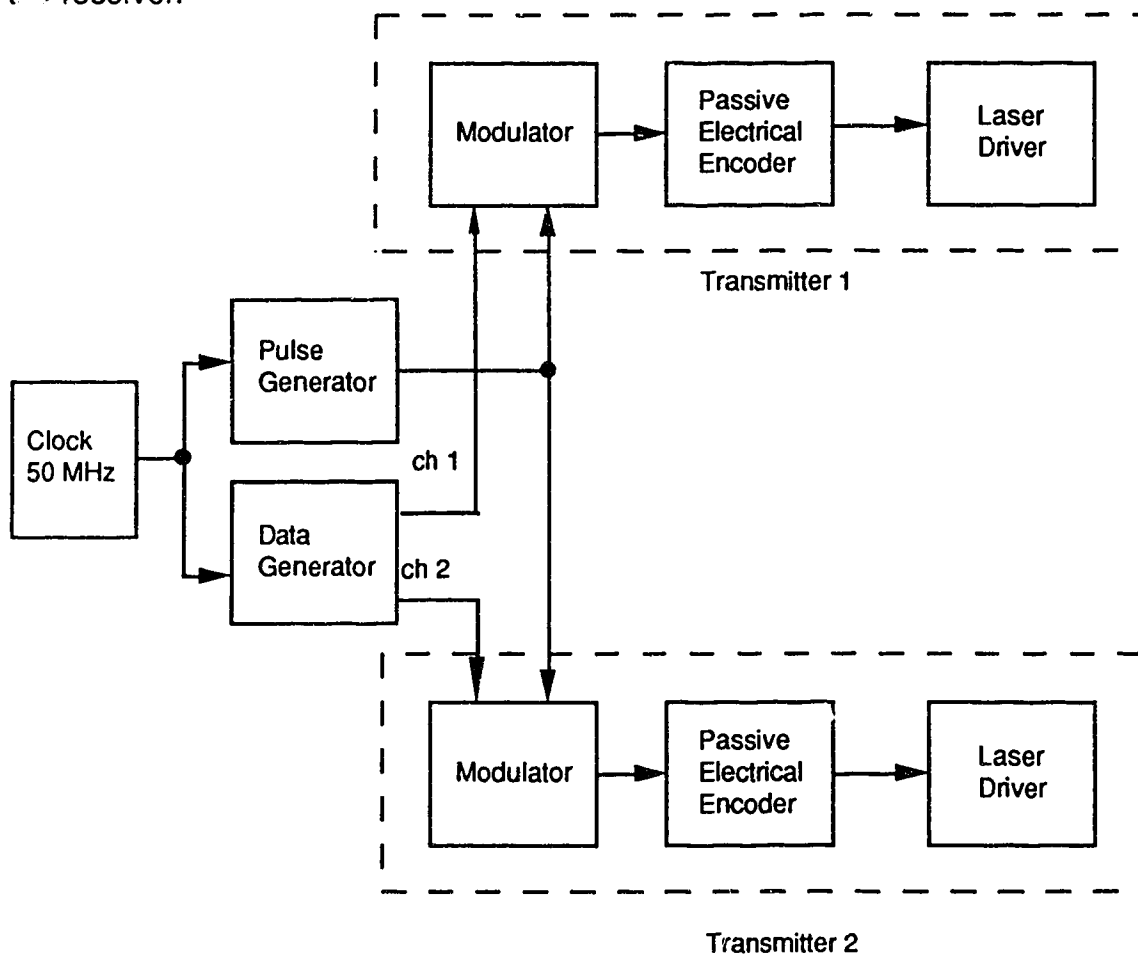


Figure 3.3 Block diagram of transmitters 1 and 2

3.3.1 THE PULSE GENERATOR

The pulse generator is used to generate electrical pulses with widths of the order of 500 ps. As explained in Section 3.1, the optical pulse width should not exceed 1.25 ns for a chip rate of 800MChips/s. Pulsing tests carried out on the ML6411C laser diode indicate that a significant widening of the pulse occurs during the electrical to optical transformation. Thus in order to obtain optical pulses with widths of 1.25 ns, it was found that electrical pulses with widths of the order of 500 ps were required at the output of the pulse generator.

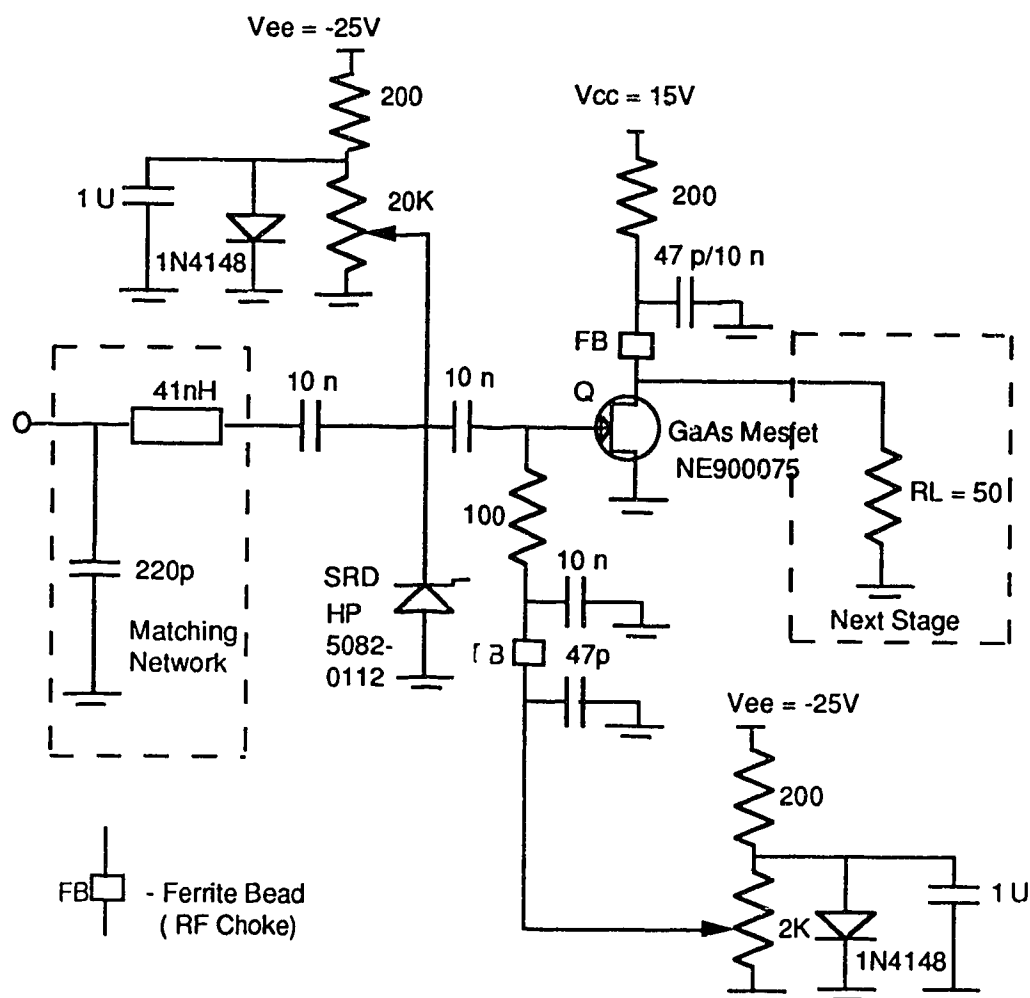


Figure 3.4 Pulse Generator circuit used to generate the 500ps wide electrical pulses

The pulse generator circuit is shown in Figure 3.4. The output from the sine wave generator has an amplitude of 6V (peak - to - peak) at 50 MHz. The Step Recovery Diode (SRD) and the associated biasing circuit convert the sinusoidal input into a train of narrow unidirectional pulses. The repetition rate of the pulses is precisely the frequency of the input.

The operation of the circuit is as follows : The SRD has a life time, τ , which is long compared to the period of the input sine wave. For the negative half of the cycle, the SRD is turned 'ON' and charge is stored on it by the current. On the positive half cycle, the generator reverses the current through the diode and the charge is thus removed. The negative bias voltage applied to the SRD is adjusted (via the variable negative bias circuit, see Figure 3.4) to make the peak reverse current through the diode a maximum when the last of the stored charge is removed. At this time the diode stops conducting and appears as a capacitor. The resulting rapid cessation of current creates a transient involving (1) the inductance of the SRD (13 nH - for the device used in the circuit) plus the stray inductance in the path due to the length of the leads etc (2) the capacitance of the step recovery diode (of the order of 1.55 pF - for the device used in the circuit) and (3) the load resistor R_L for the SRD (100 Ω in this case). The first half of the transient forms the required output pulse: then the diode becomes forward biased and the process is repeated for another cycle.

Based on the equations given in the application notes for SRD's [25], the real component of the impedance, looking into the pulse generator circuit from the 50MHz sine wave generator, was calculated to be 4.1 Ω . The 50 MHz sine wave generator is matched to 50 Ω . To avoid any reflections due to the impedance mismatch in the circuitry, an impedance matching circuit (see Figure

3.4) was designed to provide the 50Ω match for the 50 MHz sine wave generator.

Referring to Figure 3.4, the GaAs MESFET stage (the data sheets for the NE900075 are given in [26]) is introduced to provide the necessary pulse amplitude and polarity. The negative bias on the gate of the MESFET allows the transient ripples on the falling edge of the pulse to be clipped, allowing for a much cleaner output pulse shape.

3.3.2 THE MODULATOR

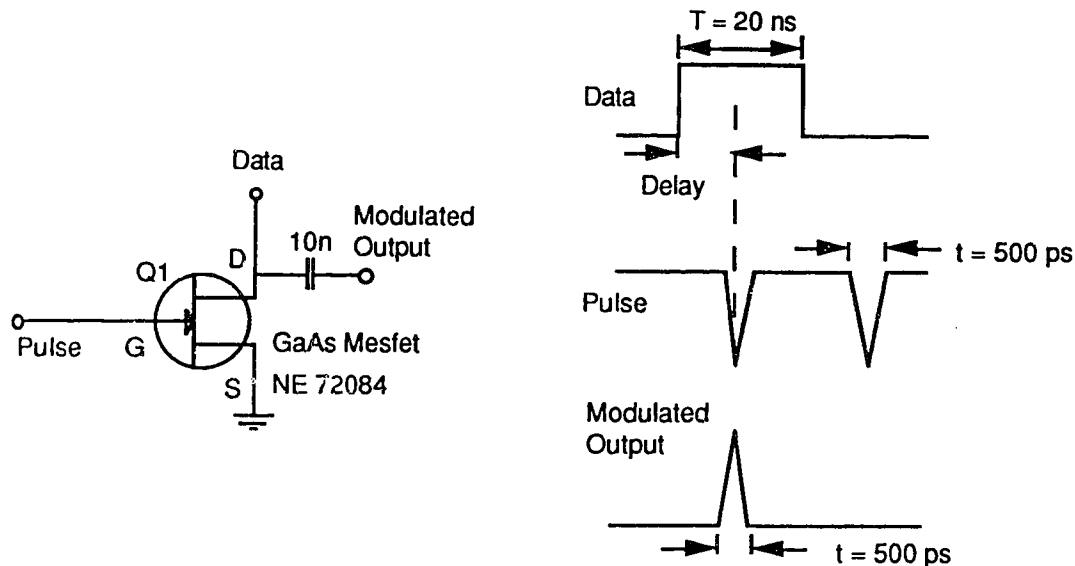
As can be seen from Figure 3.3, the pulse stream and the data stream are both applied to the modulator circuit. The operation required by the modulator is represented by the following truth table:

Table 3.1 Truth table for the operation of the modulator

Data bit	Pulse	Modulator Output
0	0	0
0	1	0
1	0	0
1	1	1

In order to satisfy the pulse width requirements mentioned in the previous sections of this chapter, it is essential that significant pulse widening does not take place as the pulses pass through the numerous stages of the transmitter. Thus a device with a very fast switching time is required. Since the pulses have rise and fall times in the 250 ps region, the effective bandwidth required is of the order of 1.4 GHz. Gallium Arsenide (GaAs) MESFET's with short gate lengths (1 μm) are ideal for such an application. The device chosen for this circuit is a

NE72084 small signal GaAs MESFET with a switching time of 10 ps (the data sheets for the NE72084 are given in [26]).



(a) Modulator Circuit

(b) Input and Output waveforms

Figure 3.5 (a) The modulator circuit (b) Timing diagram showing the timing of the data and pulse streams

The modulator circuit is shown in Figure 3.5(a). Its operation is as follows: The negative going pulse train with amplitude -4.5 V and pulse repetition frequency (PRF) 50 MHz, generated by the pulse generator circuit, is applied to the gate of the MESFET (V_{GS}). The data stream, with amplitude 5 V for a data bit '1' and 0 V for a data bit '0', is applied to the drain of the MESFET. In order to ensure that the modulation takes place correctly, the pulse stream is delayed such that the pulse occurs beyond the rising edge of the data bit (see Figure 3.5(b)). In the event of a data bit '1' occurring, 5 V is applied at the drain of the MESFET. With no pulse on the gate, $V_{GS} = 0$ V and the device conducts. When conducting, the MESFET has a low output impedance and the drain to source saturation current, I_{DSS} , is drawn by the device from the data generator. The drain to

source voltage, V_{DS} , is therefore a small value (0.6V). When the negative going pulse occurs at the gate, $V_{GS} = V_P = -3V$ (where, V_P is the gate pinch-off voltage), the device turns off and a high impedance ($1M\Omega$) is presented at the output. V_{DS} thus jumps to 5V. On the falling edge of the pulse, the reverse process takes place and V_{DS} then drops back to its low value i.e., the device turns back on. Due to the fast on-off switching time of the device (10 ps), the pulse width is not affected. When a data bit '0' occurs and a pulse occurs, there is no current being supplied by the data generator and thus even though Q1 turns off and then back on, there is no change at the output. In the event that a data bit '1' occurs but there is no pulse, there will be 0V on the gate and the device is on. Since there is a data bit '1' on the drain of Q2, there will be 5V on the drain and thus I_{DSS} will be drawn by Q2 and no change will appear at the output.

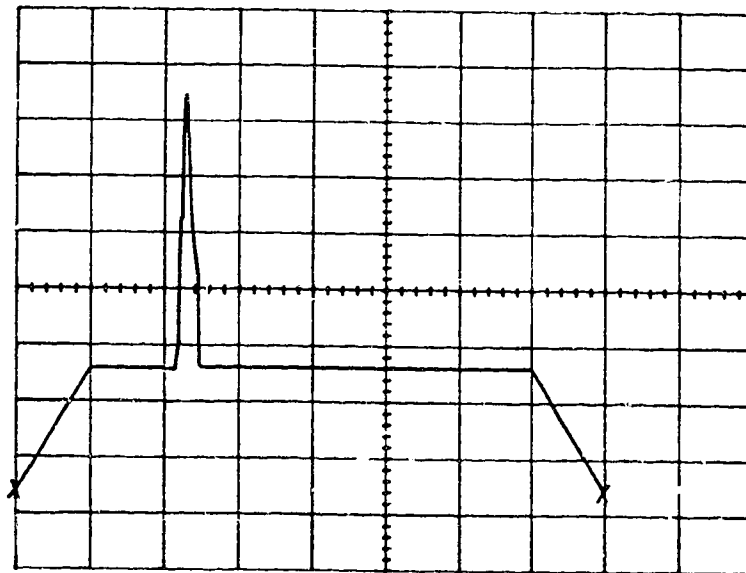


Figure 3.6 SPICE simulation of the modulator circuit showing the output for a data bit '1'. The leakage of the data signal to the output is evident
x scale: 2ns/ division y scale: arbitrary units

Figure 3.6 shows the modulated output waveform obtained with a SPICE simulation of the modulator circuit. As can be seen, the pulse width is maintained. Also, there is some leakage of the data stream to the output due mainly to the drain to source parasitic capacitance of the MESFET. This however is not a significant problem. The SPICE simulation program for the modulator is given in Appendix A.

3.3.2 THE ENCODER

As explained in Section 3.2.2, it was not possible to use passive optical encoding due to power limitations. Passive electrical encoding was thus adopted. Again, as explained in Section 3.3.1, the main concern is to maintain the pulse shape throughout all the processing steps. GaAs MESFET's were thus used for this stage as well. Figure 3.7 shows the encoder circuit for the transmitter 1 address of: 0000111100000000.

The positive going modulated pulse (of amplitude 3V) generated at the modulator circuit is applied at the gate of MESFET Q2. A negative d.c. bias of -3V is also applied at the gate of Q2 so that Q2 is normally 'OFF' (i.e., enhancement mode). A constant d.c voltage of 15 V is applied at the drain of Q2 via the 200 Ω resistor and the decoupling circuitry. Q2 is also operated as a switch. Its operation is similar to that of the modulator. The negative going pulse at the output of Q2 is then split with a 1x4 power splitter. Since Q2 switches between 'ON' and 'OFF', the resistance it offers to proceeding stages will vary between low and high resistance. It is thus difficult to match any circuitry to the output of the MESFET over a wide frequency range, as the case would be with pulses. The best that can be achieved is a compromise that will provide a reasonable match for both 'ON' and 'OFF' states rather than a good match for

one state and no match at all for the other. The encoder circuit was thus simulated with SPICE and the resistance values R1, R2, R3 and R4 (see Figure 3.7) were optimised for minimum reflections due to mismatch.

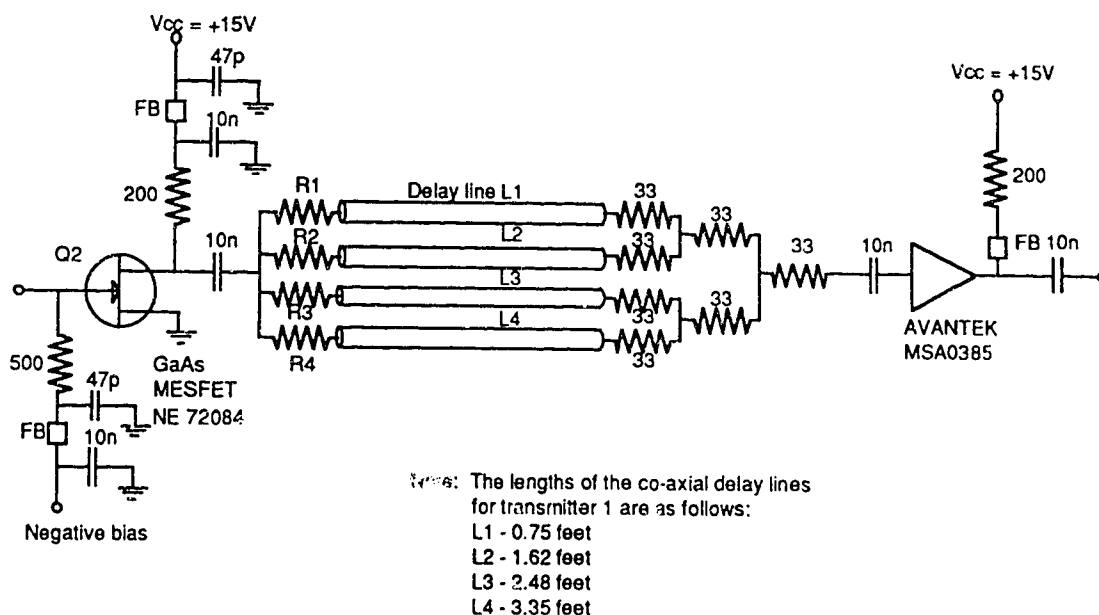


**Figure 3.7 Configuration of the encoder circuit for Transmitter 1
 Address : 0000111100000000**

The split pulses are delayed using co-axial delay lines (delay = 4.826 ns/m) [28] according to the transmitter code and then combined using a 4x1 power combiner matched to 50 Ω .

The output of the 4x1 power combiner is then applied to an AvanteK MSA0385 gain block with a gain of 12 dB and 3 dB bandwidth of 2 GHz (the data sheet is given in [51]). The gain block was added to compensate for the splitting and combining losses of 12 dB. The losses in the co-axial cables were found to be

negligible for the lengths considered. It must be noted that the Avantek gain block provides signal inversion at the output.

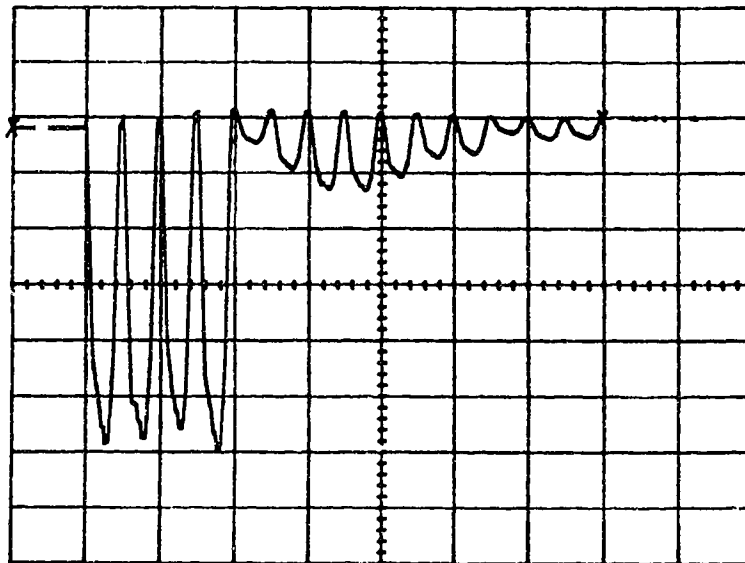


**Figure 3.8 SPICE simulation of the Encoder circuit. The data bit '1' is encoded with the address of transmitter1:
0000111100000000
x scale: 2ns/ division y scale: arbitrary units**

Figure 3.8 shows the encoded output obtained with a SPICE simulation of the encoder circuit for transmitter 1. The waveform shown is obtained at the input to the gain block. It is clearly evident from Figure 3.8 that even with the optimisation of the resistor values for the 1x4 power splitter, there is some reflection due to mismatch. The magnitude of the reflections are small as compared to the amplitude of the encoded pulse stream and can thus be clipped by adjusting the bias on the preceding stages. The simulation and optimisation operations were also performed for transmitter 2.

The SPICE simulation programs for the encoder circuit are given in Appendix A.

3.3.3 THE LASER DRIVER CIRCUIT

Referring to Appendix C, which contains the pin configuration of the Mitsubishi ML6411C laser diode, the construction of the package is such that pin 3 is connected internally to the casing. Thus, if this package is to be used in any other configuration other than with pin 3 grounded, the inductance and capacitance of the package would contribute significantly to a degradation in the frequency response of the laser. Therefore, in order to obtain as fast a response as possible from this laser package, pin 3 would have to be grounded. This limits the number of possible implementations of the laser driver. A separate circuit is not used to bias the laser. Therefore, the photodiode in the laser package (corresponding to pin 2) is not used. Since the laser needs to be switched 'ON' and 'OFF' very quickly, GaAs MESFET's were also used in this circuit design. Referring to the data sheets for the Mitsubishi ML6411C (Appendix C), the laser diode has a threshold current, I_{Th} , of around 40 mA and an operating current, I_{op} , of 80 mA in pulsed mode to produce 10 mW of peak pulsed optical power. Thus, in order to handle the higher current requirements, a NE 900075 GaAs MESFET with drain to source saturation current (I_{DSS}) of 120 mA [26] was chosen.

The laser drive circuit is shown in Figure 3.9. The operation of the circuit is as follows: A constant dc bias supply of 10 V is applied at the supply to the laser. The encoded pulse stream at the output of the encoder has the wrong polarity for the laser driver configuration. An additional MESFET, Q3, was thus added to provide the necessary inversion. It can be seen from the characteristic curves of the ML6411C (Appendix C) that the threshold current, I_{Th} , is 40 mA.

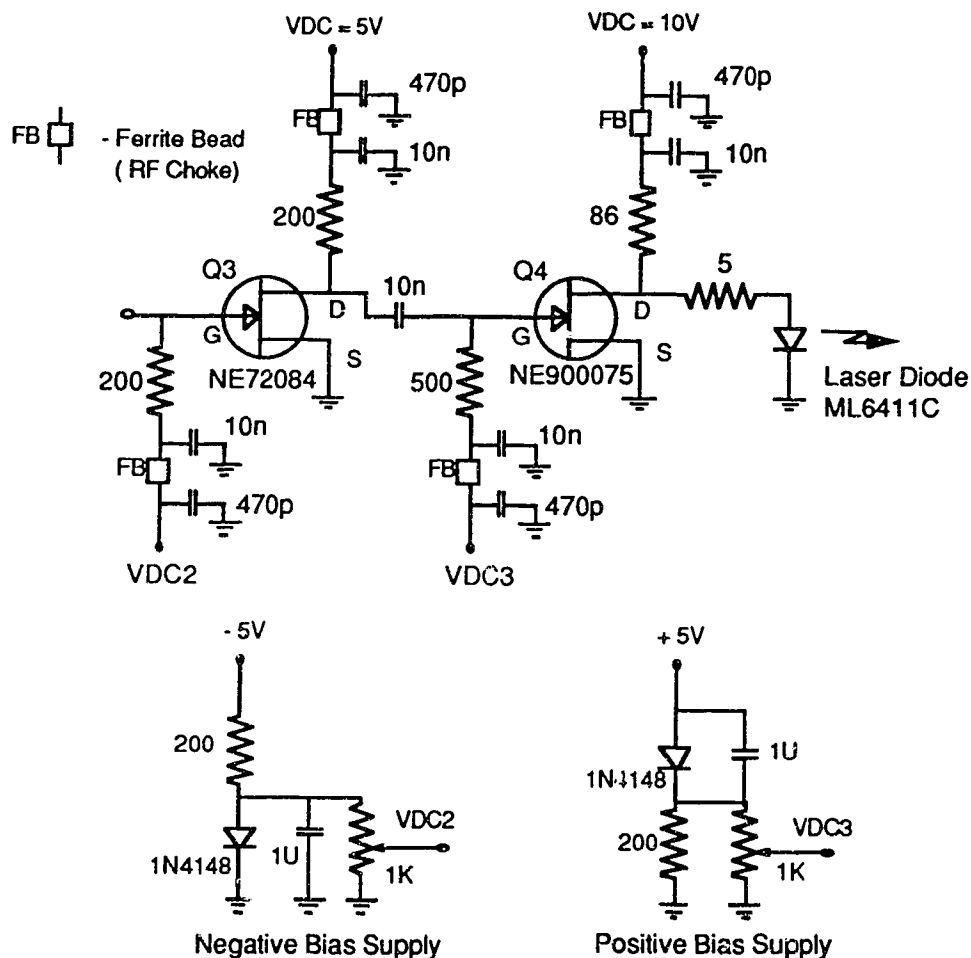


Figure 3.9 Laser driver circuit showing the positive and negative biasing supplies

The laser is biased below the threshold current level, say at 32 mA so that no light is transmitted for a data bit '0'. The NE900075 has a drain to source saturation current (I_{DSS}) of 120 mA. Therefore, with a 0V bias on the gate of the MESFET, Q4, I_{DSS} would be drawn by the device. Referring to the data sheets for the laser diode, from the forward voltage vs drive current ($V - I$) curve, the forward voltage drop for a current of 32 mA is 1.5 V. The voltage drop across the 5 Ω resistor is 0.16 V. Therefore, the voltage at the drain of Q4 (V_{DS}) is 1.66 V. The 5 Ω resistor is used for differential current measurements. A positive bias of

0.3 V is applied at the gate of Q4 to clip the reflections (see Figure 3.8) due to the mismatch at Q2 in the encoding circuit.

The NE 900075 has a pinch off voltage of -4.5 V. The amplitude of the encoded pulse stream is thus adjusted, via the bias voltage on the gate of Q3 to about -2 V (the exact value would vary from device to device) so that Q4 is only partially pinched off, i.e., the current drawn by Q4, I_{DS} , will be less than I_{DSS} . This will allow a peak pulse current of 53 mA to be diverted to the laser diode, giving the laser a peak pulse current of (32 mA + 53 mA =) 85 mA to provide the required peak pulsed optical power of 10 mW at the fibre. It must be noted that the power vs current (P vs I) curves given in the data sheets refer to the optical power generated at the facets. A 40% coupling efficiency is assumed for the coupling of light from the facets to the 50/125 μm multimode fibre.

Figure 3.10 shows the results of the SPICE simulation of the laser driver circuit in Figure 3.9. The simulation assumes that the laser is biased at threshold and thus the laser is represented by a series inductor and resistor with values 3 nH and 3 Ω respectively (the values are suggested by the manufacturer). It is seen from the simulation results that the current pulse drawn by the laser is still within the acceptable pulse width of 1.25 ns. In order to obtain an accurate estimate of the circuit performance, all possible parasitic components likely to affect the circuit performance were added to the circuit simulation. The exact circuit and SPICE program are given in Appendix A.

It is seen from the results of the simulation that a negative dip exists in the falling edge of the current pulse. This is due to the discharge from the various parasitic capacitances in the laser drive current path. Pulsing tests carried out on the laser indicate that the negative going dip on the falling edge of the pulse helps

discharge the excess carriers in the laser and this in turn improves the fall time of the generated optical pulses quite considerably. Narrower optical pulses are thus obtained.

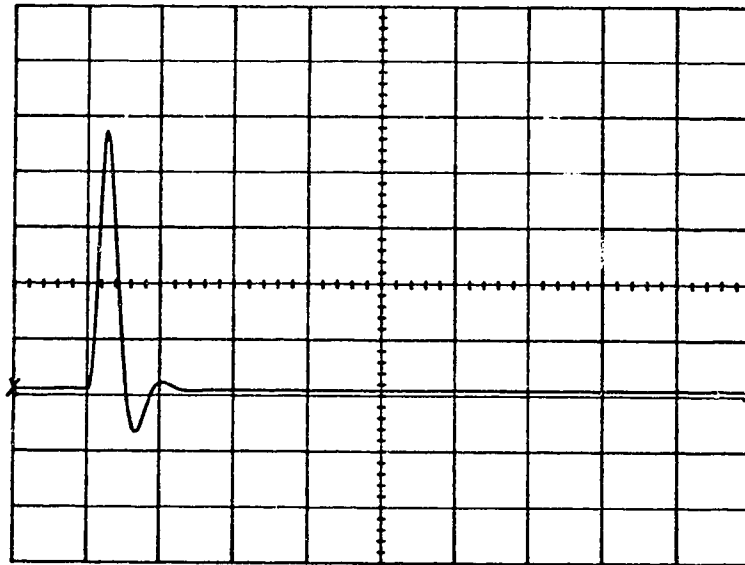


**Figure 3.10 SPICE simulation of the laser driver circuit. The figure shows the current drawn by the laser when pulsed with a 500 ps wide electrical pulse
x scale: 2ns/ division y scale: arbitrary units**

The original design for the laser driver contained a separate dc feedback circuit to provide the dc bias current and compensation for temperature variations in the laser. Simulations showed that the parasitics due to the additional circuitry were quite significant and as a result slowed the pulse response of the laser quite considerably. The laser driver circuit discussed above was thus adopted even though it provides little or no protection for the laser against temperature and drive current variations.

3.4 RECEIVER DESIGN CONSTRAINTS

3.4.1 PHOTODETECTOR REQUIREMENTS

The high speed nature of FO-CDMA systems require that the detectors used in the complementary correlator detector have very fast response times. The second requirement is that the devices chosen should have fairly flat frequency response characteristics over at least a 1 GHz bandwidth (the exact bandwidth requirement is discussed in Section 3.5) to prevent distortion of the detected optical pulses and the subsequent corruption of the correlation process. A further requirement is that the device chosen should be symmetrical with a zero-bias off state so that it would be 'OFF' for a bias voltage of 0V and 'ON' for a positive or negative bias voltage. This feature is desirable in order to achieve the subtraction of signals required for the complementary correlation but is not essential since photodiodes, for example, can be configured to produce the same effect. If photodiodes are used, they would have to be configured for a specific code and thus one would not be able to switch easily between different transmitters.

The arrays of Metal-Semiconductor-Metal photodiodes and Surface depleted photoconductors were designed originally for optoelectronic switching applications [20][40]. In the system described here device isolation is not a significant concern since all the devices in the array will be on at all times i.e., there is no switching action involved.

In addition to the requirements of bandwidth, fabrication process complexity imposes some constraints on the detector. As would be expected these

requirements are similar to those of lasers since detectors are in fact counterparts of the optical sources. These requirements include [29]:

1. Large responsivity at operating wavelengths
2. High fidelity, i.e., the detectors should be linear with respect to the optical power.
3. Low noise
4. Reliability and stability of performance characteristics, i.e., the characteristics of the device should be independent of ambient conditions
5. Ease of integration with other electronic circuitry, i.e., the compatibility of fabrication processes with those of other electronic circuitry
6. Small size to allow good coupling efficiency for light and ease of packaging
7. Low operating voltage and power consumption
8. Low cost

Very few photodetectors exist that can satisfy these requirements: GaAs surface depleted photoconductors [22], epitaxial photoconductors [30] and Metal-Semiconductor-Metal (MSM) photodiodes [18] are possible choices.

3.4.2 CHOICE OF PHOTODETECTORS

Epitaxial photoconductors [30][31] have fairly high sensitivity in the 320nm and 1300nm wavelength region due to the presence of internal gain. However, the major disadvantage with this type of photoconductor is the low dark resistance which is in the order of hundreds of ohms. The high dark current in the 'ON' state generates a DC signal pedestal that could be a few orders of magnitude greater than the AC signal. Also, these devices have fairly large bias current requirements which could be of the order of tens of milliamperes at the

operating bias voltage of 10V. This large bias current could be a significant contributor to increased detector noise [22].

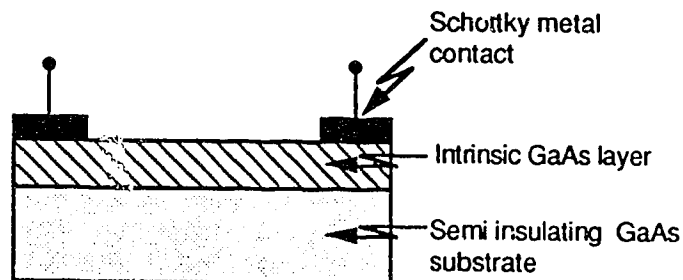


Figure 3.11 Structure of the Metal-Semiconductor-Metal photodiode

The MSM photodiode [18] consists of two Schottky barrier diodes integrated back to back (see Figure 3.11) and is formed by the deposition of an interdigitated gold-platinum-titanium (AuPtTi) or other metal anode and cathode onto the surface of a semi-insulating GaAs substrate. A Schottky contact is usually obtained by using a metal or alloy with a work function larger than that of the semiconductor. The devices are made in an interdigitated configuration so as to preserve short channel lengths for speed.

Due to its planar structure, the MSM photodiode is intrinsically compatible with the gate fabrication process of Metal-Semiconductor Field Effect Transistors (MESFET). The integration of both these types of devices is easily accomplished without the introduction of additional process stages.

The bandwidth of the MSM photodiode is limited, theoretically, by the transit time of the carriers or the RC time constant of the detector, whichever quantity is the slowest. A 10GHz GaAs MSM photodiode, limited by its transit time, has been reported [32]. A number of such devices with a 5 μm finger spacing (i.e., the spacing between the interdigitated fingers) were fabricated for the ATRC by the Communications Research Centre (CRC)[33]. The frequency response

curves for these MSM's for varying optical power (500 μW to 100 μW) is shown in Figure 3.12. The responsivity was calculated to be 0.07 A/W.

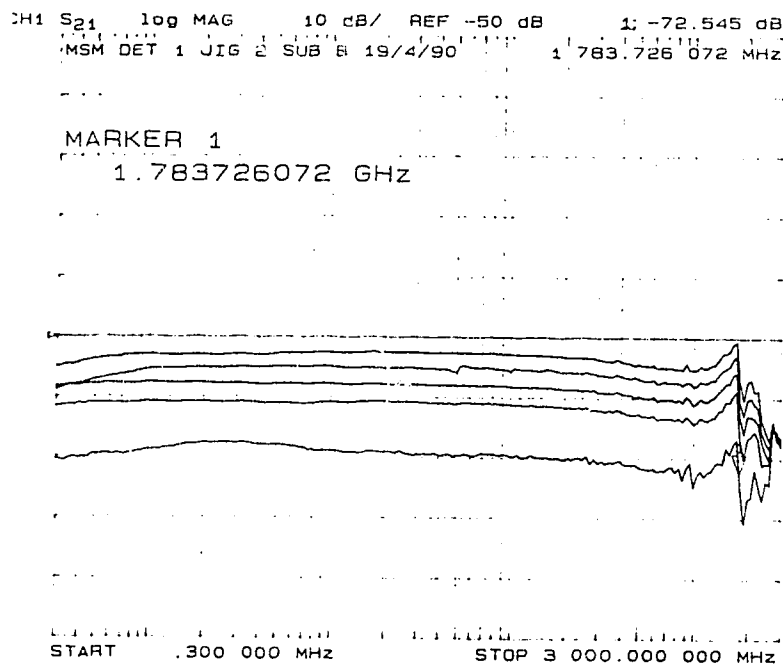


Figure 3.12 Frequency response characteristics of the MSM photodetector for varying levels of optical power (500, 400, 300, 200 and 100 μW)

The other alternative is the Surface depleted photoconductor which has been used extensively in optoelectronic switching matrices [33][34]. Surface depleted GaAs photoconductors, the structure of which is shown in Figure 3.13, are similar to MSM photodiodes except that the Schottky contacts are replaced by ohmic contacts. These devices can also be made in an interdigitated configuration so as to preserve short channel lengths for speed and gain. This technique allows for relatively large active areas for ease of coupling optical power from the fibre to the device and also retain a low capacitance value (the capacitance of the interdigitated structure has been calculated to be around 0.5pF for a digit spacing of 5 μm) [35]. The photoconductor channel is also

made thin (1 - 2 μm) so that the carriers are depleted. This results in high resistivity and therefore in reduced bias current.

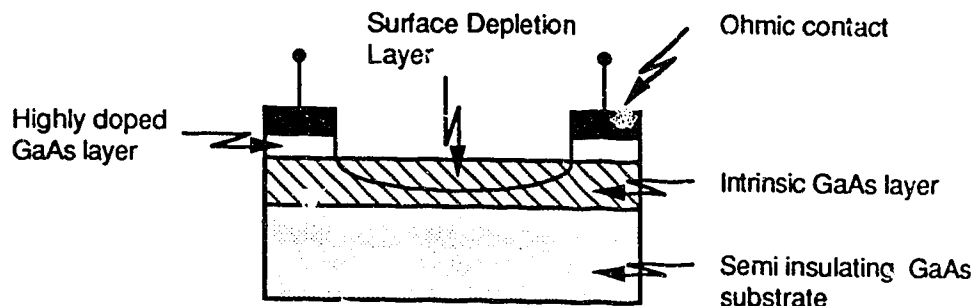


Figure 3.13 Structure of the Surface Depleted Photoconductor

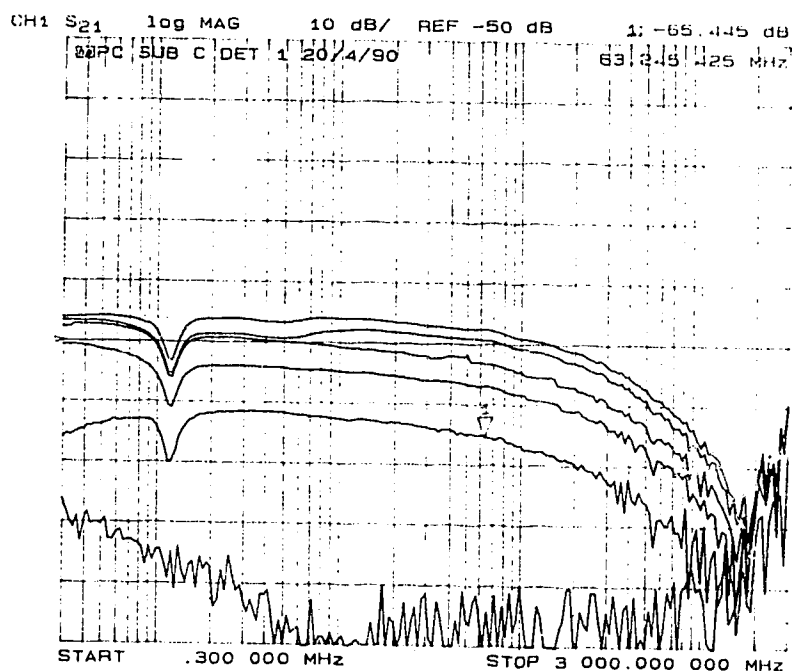


Figure 3.14 Frequency response curves for the Surface depleted photoconductors for varying levels of optical power (500, 400, 300, 200 and 100 μW)

A set of Surface depleted GaAs photoconductors with 5 μm finger spacing were fabricated by the CRC [33]. The frequency response curves for these devices are shown in Figure 3.14 for varying optical power levels (500 μW to 100 μW).

As can be seen from Figure 3.14, the usable bandwidth is around 1.4 GHz at high power levels (i.e., 500 μW) but around 300 MHz at 100 μW , the peak optical power per pulse estimated to be available at the receiver per detector. A responsivity of 0.3 A/W was calculated for these devices at 100 μW .

It must be noted that the curves in Figures 3.12 and 3.14 were obtained with an effective load of 25 Ω (i.e., a 50 Ω load resistor at the output of the detector array and a 50 Ω termination within the network analyser).

The final decision regarding the appropriate choice of photodetector is dependent on the following factors: (1) the minimum bandwidth required by the detector array for the complementary correlation to work correctly (2) the minimum responsivity required from the detector array chosen, given the optical power budget for the system and the signal to noise ratio required to achieve a BER of at least 10^{-7} . This decision was thus made once the complementary correlator requirements were quantified and this is discussed further in Section 3.5.1

3.5 RECEIVER DESIGN

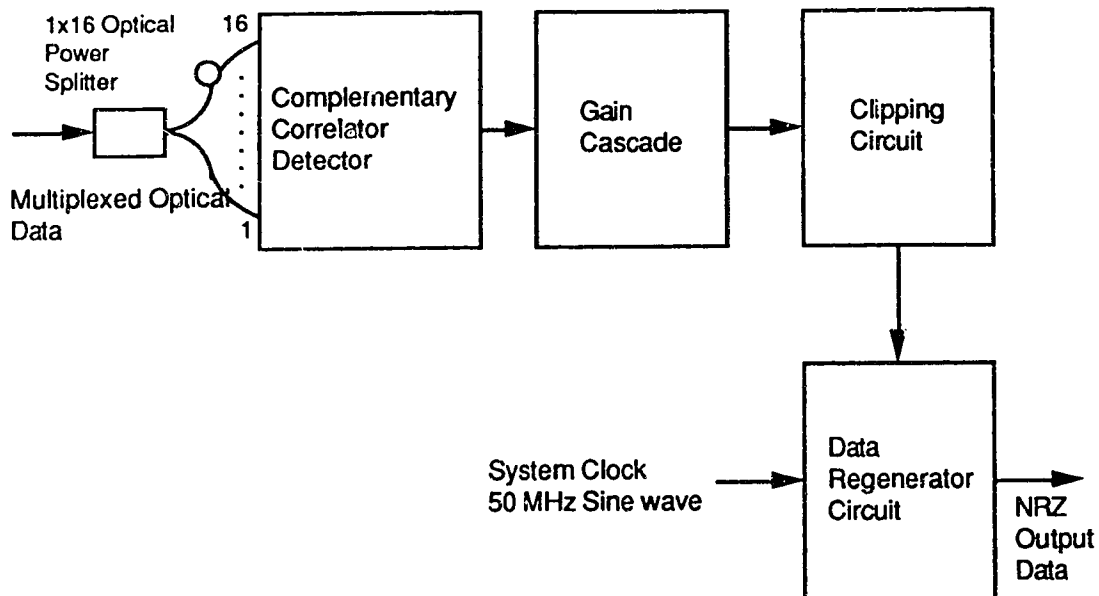


Figure 3.15 Block diagram of the Receiver that can be switched to receive transmissions from either transmitter 1 or 2

Figure 3.15 shows the block diagram of the receiver which can be switched to receive transmissions from either transmitter 1 or 2. The receiver consists of the following stages: a 1x16 optical power splitter and an array of 16 photodetectors for an Alberta code set of length $2N = 16$ and weight $w = 4$, a cascade of gain stages, a rectifier or clipping circuit to extract the auto-correlation peak from the bi-polar signal at the output of the complementary correlator detector (the bi-polar signal consists of the auto-correlation peaks, auto-correlation wings and the cross-correlation waveform) and a regenerator circuit to reconstruct the extracted auto-correlation peak back to the NRZ format. The 50 MHz sine wave clock used at the transmitters is also used at the data regenerator circuit to retime the recovered data and for BER measurements. The phase shift network,

through which the sine wave clock is fed, is used to delay or advance the rising edge of the clock.

3.5.1 THE COMPLEMENTARY CORRELATOR DETECTOR

Figure 3.16 shows the configuration of the 16 detector complementary correlator detector and the 1x16 optical power splitter. A 50 Ω load resistor is used so that standard 50 Ω gain blocks can be used to amplify the bi-polar signal at the output of the complementary correlator detector. It was felt that the thermal noise penalty in using a 50 Ω load would be compensated by the ease of amplification using standard 50 Ω gain blocks.

It can be seen from the explanation of the complementary correlator detector circuit in Chapter 2 that each detector in the detector array requires a certain bandwidth for the complementary correlation to work correctly. To determine this bandwidth and thus to make a decision regarding the choice of photodetector, the Surface depleted photoconductor and MSM photodetector were modeled using SPICE and the 16 detector complementary correlator was also modeled in turn.

Figure 3.17(a) shows the SPICE model of a MSM photodetector/Surface depleted photoconductor obtained from [36]. As explained in Section 3.4, the physical structure of the two devices is the same. The values of the parasitic components in the SPICE simulation model can then be modified to represent the effects of the device characteristics in each case.

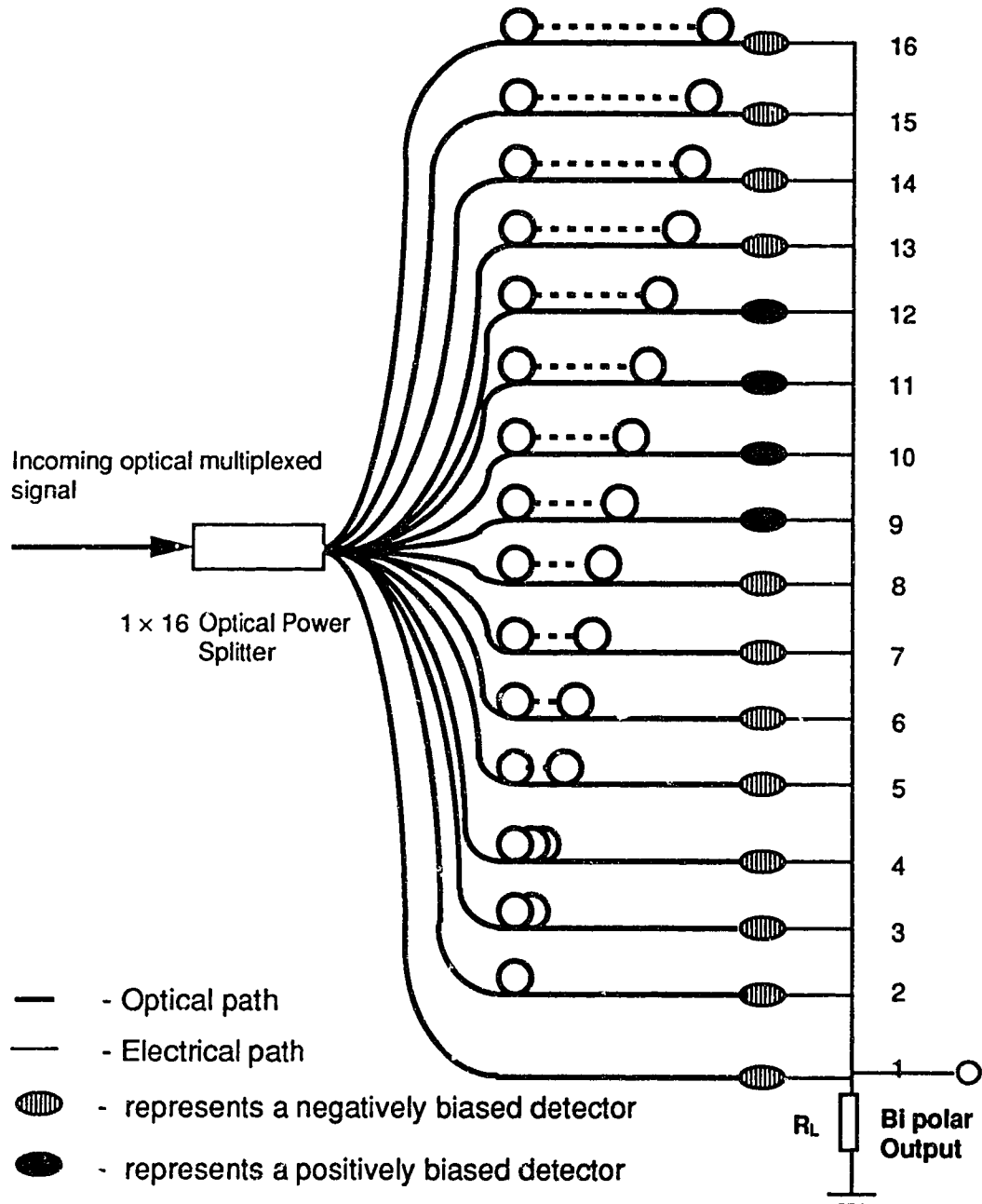
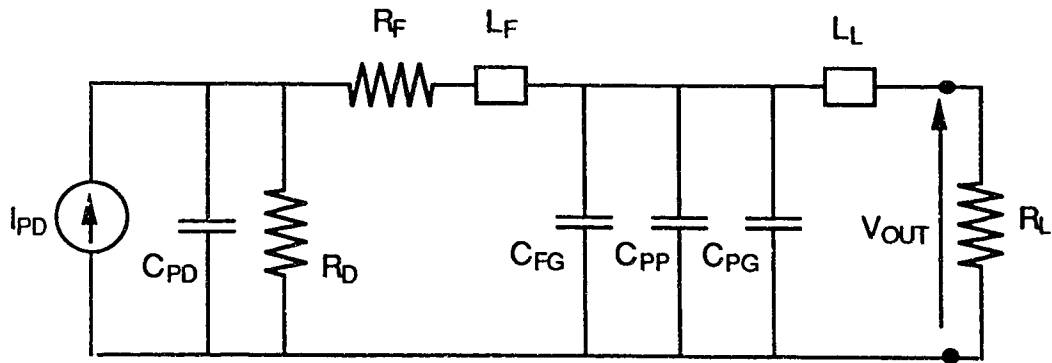


Figure 3.16 Schematic diagram of the complementary correlator detector for an Alberta code set of length $2N = 16$ and weight $w = 4$



The parasitic components are as follows:

- | | |
|---|---|
| C_{PD} - Capacitance between fingers | C_{FG} - Capacitance between fingers and ground |
| R_D - Leakage resistance | C_{PP} - Capacitance between bond pads |
| R_F - Resistive component of finger impedance | C_{PG} - Capacitance between bond pads and ground |
| L_F - Inductive component of finger impedance | L_L - Inductance of bond wire |
| | R_L - Load resistor |

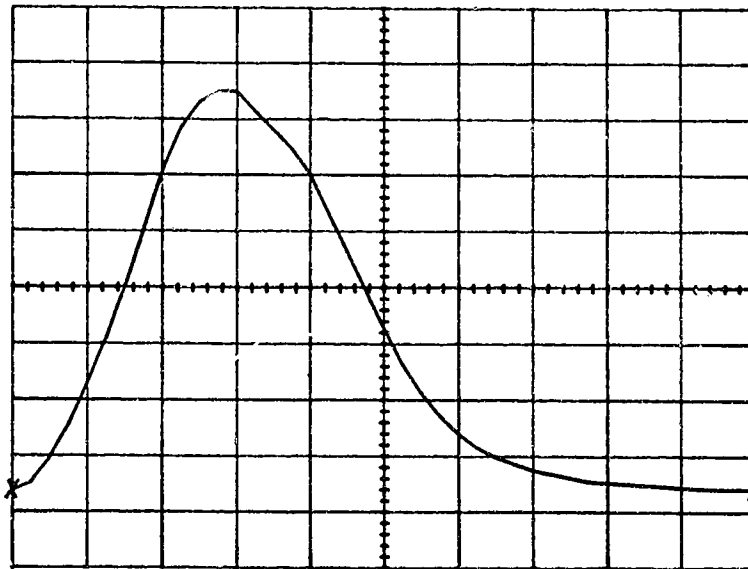


Figure 3.17 (a) SPICE model of the MSM photodiode/ surface depleted photoconductor [36]

(b) Simulated pulse response of the surface depleted photoconductor

x scale: 300 ps/division y scale: arbitrary units

The Surface depleted photoconductors have a responsivity of 0.3 A/W while the MSM photodetectors have a responsivity of 0.07 A/W. Thus from a responsivity point of view, the surface depleted photoconductors would be a better choice of device since they would allow for a better signal to noise ratio at the receiver (based on the power available at the receiver, per pulse). Also, less signal amplification would be required before further signal processing can be carried out.

As a first step in modelling process, the pulse response of a surface depleted photoconductor was measured using an optical pulse of known width. The values of the parasitic components in the model were then adjusted such that the pulse response of the SPICE simulation corresponded with that of the measured pulse response. Sixteen such photodetector models were then connected to a common load as shown in Figure 3.16 and the delayed pulse stream reaching each detector was simulated in SPICE (the delayed pulse stream reaching the 16 detector array has the form shown in Figure 2.4). It was found that the correlation did not work due to the fact that the long tail on the falling edge of the electrical pulse at the output of the detector (seen quite clearly in Figure 3.17(b)) interfered with the following chip and so on. As a result, when a large number of pulses added up, there was a cumulative effect of charge storage which meant that the signal did not return to the zero level between chips. Thus, the addition/subtraction operations that should have been confined to a chip width of 1.25ns were not and the whole correlation was corrupted. This implied that a minimum band width was essential for the complementary correlation detection to work correctly. In order to determine this bandwidth a series resistor-inductor (RL) equaliser circuit was added as a shunt circuit across the biasing input of each of the 16 detectors in the detector array.

A series of simulations were then run for varying values of R and L. It was found that a minimum 3 dB bandwidth of 1.26 GHz was required for the complementary correlator to work correctly. Figure 3.18 shown the simulated output from the complementary correlator detector for the system shown in Figure 3.1 with the receiver switched to transmitter 1. The data sequence input to transmitter 1 is 010.

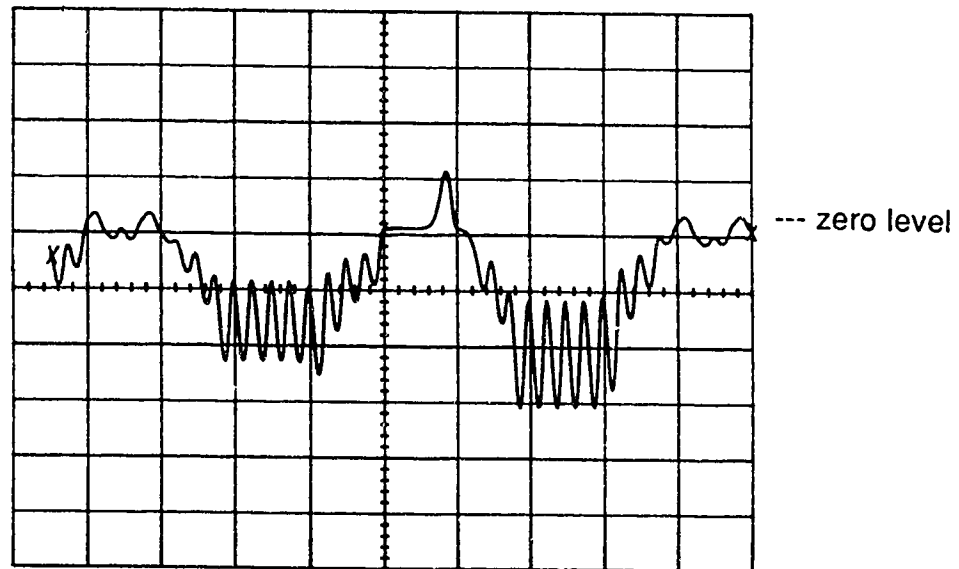


Figure 3.18 Simulated output from the complementary correlator detector circuit for an input data stream of 010. The auto-correlation peaks correspond to 010 as expected.

x scale: 5 ns/division y scale: arbitrary units

As expected, the result of the complementary correlation process is a bi-polar signal with a positive auto-correlation peak and the positive part of the bi-polar signal is in fact 010, which is the required data sequence. The SPICE simulation program for the complementary correlator detector is given in Appendix B.

Referring to the frequency response curves for the Surface depleted photoconductors (Figure 3.14), it can be seen that it would be difficult to equalise these devices to the required bandwidth of 1.3 GHz because the roll off of the frequency response is not 10 dB per decade and therefore simple RC equaliser circuits cannot be used. Also, even if equalisation could be carried out, the equalised response would be so low (of the order of 0.005 A/W) that a significant amount of optical power ($\gg 100 \mu\text{W}$ peak per pulse) would be required in order to obtain a signal to noise ratio sufficient to achieve a BER of 10^{-7} .

Referring to Figure 3.12, the MSM photodiodes have a bandwidth per device of 1.8 GHz and an overall bandwidth (considering all 16 detectors in parallel) of 1.3 GHz.

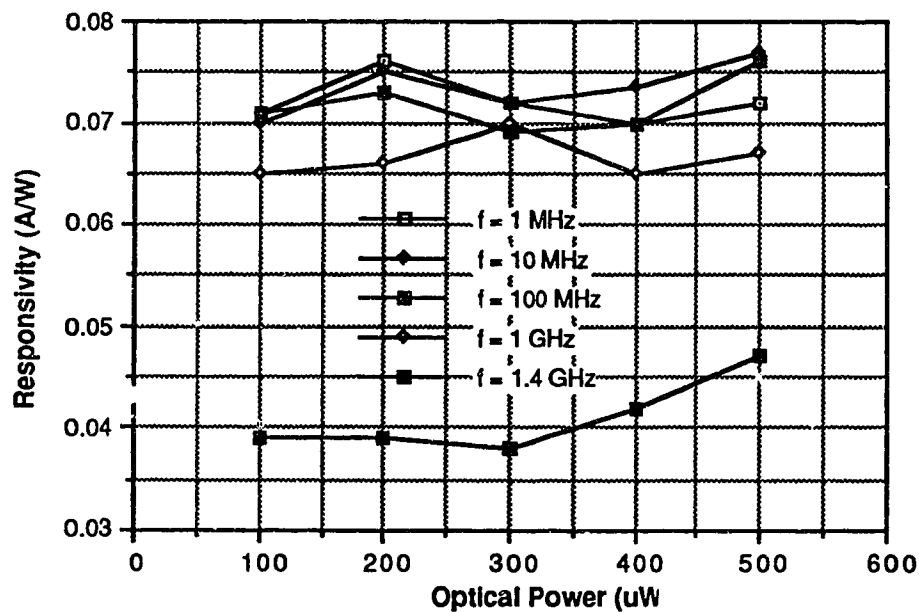


Figure 3.19 Responsivity vs optical power curves for the MSM photodetector for different frequency ranges

Figure 3.19 shows the responsivity of the MSM photodiodes vs optical power curves for varying frequencies. It is apparent that the responsivity is independent of the incident optical power. Also, within the limits of experimental error, the responsivity may be assumed to be the same for the frequency ranges considered (the curve for $f = 1.4$ GHz must be ignored since it refers to a frequency beyond the 3 dB roll off of the devices in question). Therefore, there will be no distortion of the electrical pulse at the output of the detector due to the boosting of some frequency components and suppression of others. MSM photodiodes were thus chosen for the complementary correlator.

3.5.2 THE CLIPPING CIRCUIT

With reference to the simulated output from the complementary correlator detector (Figure 3.18), it can be seen that the positive auto-correlation peaks can be extracted from the bi-polar signal by clipping the unwanted negative part of the signal which may be considered to be 'noise'. The clipping can be performed by a high speed switching or schottky diode [37]. A bi-polar transistor or FET can be configured to produce the same clipping effect (i.e., the so called clipping effect is in fact an expansion or amplification of the wanted part of the signal and the compression of the unwanted part). The objective of this circuit was twofold, the first being to clip the unwanted part of the output from the complementary correlator detector and the other to provide some gain to the clipped signal so that further signal processing could be carried out without the need for additional gain stages.

In order to determine the device (diode, bi-polar transistor or field effect transistor) best suited to perform the clipping function, the devices mentioned above were modeled in SPICE. The simulations confirmed that the bi-polar

transistor was best suited to the task due to its high forward current transfer ratio (h_{FE}) which allows the auto-correlation peak to be amplified. Due to the pulse nature of the signal (and hence its wide bandwidth requirement) a device with a high gain.bandwidth ratio (f_T) was chosen. The device chosen was an Avantek AT42085 which in addition to having a high gain.bandwidth ratio, also has a low noise figure (1.9 dB typically at 2.0 GHz). The data sheets for the Avantek AT42085 are given in [51].

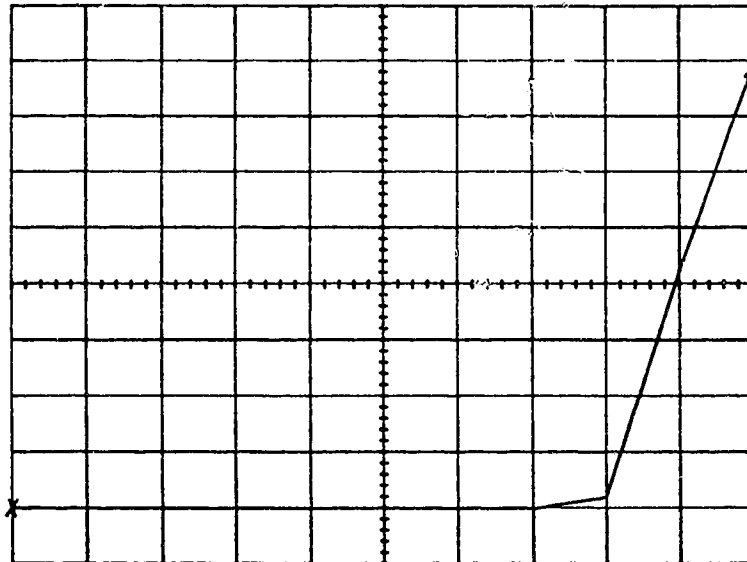


Figure 3.20 Simulated Base voltage vs Collector current characteristics of the Avantek AT42085 bi-polar transistor
x scale: 0.1 V/division y scale: 10 mA/division

Figure 3.20 shows the simulated base voltage (V_B) versus collector current (I_C) characteristics of the Avantek AT42085. Referring to Figure 3.20 and Figure 3.18, it can be seen that if the 'zero' level of the complementary correlator output is set at 0.8 V, then the auto-correlation peak will be passed through and amplified while all the signal content below the 0.8V level (i.e., the noise) will be clipped or compressed.

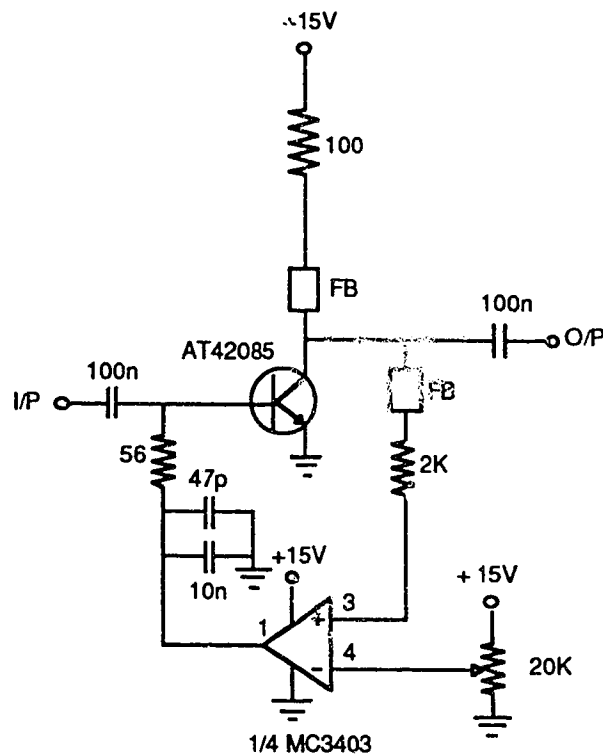


Figure 3.21 Clipping circuit used to recover the auto-correlation peak from the bi-polar signal at the output of the complementary correlator detector array

Figure 3.21 shows the circuit that performs the clipping operation. The operation of the circuit is as follows: Referring to Figure 2.6, it can be seen that the negative content of the bi-polar signal at the output of the complementary correlator detector depends on the number of users present and on the history of the data stream of each user. The only part of the bi-polar signal that always has the same amplitude is the auto-correlation peak, which has a fixed magnitude of w for a given code set of weight w . The 20K variable resistor in the circuit (Figure 3.21) is used to adjust the bias voltage applied to the inverting input of the op-amp (1/4 MC3403) such that the base of the transistor is clamped to the autocorrelation peak and the 'zero' level of the bi-polar signal (see Figure 3.18) is at the 0.8 V knee of the V_B vs I_C curve shown in Figure 3.20.

The auto-correlation peak is thus amplified by the h_{FE} of the transistor while the negative content is compressed by slope of the curve in the 0 V to 0.8 V region of the curve (see Figure 3.20).

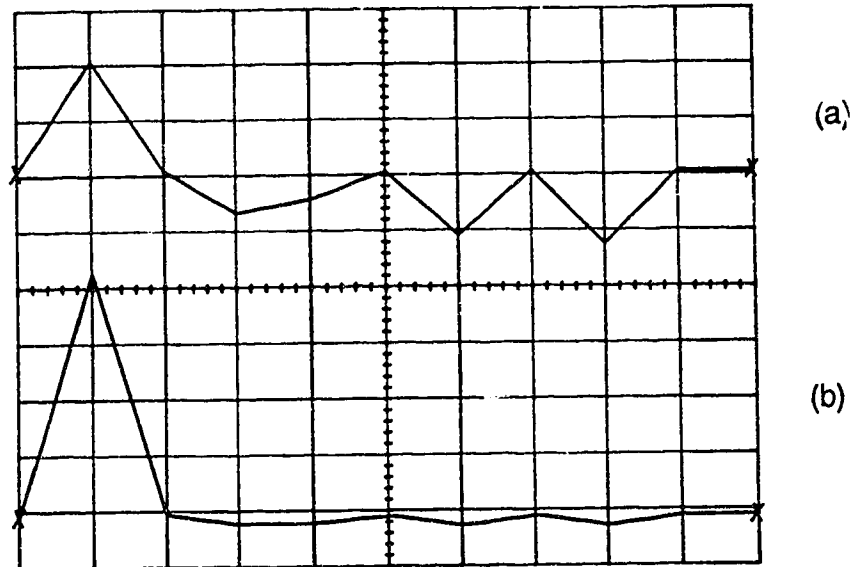


Figure 3.22 Simulation results for the clipping circuit showing
(a) the voltage waveform input to the circuit
(b) the current waveform at the output
x scale: 500 ps/division y scale: arbitrary units

Figure 3.22 shows the simulation results for the circuit obtained with SPICE. Figure 3.22(a) shows the waveform input to the circuit (it represents part of the waveform shown in Figure 3.18) and Figure 3.22(b) shows the current waveform at the output of the clipping circuit. It must be noted that there will be an inversion of the waveform at the output of the circuit (as would be expected from the common-emitter configuration of the bi-polar transistor). It is seen clearly from Figure 3.22(a) and (b) that the clipping operation takes place. Also, the auto correlation peak is amplified as expected. The gain provided by the bi-polar transistor is of the order of 18.0 dB. The load resistance of the following

stage was then adjusted such that the amplitude of the auto-correlation peak was ECL (Emitter Coupled Logic) compatible.

The degree of dc wander is dependent on the low end frequency response available from the circuit and also on the number of zero's that can occur consecutively. Since the system was designed for a pseudo random bit sequence (PRBS) of length $2^9 - 1$, the worst case data pattern that can occur is eight zero's followed by a one. The values of the de-coupling capacitors were thus chosen such that the discharge time of the capacitors were much longer than the time corresponding to eight consecutive zero's in the data stream.

3.5.3 THE GAIN CIRCUITS

As a result of the simulations carried out for the clipping circuit, it was found that a minimum value of 0.12 Volts was required for the amplitude of the auto-correlation peak for the clipping action to take place. Now, with $100 \mu W$ of peak pulsed optical power incident on a detector for a chip '1', the auto-correlation peak will have a magnitude of 0.35 mV at the 50Ω load (at the output of the complementary correlator detector). The gain required is therefore of the order of 37.0 dB. Since one gain block cannot provide the necessary gain, a cascade of gain stages was used. Figure 3.23 shows the configuration of the gain circuit which consists of an Avantek INA-03170 and an Avantek MSA-0885 with feedback, both of which are standard 50Ω gain blocks. The INA-03170 is used as the pre-amplifier due to its low noise figure of 2.5 dB (typical). The predominant source of noise in the receiver is thus the thermal noise due to the 50Ω load resistor R_L in the complementary correlator detector array (see Figure 3.16).

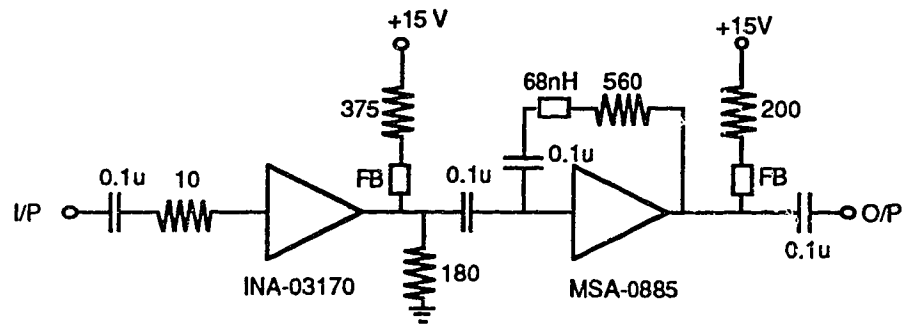


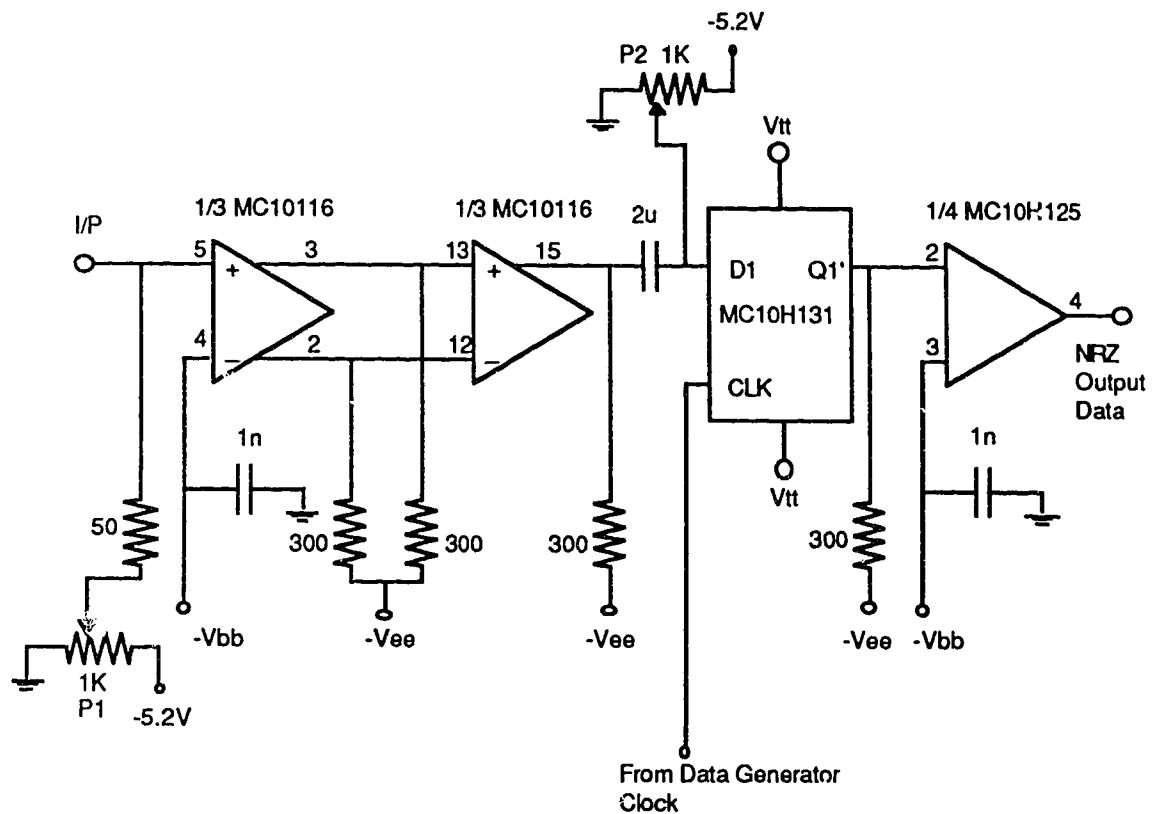
Figure 3.23 Configuration of the gain circuit cascade

Although the INA-03170 is by itself unconditionally stable, it was found to be only conditionally stable when used in conjunction with the 16 detector array. This is due to the fact that the impedance seen by the gain block is not exactly 50 Ω . There is also a significant capacitive component. This result was observed during simulations carried out with C/NL, a frequency domain analysis package. A small series resistance of 10 Ω at the input and a shunt resistance of 180 Ω at the output were added to make the 16 photodetector array-gain block combination unconditionally stable. As a result of the stabilisation, the gain obtained during simulation was around 20 dB with a bandwidth of 1.6 GHz.

An Avantek MSA-0885 was used as the second gain stage. Referring to the power gain vs frequency curve given in the data sheets for the MSA-0885 (given in [51]), it can be seen that a feedback circuit can be used to extend the bandwidth of the amplifier to 2.0 GHz. This is achieved by lowering the low frequency gain. As shown in Figure 3.23, the feedback circuit consists of a resistor-inductor (RL) combination. The 0.1 μF capacitor is used in the feedback path to prevent the dc signal affecting the bias point of the gain block. In order to determine the optimum values for the resistor and inductor, a C/NL simulation was performed on the above circuit. The results of the simulation indicated that

a gain of 18 dB could be achieved with a 3 dB bandwidth of 1.8 GHz using the values of R and L shown in Figure 3.23 for the feedback circuit. A total gain of 38 dB was thus achieved, the total gain requirement being 37 dB.

3.5.4 THE DATA REGENERATOR CIRCUIT



P1 and P2 are used to set the slicing level for the decision threshold of the D flip-flop

Figure 3.24 Regenerator circuit used to regenerate the NRZ data from the recovered auto-correlation peaks

Figure 3.24 above shows the circuit used to regenerate the NRZ data from the recovered auto-correlation peak which may be considered to be RZ data with a 6.25% duty cycle. The circuit consists of two ECL line receivers (MC10116), a

ECL D Master-Slave Flop-Flop (MC10H131) and an ECL to TTL translator (MC10H125). The data sheets for these devices are given in [39].

ECL logic is used throughout the circuit except at the final stage where an ECL to TTL transfer takes place. This is due to the fact that the amplitude of the signals leaving the clipping circuit are still small, i.e., around 1.0V (between a logic '1' and logic '0'). TTL logic requires that the signal amplitude be at least 1.5V between a logic '1' and logic '0' for a correct decision to be made at all times [38] while ECL logic requires only 0.8V [39]. Thus the requirements for ECL are easily satisfied without the need for additional gain. The HP3780 data generator/BER tester requires TTL compatible signals for BER measurements, hence the need for the ECL to TTL translator.

The operation of the circuit is as follows: As expected, the recovered auto-correlation peak at the output of the clipping circuit is still narrow with a pulse width of around 1.5 ns. For the D flip-flop to make a decision between a logic '1' and '0', ECL logic requires a setup time typically of the order of 0.7 ns. Also, the ECL logic has a maximum operating frequency of 250 MHz with the standard DIP (Dual Inline Package) packaging. Thus rather than filter the signal and then amplify it to achieve compatibility with ECL logic, the low pass filtering effect of the parasitic components in the packaging of the ECL circuitry is used to filter the signal (i.e., effectively a low pass filter with a cut-off frequency of 250 MHz) and then amplify it since the differential amplifier has a gain of around 15 dB. Two such stages are cascaded together to obtain the necessary filtering and signal amplitude. The signal at the output of the line receiver cascade is then applied to the D input of the D Master-Slave flip-flop. The sine wave master clock at 50 MHz is also applied to the D flip-flop via a phase shift network. The phase shift network is used to adjust the phase of the sine wave clock so that

the rising edge of the clock pulse occurs at the peak of the pulse (i.e., at the centre of the 'eye' opening for a PRBS data pattern) and a correct decision is made by the D flip-flop. Due to the master-slave action of the D flip-flop, the data is regenerated back into the NRZ format. The output of the D flip-flop is then applied to the ECL to TTL translator which as the name suggests translates the ECL logic levels to TTL logic compatible ones. Referring to Figure 3.24, the variable resistors P1 and P2 are used to set the slicing level for the decision threshold of the D flip-flop.

3.6 SYSTEM CONSTRUCTION

3.6.1 THE TRANSMITTER

The layout of the printed circuit boards of the two transmitters is given in page of Appendix D. Each transmitter is divided into two stages; one containing the modulator and part of the encoder, the other, the remainder of the encoder and the laser drive circuit. Stage one is common to both transmitters. The output of the pulse generator is split two ways within stage 1 and fed directly to the gates of the MESFET's that make up the modulator circuits. Therefore in order to avoid reflections due to mismatch at the split, the lengths of the tracks from the pulse input port to the gate of the MESFET in the modulator circuit were made as short as possible. Also, since the pulses travel the same distance in order to reach the modulators, the possibility of synchronisation problems are eliminated. Due to the high speeds involved, all critical track lengths were kept to a minimum and RF design rules were followed throughout the board design process.

The two stages of each transmitter are connected together via the co-axial cables (semi-rigid, 0.034 inch outer diameter) that are used as delay elements

in the encoder. The circuitry for transmitters 1 and 2 are physically identical except for the lengths of the co-axial delay lines (i.e., the transmitter codes).

Referring to the printed circuit board layout of stage 2 of the transmitter (Appendix D), four 'U' shaped 50 Ω copper tracks are present, one per delay path. These copper tracks are used as variable delay lines and provide an additional delay of between 0 and 400 ps. They are used as fine delay adjustments to compensate for any errors incurred in cutting the co-axial cables to their correct lengths.



Figure 3.25 Photograph of transmitters 1 and 2 showing the two stages of each transmitter, the co-axial delay lines and the laser diodes mounted on the casing of stage 2 of each transmitter

Figure 3.25 shows a photograph of transmitters 1 and 2. The coiled co-axial cable delay lines connecting stages 1 and 2 of each transmitter are clearly

evident. The mounted pig tailed lasers can be seen on the far right hand side of the photograph. The laser diodes were bolted onto the metal case of stage 2 of each transmitter which was in turn bolted to the optical table. Additional cooling circuitry was thus found to be unnecessary.

3.6.2 THE RECEIVER

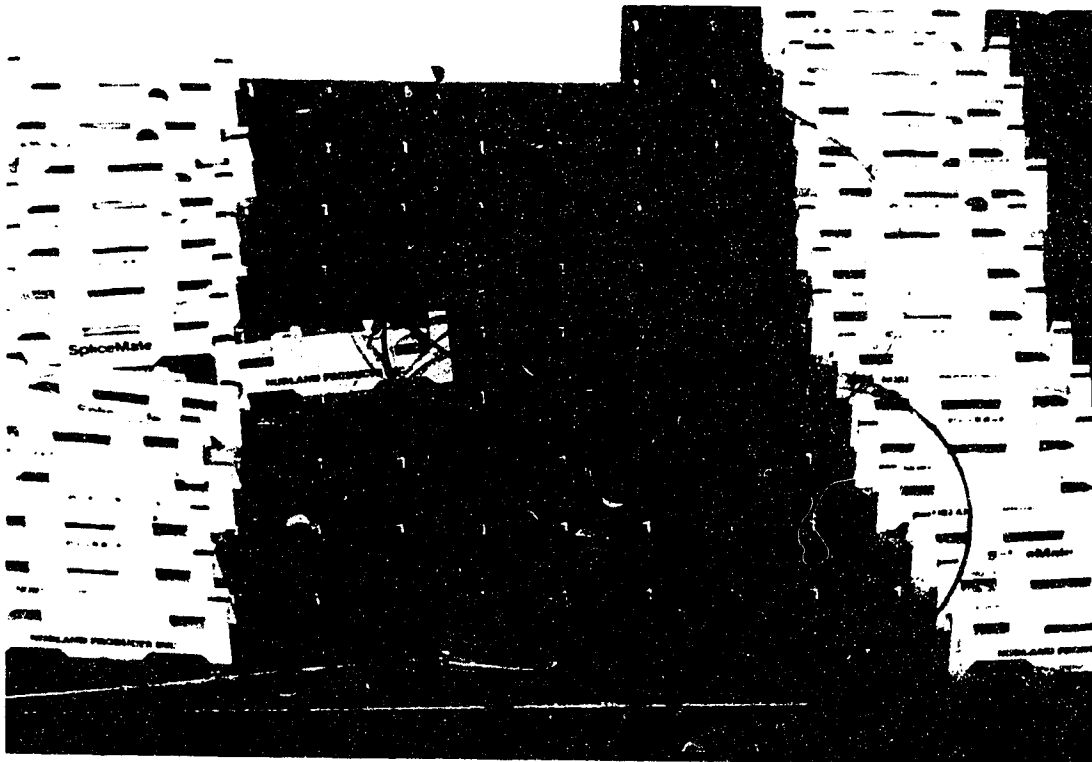


Figure 3.26 Photograph showing the optical delay lines

As explained in Chapter 2.0, the encoded and multiplexed data arriving at the receiver are split 16 ways using a passive optical power splitter and delayed optically with lengths of 50/125 micrometre diameter fibre. The delays are such that the optical coded data stream following split 2 is delayed by one chip interval with respect to the optical coded data stream following split 1 and the optical encoded data stream following split 16 is delayed by 16 chip widths relative to the optical encoded data stream following split 1 and so on. Figure

3.26 shows a photograph of the optical delay lines, coiled and connected to the rest of the optical system using 'Norland' splices which have splicing losses of the order of 0.3 to 0.4 dB per splice.



Figure 3.27 Part of the monolithically integrated array of 16 MSM photodetectors with 16 independent bias lines and one common output. The gold wire bonds are evident.

Figure 3.27 shows a photograph of part the 16 detector array with a single common output and 16 individual biasing lines fabricated specifically for this project by the CRC. The array is mounted in a 40 pin Monolithic Microwave Integrated Circuit (MMIC) package and bonded to the pins of the package with gold wire. This approach minimises the length of the bond wires which in turn limits the parasitic reactances added to the circuit.

A point of concern with such an approach was the parasitic reactances introduced by the package itself. In order to determine the effect, if any, of the MMIC package on the photodetector array, the frequency response of the package was measured using a 'through' measurement. It was found that the

frequency response of the package was flat to 2.0 GHz. It was thus concluded that the performance of the package was quite sufficient for the frequency range of interest (i.e., dc to 1.2 GHz). One of the advantages of using such a package is the good electrical isolation provided by the MMIC package. This is due to the fact that alternate pins of the package are grounded.

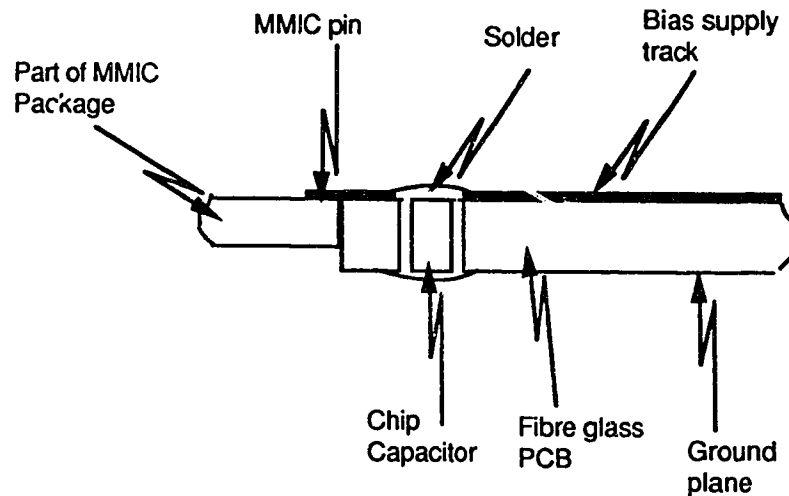


Figure 3.28 Cross section of the complementary correlator detector module showing the position of the de-coupling capacitors and the dc bias lines

In order to minimise the length of the RF path between the devices and the de-coupling capacitors in the biasing circuitry, the de-coupling capacitors were mounted as close to the shortened pins of the MMIC package as possible. This was achieved by drilling holes through the printed circuit boards and placing the surface mount chip capacitors in these holes. The relative positions of the pins, the de-coupling capacitors and the biasing lines are shown in Figure 3.28.

The printed circuit board (PCB) layout of the complementary correlator detector module is given in Appendix D. The MMIC package is placed within the rectangular block shown in the layout. The 16 independent d.c biasing lines and the common 50 Ω output track are clearly seen. The MMIC package

mounted within the complementary correlator detector module is seen quite clearly in Figure 3.29.

In order to align and hold the 16 fibres vertically on the photosensitive surface of each of the 16 detectors, a set of 'V' shaped grooves were etched on a 3mmX4mm silicon wafer. This work was performed by the Alberta Microelectronics Centre (AMC). The dimensions of the 'V' grooves are such that the fibres, when placed in the grooves, are exactly 250 micrometres apart from centre to centre, the exact spacing of the photodetectors in the array. The fibres are held in the 'V' grooves with Ultra Violet (UV) cured epoxy [33].

The 'V' groove, with the fibres in place, was then attached to a specially made clamp attached to a vacuum pump [33]. The vacuum is used to hold the 'V' groove vertically. The entire mechanism was then mounted on a three way micro-positioner for ease of alignment of the 16 fibres with the 16 photodetectors. Figure 3.29 shows the setup of the complementary correlator detector module. The 16 fibres, the 'V' groove and the special clamp used to hold the 'V' groove in place are clearly seen.

The 16 fibres were aligned with the 16 photodetectors as follows: Two separate lasers were modulated at two different frequencies. The modulated optical output of the lasers were injected into the two end fibres. The 'V' groove was then placed above the 16 detector array and the outputs of the two end detectors were monitored with a spectrum analyser [33]. The 'V' groove was then positioned such that the readings of the two reference signals were maximised on the spectrum analyser. Once the coupling of the reference signals were optimised, the 'V' groove was lowered on to the detector array and held in place by the micro-positioner/ vacuum pump setup. The optical uniformity at the 16

detector array was found to be within about 1 dB. The remainder of the receiver circuitry was constructed using standard RF practices.

The second gain stage consisting of the Avantek MSA 0885 with feedback is seen at the right of Figure 3.29.

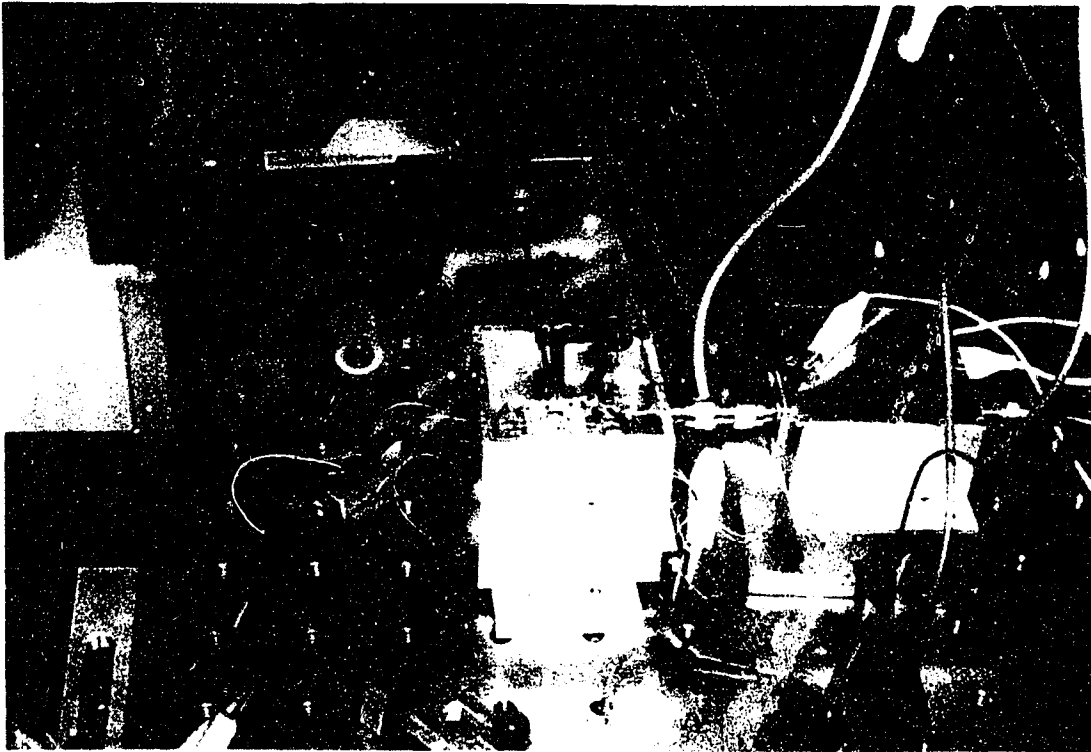


Figure 3.29 Configuration of the Complementary correlator detector showing the 16 fibres, the 'V' groove and the 'V' groove holder setup

3.7 SUMMARY

The experimental set up used to demonstrate a FO-CDMA system using Alberta codes and complementary correlation detection has been presented. The circuits used to achieve the objective have been discussed and simulation results presented. The construction of the experimental system has been

discussed with some emphasis on the construction of the complementary correlator detector module.

CHAPTER 4

EXPERIMENTAL RESULTS

This chapter discusses the measurements made with the experimental system presented in Chapter 3. Waveforms obtained at important points in the network and the performance achieved by the various blocks in the circuitry are presented in the first part of the chapter. Bit Error Rate (BER) measurements made with the system are then discussed. The variation of the BER with transmitter optical power is presented for the cases of no interfering users and one interfering user. Finally, the spectra of the uncoded, coded, correlated and recovered data are presented at the transmitter and receiver to illustrate the spreading and de-spreading that is achieved with Alberta codes applied to a FO-CDMA system.

Figure 4.1 shows the configuration of the experimental FO-CDMA system used for the demonstration of Alberta codes and complementary correlation detection.

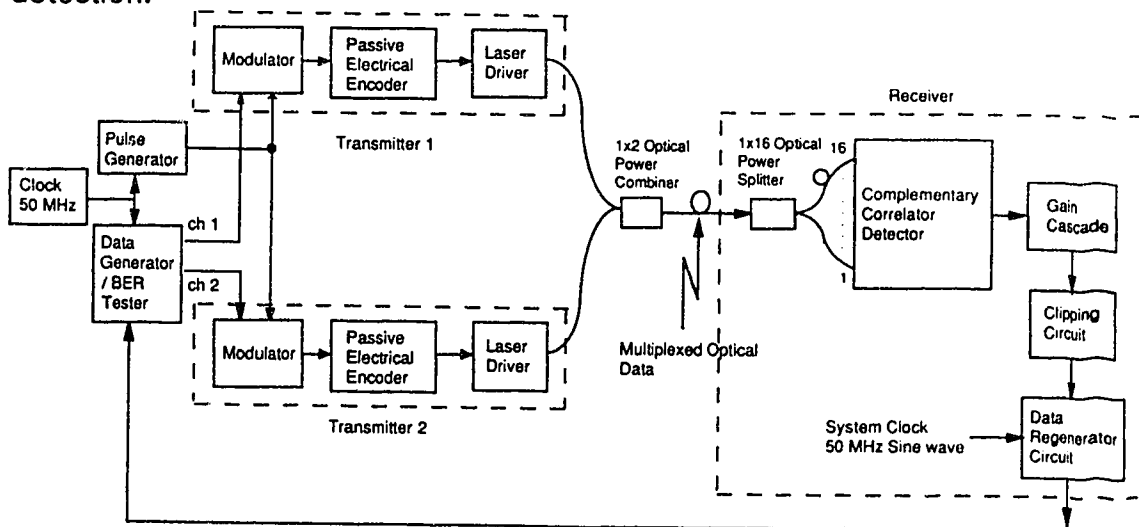
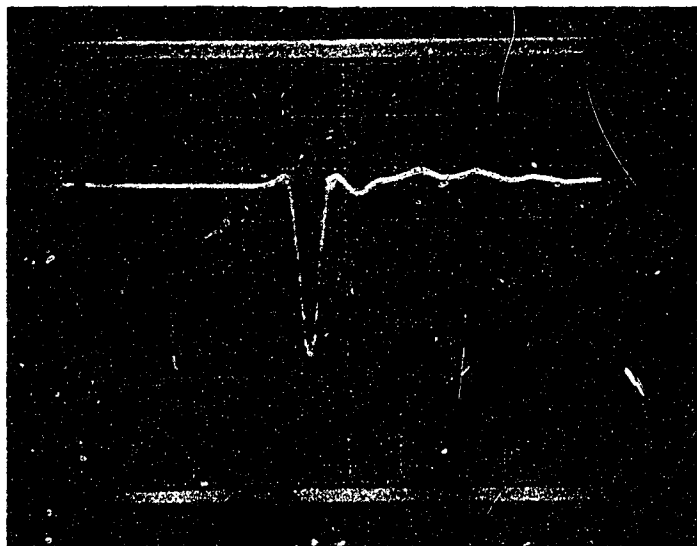


Figure 4.1 Configuration of the experimental FO-CDMA system

4.1 TRANSMITTER PERFORMANCE

4.1.1 THE PULSE GENERATOR

With reference to the pulse generator circuit shown in Figure 3.4 and the description of its operation given in Section 3.3.1, the photograph below (Figure 4.2) shows the output of the pulse generator circuit. As expected from the design calculations, the pulse width is around 500 ps (439.5 ps at the base with a Full Width Half Maximum (FWHM) of 214.8 ps). The pulse repetition frequency is 50 MHz. The output of the SRD is a damped high frequency sine wave, the first half cycle of which forms the required narrow pulse. The ripples that can be observed beyond the falling edge of the pulse are due to the following cycles of this damped high frequency sine wave and have been clipped to a large extent by the MESFET stage following the pulse generator. The pulse amplitude is 3.4 V.



**Figure 4.2 Output pulse from the pulse generator circuit.
with pulse width 439.5 ps (at the base) and
amplitude 3.4 V
x scale: 500 ps/division y scale: 1 V/division**

4.1.2 THE MODULATOR CIRCUIT

As described in Section 3.3.2, the output of the pulse generator is applied to the gate of the MESFET (see Figure 3.5). The data pattern generated by the Hewlett Packard HP3780A Pattern Generator/ BER Tester is applied to the drain of the MESFET. Referring to Figure 4.3, Figure 4.3 (a) shows the pulse stream applied to the gate of the MESFET and Figure 4.3 (b) shows a 1010 data pattern that is applied to the drain of the MESFET.

As noted in Section 3.3.2, the output from the pulse generator is delayed such that the peak of the pulse occurs beyond the rising edge of the data bit. Figure 4.4 shows the output of the modulator circuit for the 1010 data pattern. As expected, there is some leakage of the data pattern to the output due to the drain to source parasitic capacitances. However, the magnitude of the leakage is small compared to the amplitude of the pulse signal.

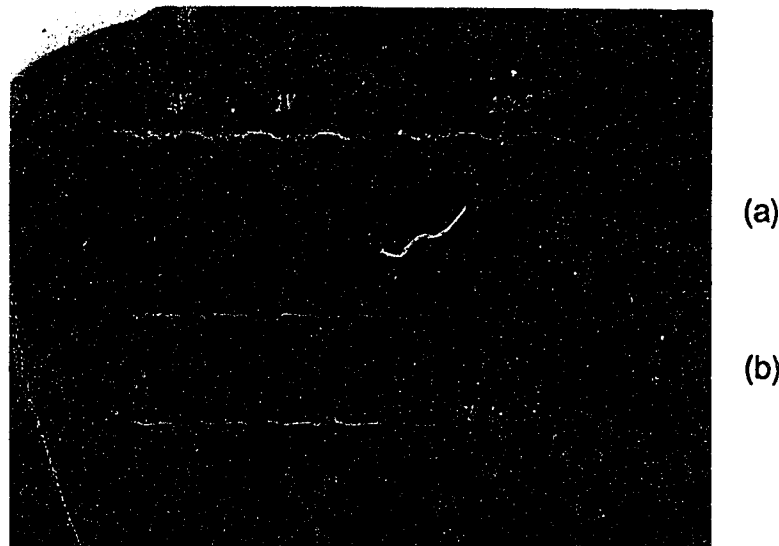


Figure 4.3 (a) Pulse stream at the output of the pulse generator with repetition frequency 50 MHz
(b) 1010 data pattern produced by the HP3780A pattern generator/BER tester
x scale: 10 ns/division y scale: 1 V/division

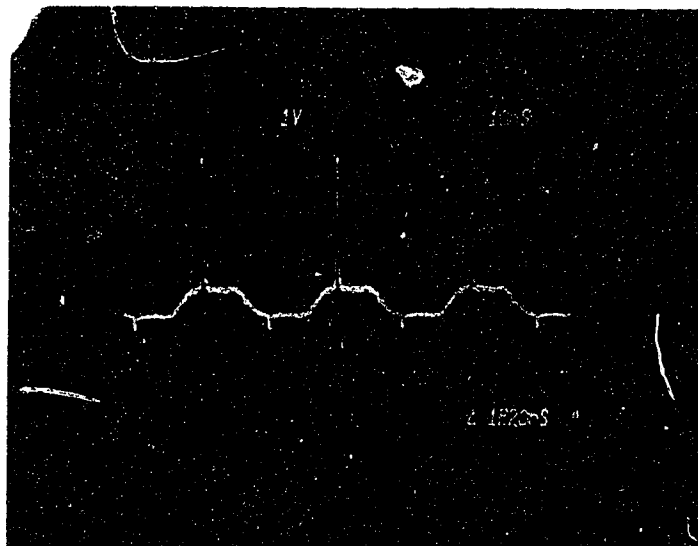


Figure 4.4 Output of the modulator circuit for a 1010 data pattern

x scale: 10 ns/division y scale: 1 V/division



Figure 4.5 Output of the passive encoder circuit for the transmitter 1 code of 0000111100000000. It must be noted that only the 1's in the code are shown above.

x scale: 500 ps/division y scale:10x50 mV/division

4.1.3 THE ENCODER CIRCUIT

As explained in Section 3.3.2, the encoder circuit is used to encode the modulated data with the address of the transmitter from which the information is being transmitted. Figure 4.5 shows the encoded output for the transmitter 1 code of 0000111100000000. Only the 1's in the code are shown so as to show the widths of the pulses at the output of the encoder.

Comparing the four pulses that make up the 1's in the code, it can be seen that fairly good uniformity is achieved with respect to pulse widths. However, the pulses have widened, with widths between 770 ps and 820 ps. Comparing Figures 4.4 and 4.5, it can also be seen that the pedestal under the modulated pulse stream, due to the data leaking to the output, has been eliminated. This was achieved by adjusting the negative bias on the gate of MESFET Q2 (Figure 3.7) such that the base of the pulse occurred at the pinch off voltage (V_P) of the MESFET. Since the pedestal occurred below the pinch off voltage and since the device Q2 is effectively OFF for all negative voltages below V_P , the pedestal is effectively clipped.

The pulse widening mentioned above is due to the frequency response characteristics of the semi-rigid co-axial cables used as delay elements. Appendix C gives the data sheet for the attenuation vs frequency characteristics of the co-axial cable. It can be seen that the attenuation of the co-axial cable is 15 dB/100 feet at 100 MHz and 104 dB/100 feet at 1.0 GHz. The co-axial cable thus behaves as a low pass filter with a wide cut-off region. The pulse is thus 'smeared' or widened by the limited bandwidth of the transmission medium. However, the pulse widths are still within the allotted time slots of 1.25 ns.

As expected, some reflection was observed at the output of the encoder circuit due to the impedance mismatch at the output of the MESFET Q2. Since the reflections effectively travel twice the length of the delay line before appearing at the output, they are delayed by twice the delay of each delay line and do not affect the encoded data in any way. The reflections are also attenuated twice before appearing at the output. The reflections at the output of the encoder were found by measurement to be reduced in amplitude by 82% relative to the amplitude of the encoded data.

4.1.4 THE LASER DRIVER CIRCUIT

With reference to the laser driver circuit in Figure 3.9 and Section 3.3.3, Figure 4.6 shows the current waveform measured with a 300 Ω probe and the high speed sampling head of a Tektronix 7854 storage oscilloscope.

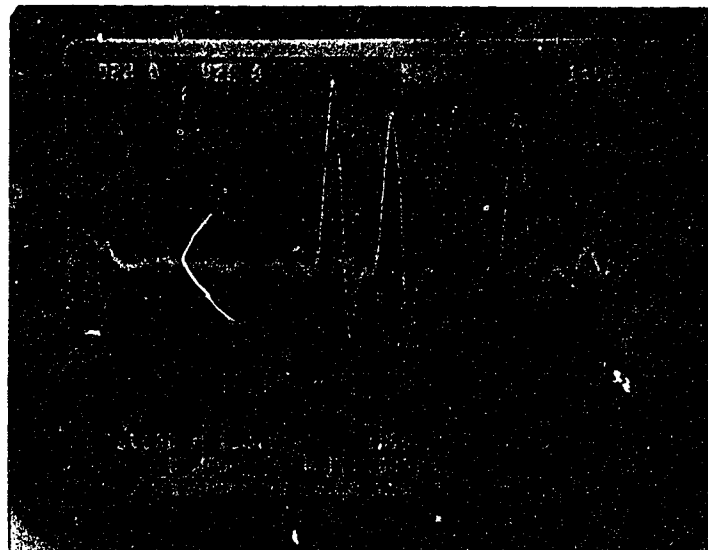


Figure 4.6 Current waveform going to the laser measured with the sampling head of a high speed storage oscilloscope
x scale: 1ns/division y scale: 500 mV/division

As expected from the simulations (Figure 3.10), a negative going dip exists on the falling edge of each pulse making up the coded waveform. This is due to the discharge of the parasitic capacitances in the laser drive current path. Figure 4.7 shows the optical output of transmitter 1 for a data bit '1' detected with a single Metal-Semiconductor-Metal (MSM) photodiode with a 3 dB bandwidth of 1.8 GHz and responsivity 0.07 A/W. The detected signal is amplified by a gain of 40 dB.

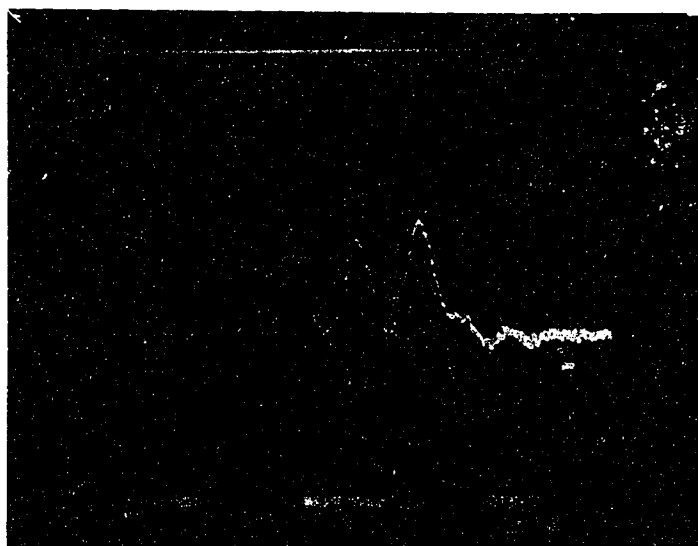
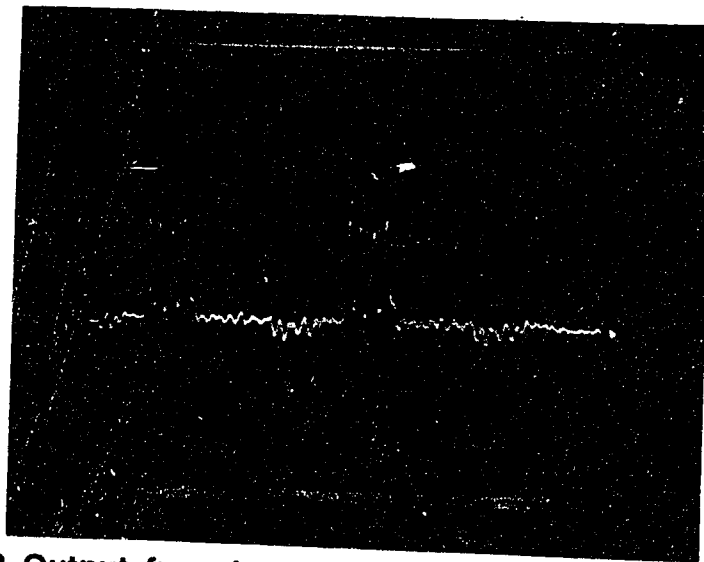


Figure 4.7 Optical output from transmitter 1 for a data bit '1' detected with a single MSM photodiode. Transmitter 1 code: 0000111100000000. Only the part corresponding to the 1's is shown for clarity x scale: 1ns/division y scale: 200 mV/division

In order to obtain complete extinction between the ON and OFF states, the laser was biased well below threshold and then pulsed. As a result of this biasing condition and because of the narrow width of the current pulse (approx. 800 ps, see Figure 4.6), it was found that sufficient charge was not generated within the laser for the first pulse in the coded data to reach its full optical amplitude. Therefore, in order to obtain equal optical amplitudes for all the 1's in the coded

data sequence, the 1x4 pulse splitter/combiner in the encoder circuit was made unequal to give a boost to the first optical pulse. As a result of this unequal splitting/combining, some worsening of the reflections were observed in the encoder output waveform due to increased mismatch. This degradation was compensated by adjusting the bias on the gates of MESFET's Q3 and Q4 (Figure 3.9) so that the reflections were clipped as much as possible. The optical output for a data '1' shown in Figure 4.7 is in fact that obtained with the modified encoder circuit. As can be seen, the optical pulses all have the same amplitude, the variation in amplitude being within 10 %. Also, the optical pulses are all within the allocated 1.25 ns time slots.



**Figure 4.8 Output from transmitter 1 for two adjacent data bit 1's. The ripple due to reflections can be seen in the region corresponding to zero's.
x scale: 5 ns/division y scale: 200 mV/division**

Figure 4.8 shows the optical output from transmitter 1 for two adjacent '1' bits, again detected with a single MSM photodiode. It can be seen that the pulses do not go all the way down to zero between pulses. This is due to the bandwidth limitation (1 GHz) of the oscilloscope channel used for this measurement. The

ripples due to the mismatch in the encoder circuit are evident to some extent in the region corresponding to the 0's in the code sequence.

A similar optimisation process was performed for transmitter 2 in order to obtain optical pulses of the same amplitude. Figure 4.9 shows the encoded output from transmitter 2 for two adjacent data bit 1's. The address of transmitter 2 is 0000110011000000.

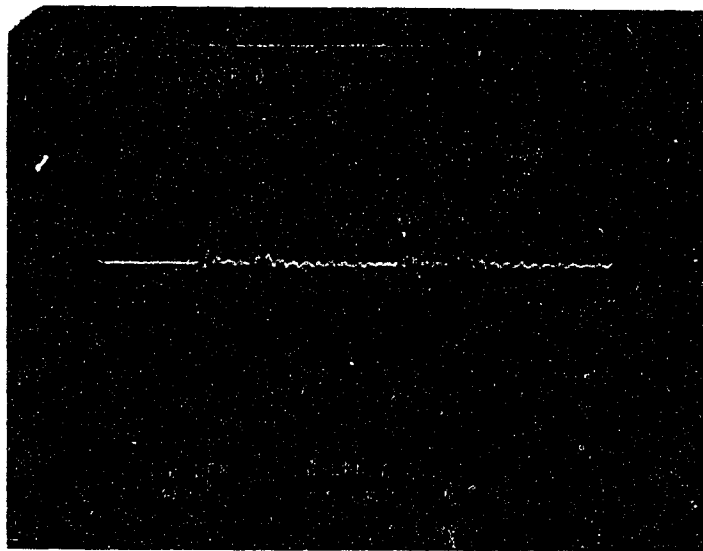


Figure 4.9 Optical output from transmitter 2 for adjacent data bit 1's.

Transmitter 2 code: 0000110011000000

x scale: 5 ns/division y scale: 10x20 mV/division

4.2 THE PASSIVE OPTICAL MULTIPLEXER

With reference to the experimental system shown in Figure 4.1, the encoded data leaving transmitters 1 and 2 are multiplexed using a passive 1x3 optical power combiner. Since the two transmitters are synchronised and the multiplexer is equi-distant from both transmitters, the encoded data from the two transmitters will arrive at the passive multiplexer at the same time and the

optical powers will thus add incoherently. Figure 4.10 shows the optical signal at the output of the multiplexer for a data '1' from transmitters 1 and 2. The code for transmitter 1 is 0000111110000000 and that for transmitter 2 is 0000110011000000. Therefore with correct synchronisation the coded output of the multiplexer will be 0000221111000. This is seen in Figure 4.10. It can also be observed from Figure 4.10 that transmitter 2 was transmitting slightly more optical power than transmitter 1. This was corrected when the actual measurements were made.

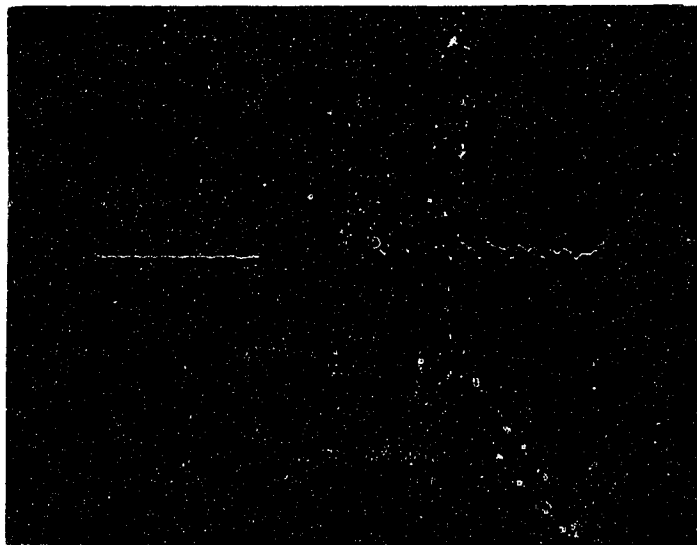


**Figure 4.10 Multiplexed Optical output from the passive optical multiplexer for a data '1' from both transmitters 1 and 2.
x scale: 2 ns/division y scale: 20x10 mV/division**

4.3 RECEIVER PERFORMANCE

4.3.1 THE COMPLEMENTARY CORRELATOR DETECTOR PLUS GAIN STAGE CASCADE

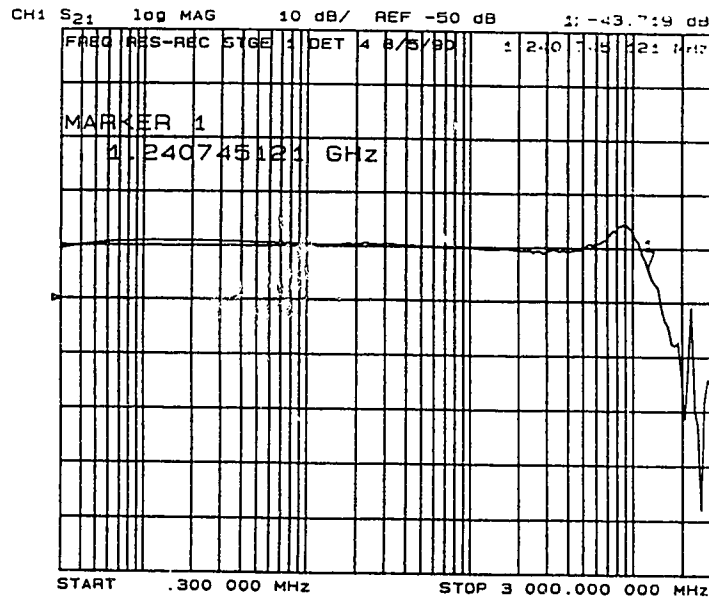


Figure 4.11 Frequency response of the complementary correlator detector - INA03170 cascade with a single detector illuminated with 0.1 mW of optical power

As explained in Section 3.6, the INA-03170 front end amplifier was incorporated with the 16 detector array in a single module. Figure 4.11 shows the frequency response of the the 16 detector array - INA-03170 cascade with one detector in the array illuminated. This measurement was obtained with all the detectors in the array biased with a 5 V supply. The frequency response curve illustrates the response of the cascade when a detector is illuminated with a 100 μ W carrier modulated with a modulation depth of 10 %.

The remaining 15 detectors in the array were tested in a similar manner. The frequency response was found to be uniform within +/- 1 dB. The usable bandwidth is 1.24 GHz. Due to the high dynamic resistance of the MSM

photodiode (measured to be $1 \text{ M}\Omega$ at a constant dc bias of 5 V) the frequency response of the circuit was found to be independent of the number of photodiodes illuminated at any one time. It must be noted that the effective bandwidth of the 16 detector array is 1.24 GHz while that of a single device was found to 1.8 GHz (see Figure 3.12). It is possible that the frequency response, in the case of a single device was limited by the transit time of the carriers while in the case of the 16 detector array the frequency response is limited by the RC time constant. The capacitance of the array becomes quite substantial when 16 such detectors are connected in parallel.

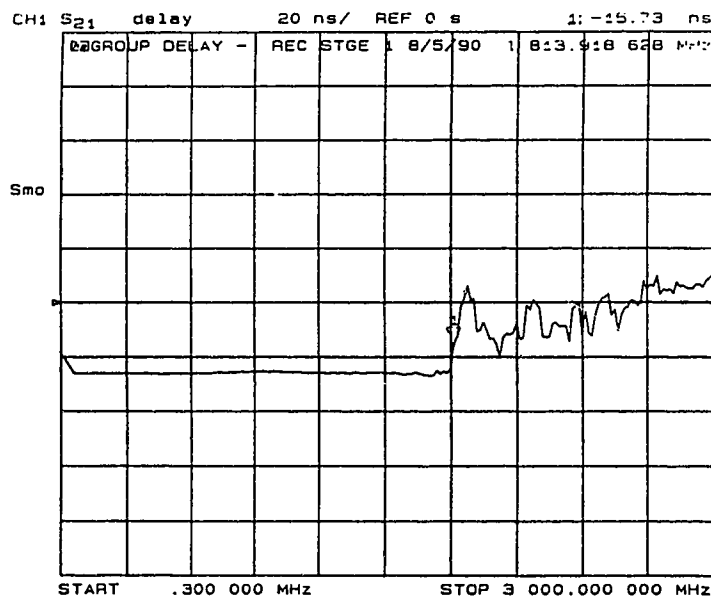


Figure 4.12 Group delay measurement of the complementary correlator detector - INA-03170 cascade

In order to determine the effect, if any, of the peaking observed in the 800 MHz region of the frequency response curve (Figure 4.11) on the encoded optical data reaching a detector in the array, the group delay of the complementary correlator detector - INA-03170 cascade was measured. The result is shown in 4.12. It can be seen that there are no significant changes in the group delay till 1.8 GHz. There is no usable gain beyond 1.2 GHz (Figure 4.11) anyway. It was

concluded that the effect of the peaking would be to provide a boost to the high frequency components in the encoded data.

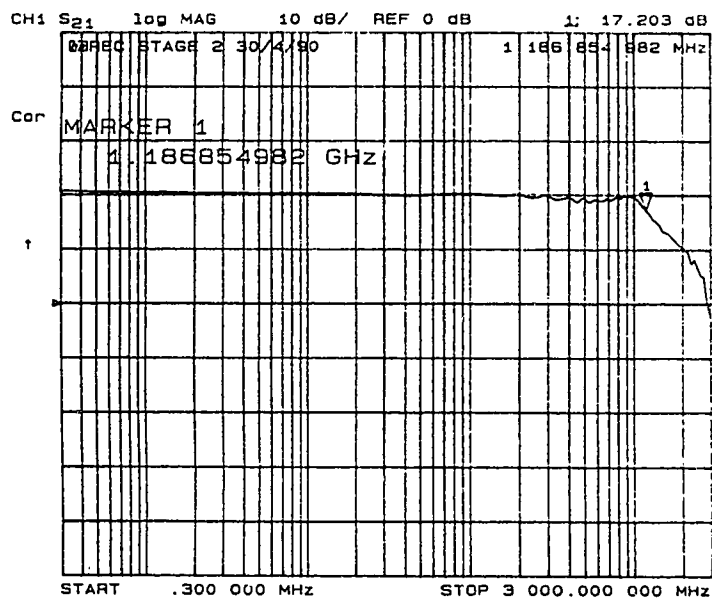
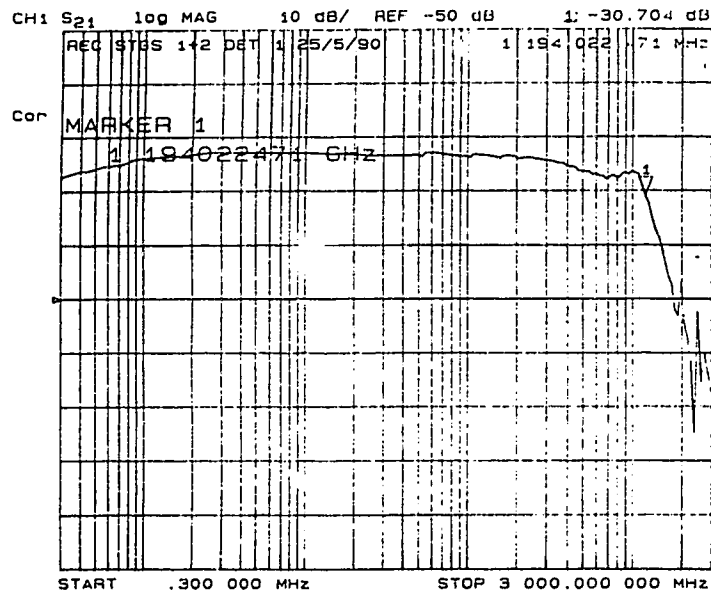


Figure 4.13 Frequency response of the MSA-0885 gain stage with feedback. Gain = 21.56 dB 3 dB Bandwidth = 1.2 GHz Measured noise figure = 4.2 dB

Figure 4.13 shows the frequency response of the MSA-0885 with feedback. The gain obtained is 21.56 dB with a 3 dB bandwidth of 1.2 GHz. A noise figure (NF) of 4.2 dB was measured. The noise figure of the gain block without feedback is 3.5 dB (see data sheet in [51]). Thus as would be expected, the noise figure is degraded by the presence of a resistor in the feedback path.

On cascading the MSA-0885 gain stage with the complementary correlator - INA 03170 cascade, a large resonance peak of relative amplitude 15 dB was observed at 1.0 GHz. It was concluded that the gain in the 1 GHz region of the MSA-0885 increased the instability of the already marginal stability of the complementary correlator detector - INA-03170 cascade. In order to make the whole cascade more stable, the 3 dB corner frequency of the MSA-0885 was moved from 1.2 GHz to 600 MHz by modifying the feedback circuit. Figure 4.14

shows the frequency response of the cascade using the modified MSA-0885 with feedback. As can be seen, the usable bandwidth is still 1.2 GHz but the peaking is greatly reduced. Again, the uniformity in the frequency response of the 16 detectors was found to be within ± 1 dB.



**Figure 4.14 Frequency response of the complementary correlator detector- INA 03170 - MSA 0885 cascade.
 Usable bandwidth = 1.2 GHz**

Considering the time domain performance of the receiver stages discussed above, Figure 4.15 shows the amplified output of the complementary correlator detector for a PRBS sequence of length 2^9-1 , encoded and transmitted by transmitter 1. There are no interfering users present in the system.

The waveform shown in Figure 4.15 was obtained with the high speed sampling head of the Tektronix 7854 storage oscilloscope. As explained in Chapter 2 and shown by simulation in Chapter 3, the positive part of the waveform in Figure 4.15 corresponds to the auto-correlation peaks. The part of the PRBS sequence captured in the photograph thus corresponds to 011. The auto-correlation wings observed on either side of the auto-correlation peak (for a data bit '1') are as

expected. This is a peculiarity observed with Alberta codes when only a single user is present in the system.

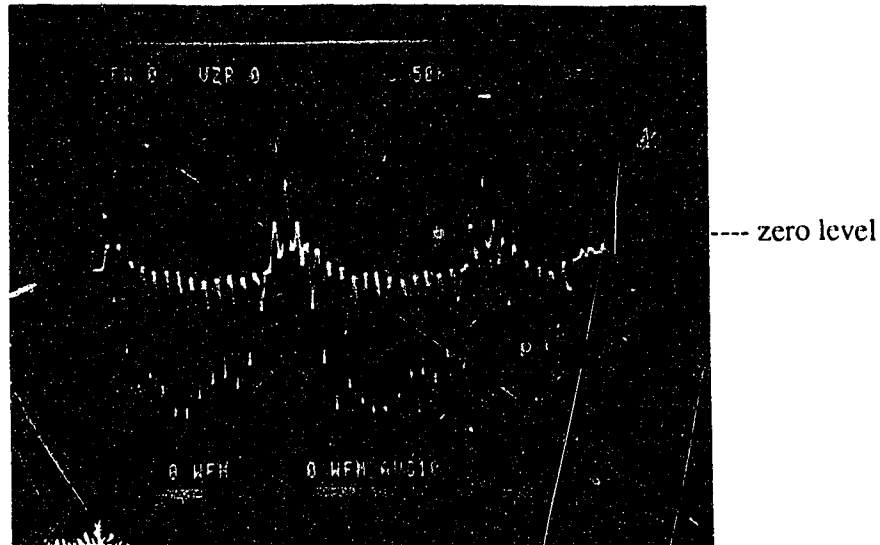


Figure 4.15 Amplified output from the complementary correlator detector for the transmitted PRBS data sequence. The auto-correlation peaks correspond to 011. No interfering users present. x scale: 5 ns/division y scale: 50 mV/division

With reference to Figure 4.15, it was found that the degree of 'sag' (i.e., the degree of negative offset from the 'zero' level) between the auto-correlation peaks for two adjacent one's in the data stream was dependent on the dc optical power incident on the detector array. No sag was observed when the laser was biased well below threshold and then pulsed so that no light was transmitted for a chip '0'. The general shape of the complementary correlator output is as expected from the theory (Chapter 2) and simulation (see Figure 3.19).



Figure 4.16 Amplified output from the complementary correlator detector for a PRBS pattern of length 2^9-1 with one interfering user present
x scale: 5 ns/division y scale: 2.5X20 mV/division

Figure 4.16 shows the amplified output from the complementary correlator detector, with the receiver switched to transmitter 1, for a PRBS sequence of length 2^9-1 encoded and transmitted by transmitter 1. In this case transmitter 2 is also encoding and transmitting a PRBS sequence of length 2^9-1 . It must be noted that the two PRBS sequences are uncorrelated. The transmitted data from transmitter 2 thus acts as a source of interference to the data stream from transmitter 1. Comparing Figures 4.15 and 4.16, it can be seen that there is no significant difference between the two waveforms except for the increased negative content that is present in the case where transmitter 2 is interfering. The increased negative content is to be expected since the correlation of the receiver address sequence with a data stream coded with the address of transmitter 2 would simply result in a cross-correlation waveform with a maximum amplitude of zero. Also, the auto-correlation peaks in the two cases are unchanged i.e., the auto-correlation peak in case two is unaffected by the

presence of the interfering user. This result provides some proof to the claim made in Chapter 2 that the performance of a FO-CDMA system using Alberta codes and complementary correlation is independent of the number of interfering users in the system, i.e., the codes are truly orthogonal.

Referring to Figures 4.15 and 4.16, it can also be seen that the auto-correlation peaks occur at exactly 20 ns intervals for two consecutive data bit one's in the data stream. The auto-correlation peaks occur at the sixteenth time slot of the sixteen chip code, as expected. It can also be seen that the auto-correlation peak is still within the 1.25 ns time slot allocated for a chip.

4.3.2 THE CLIPPING CIRCUIT

With reference to the clipping circuit shown in Figure 3.21 and the simulation results shown in Figure 3.22, Figure 4.17 shows the recovered auto-correlation peak at the output of the clipping circuit. The waveform input to the circuit has the form shown in Figure 4.15. The two auto-correlation wings observed on either side of the recovered auto-correlation peak correspond to the two wings seen in Figure 4.15.

The signal inversion is as expected due to the common-emitter configuration of the clipping circuit. Comparing the magnitude of the auto-correlation peaks in Figures 4.15 and 4.17, the gain provided by the clipping circuit is 17.62 dB. This is close to the calculated gain of 18.0 dB. The clipping circuit thus achieves both its objectives: (i) recover the auto-correlation peak and (ii) provide a gain of 18 dB. The need for additional gain stages is thus avoided. The gain of 18 dB is required to make the output of the clipping circuit ECL logic compatible.

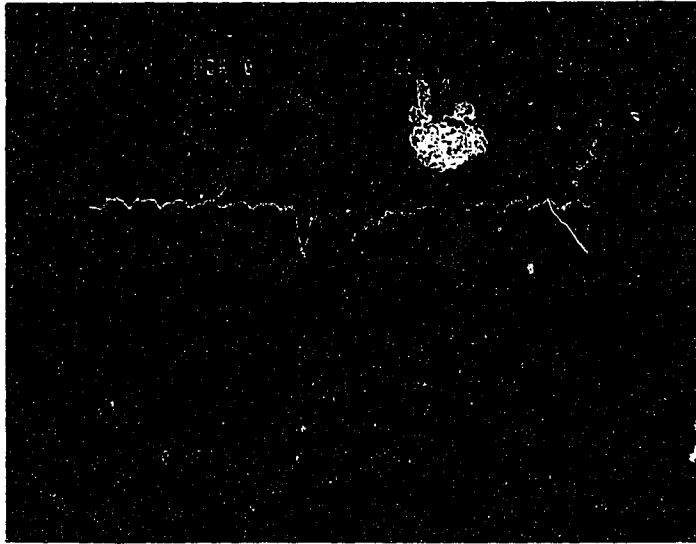


Figure 4.17 Output of the Clipping circuit showing a recovered auto-correlation peak for a PRBS pattern of length 2^9-1 .

x scale: 2 ns/division y scale: 200 mV/division

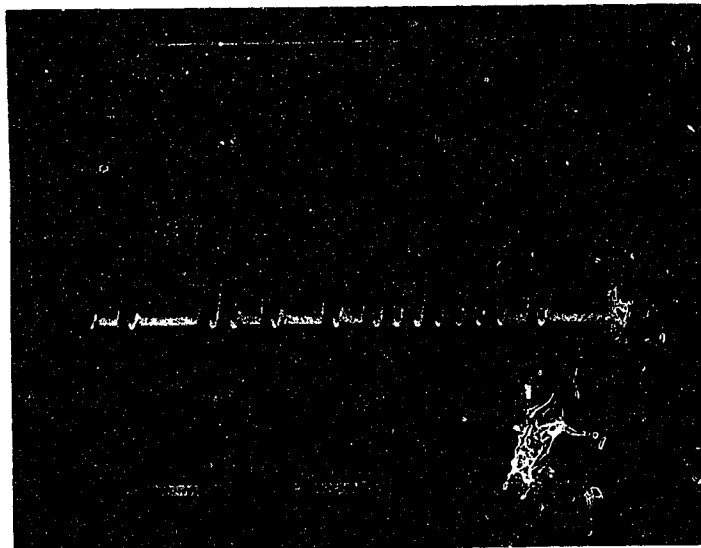


Figure 4.18 Output of the Clipping circuit for a PRBS = 2^9-1 data pattern obtained with an oscilloscope with a 1 GHz bandwidth.

x scale: 50 ns/division y scale: 500 mV/division

It must be noted that the waveform shown in Figure 4.18 has been inverted using the inversion facility of the oscilloscope. The correct orientation of the waveform is that shown in Figure 4.17. Referring to Figure 4.18, the smearing observed at the tips of the auto-correlation peaks are possibly due to the limited bandwidth (1GHz) of the oscilloscope used since this is not apparent in Figure 4.17. The waveform shown in Figure 4.17 was obtained with the high speed sampling head (rise time < 25 ps) of a storage oscilloscope (Tektronix 7854) which has an effective bandwidth of the order of 14 GHz. The 'noise' observed along the zero level of Figure 4.18 is due to the compression of the negative part of the bi-polar signal at the output of the complementary correlator detector.

On comparing the output of the clipping circuit in the absence and presence of the interfering transmitter, no significant difference in the 'noise' was observed when the second transmitter was present. However, the increase in 'noise' could be significant if all the transmitters that the system is capable of supporting are present.

4.3.3 THE DATA REGENERATOR CIRCUIT

As explained in Section 3.5.4, the data regenerator circuit consists of three stages: (i) the differential amplifier cascade (ii) the ECL D-type master-slave flip flop and (iii) the ECL to TTL translator.

Figure 4.19 (b) shows the waveform at the output of the second differential amplifier stage. Figure 4.19 (a) shows the part of the PRBS = 2^9-1 data pattern transmitted by transmitter 1. The distortions observed in the waveform are due to the mismatch created by the 500 Ω resistor used to tap off part of the transmitted data pattern. Comparing the two waveforms, the system delay of 78

ns is clearly seen. The output from the differential amplifier cascade is ECL compatible. Also, the recovered auto-correlation peaks have been widened to about 10 ns (at the base) by the low pass filtering effect (effective cut off frequency 250 MHz) of the ECL circuitry. In order to obtain the maximum gain of 15 dB provided by each stage, the differential amplifiers were operated non-linearly.

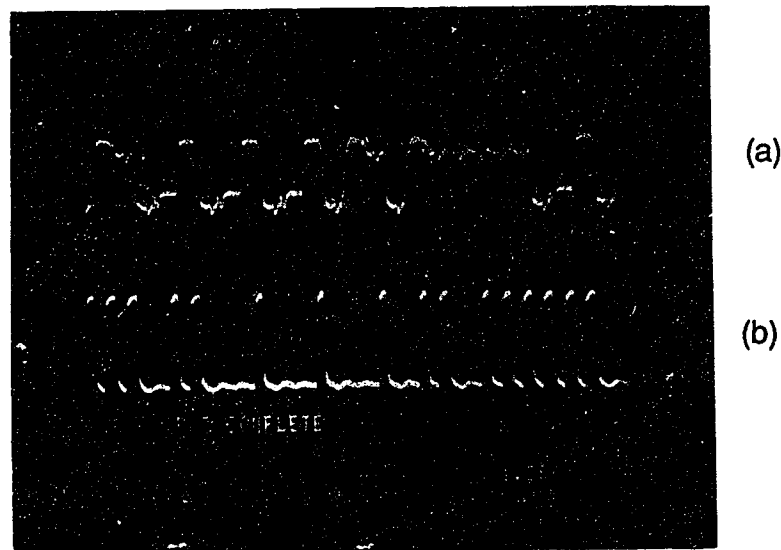


Figure 4.19 (a) PRBS = 2^9-1 data pattern transmitted by transmitter 1.
(b) Waveform at the output of the second differential amplifier
x scale:50 ns/division y scale(a): 10X50 mV/division
(b): 10X50 mV/division

Figure 4.20 (b) shows the output of the ECL D flip-flop. The master clock (50 MHz sine wave) is used, via a phase shift network, to clock the D flip-flop. The phase shift network is used to provide a fine adjustment for the clock so that the rise time of the clock occurs at the centre of the data pulse (i.e., the maximum eye opening) for a correct decision to be made by the D flip flop. Figure 4.20 (a) shows part of the transmitted PRBS pattern of length 2^9-1 . It can be seen from

Figure 4.20 (b) that the data has been regenerated to the correct NRZ format by the master slave action of the D flip flop which holds a given flip flop state for a whole clock period, since the device only changes state on the positive going edge of a clock pulse.

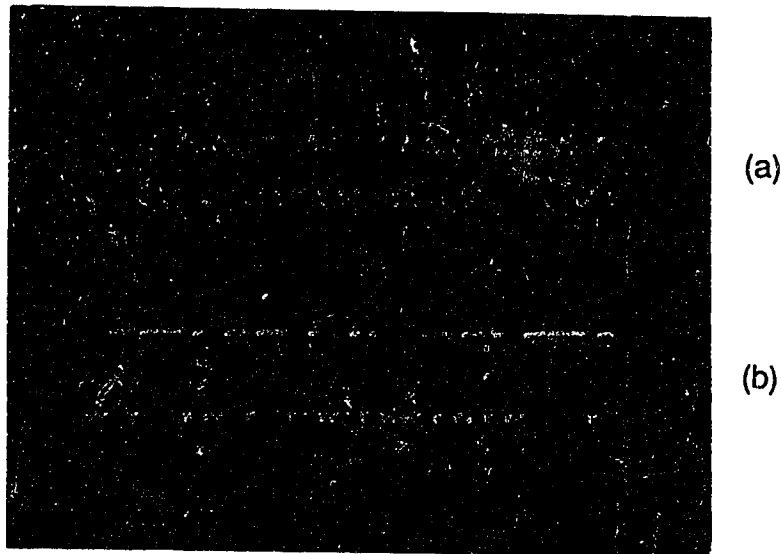


Figure 4.20 (a) PRBS = 2^9-1 data pattern transmitted by transmitter1.

(b) Regenerated data at the output of the ECL D flip-flop. No interfering transmitters present

x scale: 100 ns/div y scale (a): 200 mV/division

(b): 500 mV/division

Figure 4.21 (b) shows the regenerated data at the output of the ECL to TTL translator. Figure 4.21 (a) shows part of the PRBS = 2^9-1 data pattern transmitted by transmitter 1. Comparing the two waveforms the system delay of 78 ns is apparent.

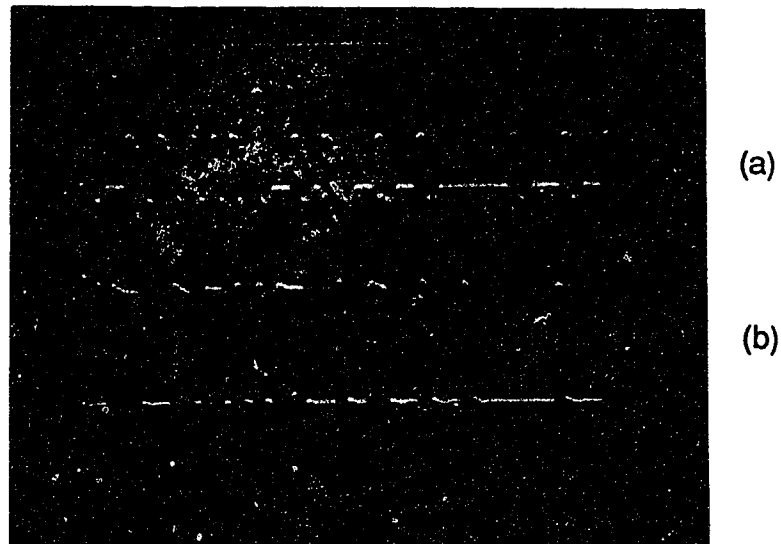


Figure 4.21 (a) PRBS = 2^9-1 data pattern transmitted by transmitter 1
(b) Output of the ECL to TTL translator. No interfering transmitters present
x scale: 100 ns/div y scale (a): 200 mV/division
(b): 1 V/division

4.4 BIT ERROR RATE (BER) PERFORMANCE

Since the receiver can be switched to receive transmissions from either transmitter in the system, BER tests were performed for two possible conditions (i) receiver switched to receive transmissions from transmitter 1 and (ii) receiver switched to receive transmissions from transmitter 2. In order to determine the effect, if any, of an interfering user on the BER performance of a channel, the above mentioned tests were performed with and without the presence of the interfering transmitter (i.e., in case (i) the interfering transmitter is transmitter 2 and in case (ii) the interfering transmitter is transmitter 1).

(i) BER performance of the system with the receiver switched to transmitter1

Figure 4.22 shows the BER curves obtained with the receiver switched to transmitter 1. Curve (a) shows the BER performance of the system without the interfering transmitter and curve (b) shows the performance of the system in the presence of an interfering user, i.e., transmitter 2.

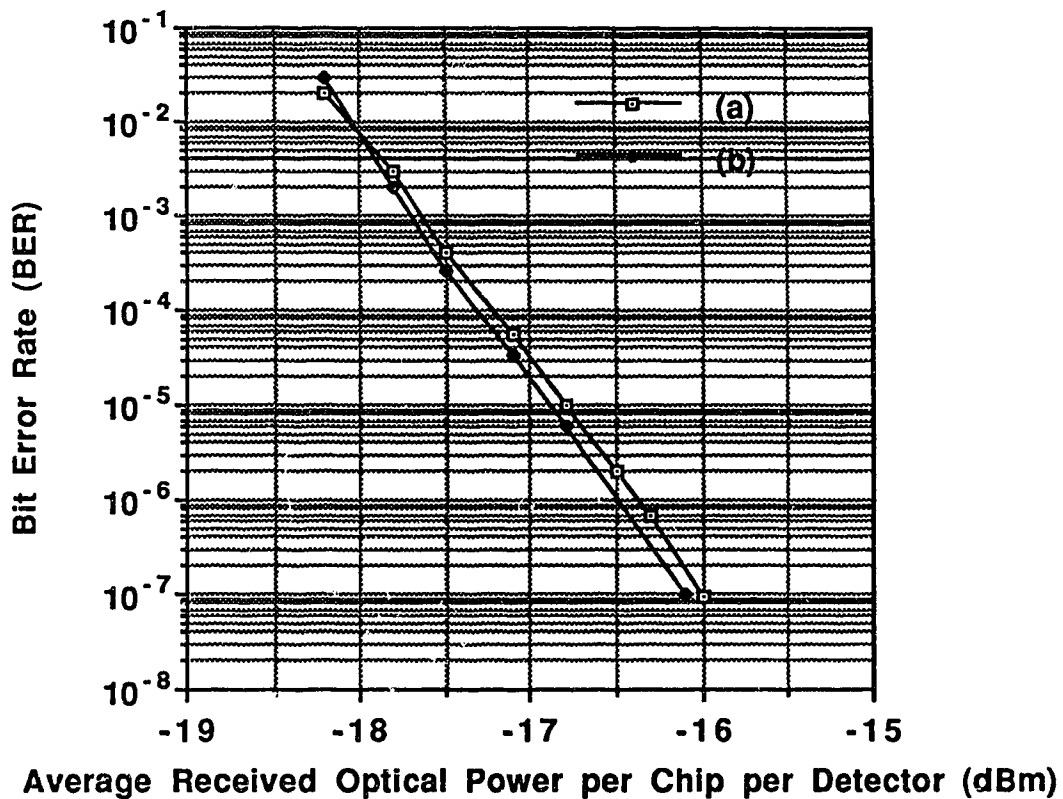


**Figure 4.22 BER vs Average Received Optical Power per Detector per Chip. Receiver switched to Transmitter 1
(a) No interfering users (b) Transmitter 2 interfering**

The BER measurements were made with respect to the average received optical power per chip per detector. In the case of curve (a) the optical power

from transmitter 1 was varied from the maximum possible value to a value below which synchronisation was lost between the transmitter and receiver. In case of curve (b) the optical power from transmitter 2 was fixed at the maximum value and the optical power from transmitter 1 was varied as before. It was not possible to increase the optical power from transmitter 2 in order to determine the swamping effect, if any, of transmitter 2 due to the power limitations discussed previously.

(ii) BER performance of the system with the receiver switched to transmitter 2

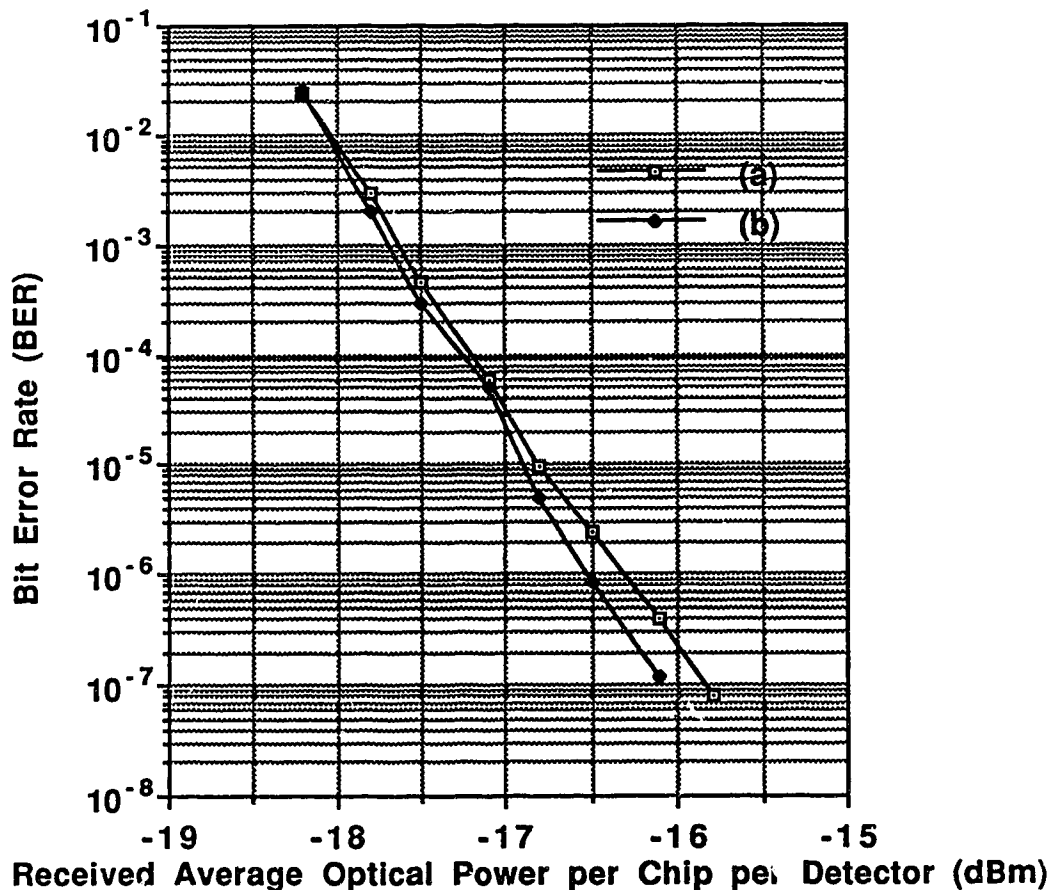


**Figure 4.23 Plot of BER vs Average Received Optical Power per Chip per Detector. Receiver switched to transmitter 2
(a) No interfering user (b) Transmitter 2 interfering**

Figure 4.23 shows the BER performance achieved with the receiver switched to receive transmissions from transmitter 2. Curves (a) and (b) show the performance of the system with and without the interfering user respectively. The interfering user in this case being transmitter 1. The curves shown in Figure 4.23 were obtained in the same manner as those in Figure 4.22.

Since the BER performance of the main channel is of interest (i.e., transmitter 1 - receiver 1 in (i) and transmitter 2 - receiver 2 in (ii)), the received average optical power per detector per chip values given in the abscissa of Figures 4.22 and 4.23 do not include the constant optical power of the interfering transmitters, i.e., transmitter 2 in (i) and transmitter 1 in (ii).

Comparing Figures 4.22 and 4.23, there is no significant difference between the two sets of curves. The best BER performance achieved in each case was of the order of 10^{-7} . Lower BER performance could not be achieved due to (i) high system losses (20.6 dB) and (ii) poor responsivity of the MSM photodiodes used in the receiver. The responsivity of 0.07 A/W achieved with the devices in question is about a factor of 4 lower than values published in current literature [40]. Due to these limitations, the BER performance achieved is consistent with expected results. With the laser operating at peak pulsed power (10 mW into the fibre at the transmitter), the average received optical power per detector per chip is $25 \mu\text{W}$ for a PRBS data pattern. Based on receiver noise calculations $25 \mu\text{W}$ corresponds to an error rate of 10^{-7} . This ties in with the experimentally measured results.

Referring to Figures 4.22 and 4.23, no error floor is apparent and the trend of the curves give no indication of one. It can thus be concluded that BER performance of the order of 10^{-9} can be achieved if (i) more optical power is

available or (ii) photodetectors with better responsivities are used. A factor of 4 improvement in the device responsivity would correspond to a 12 dB increase in electrical power or a 6 dB improvement in optical power. Thus with the absence of any noise floor, a BER better than 10^{-9} could be achieved. The poor responsivity of the MSM photodetector was therefore a major limitation on the system performance.

Comparing curves (a) and (b) in each of the cases considered above, there appears to be a consistent improvement in the BER performance of the system when the interfering transmitter is present and transmitting at almost equal power as the legitimate transmitter. Thus although the Alberta codes are orthogonal as discussed, the presence of the interfering transmitter shifts the cross-correlation further negative. Also, the presence of the interfering transmitter removes the auto-correlation wings on either side of the auto-correlation peak. This can be observed by comparing Figures 4.15 and 4.16. Thus the increased negative shift and the removal of the auto-correlation wings could result in an improved BER performance in the presence of the second interfering transmitter.

With an increased number of users in the system, there would be increased noise in the receiver due to (i) increased noise current caused by increased optical power incident on the each detector in the array and (ii) increased negative content in the signal at the output of the complementary correlator detector. This increased negative content will result in increased 'noise' at the output of the clipping circuit due the increased compression that will be performed by the clipping circuit. A reduction in the eye opening could result leading to a degradation in the BER performance of the system in the presence of the interfering users. Based on the results obtained with a single interfering

transmitter, it could be concluded that effect of the increased noise would be fairly nominal.

The two mechanisms mentioned above have opposing effects on the BER performance of the system. Based on the BER performance curves shown in Figures 4.22 and 4.23, it would appear that there is a net gain due to the presence of the interfering transmitter, i.e., the gain due to coding is greater than the degradation due to increased 'noise'. Further investigation with more transmitters is required before this hypothesis can be confirmed with some degree of certainty. It was not possible to use more transmitters due to optical power limitations caused by poor responsivity of the MSM photodetectors used in this demonstration.

4.5 POWER SPECTRUM MEASUREMENTS

As implied by the name spread spectrum, the data that is input to such a system is modulated such that the spectrum of the modulated data is much wider than that of the original data, i.e., the spectrum of the data has been spread. Thus in order to determine the performance of the FO-CDMA system with respect to spectral spreading and de-spreading, the power spectrum was checked at various points of the experimental system.

Figure 4.24 shows the spectrum of the 50 Mbits/s PRBS data pattern of length 2^9-1 that is applied to the input of one channel of the experimental system. This PRBS data pattern is modulated and encoded with the address of the transmitter in question. Figure 4.25 shows the spectrum of the signal at the output of the passive electrical encoder. For reasons of clarity, only one side of the spectral pattern is shown. Comparing the spectra in Figures 4.24 and 4.25,

the spreading achieved is clearly seen. The bandwidth of the spread signal is 2.8 GHz.

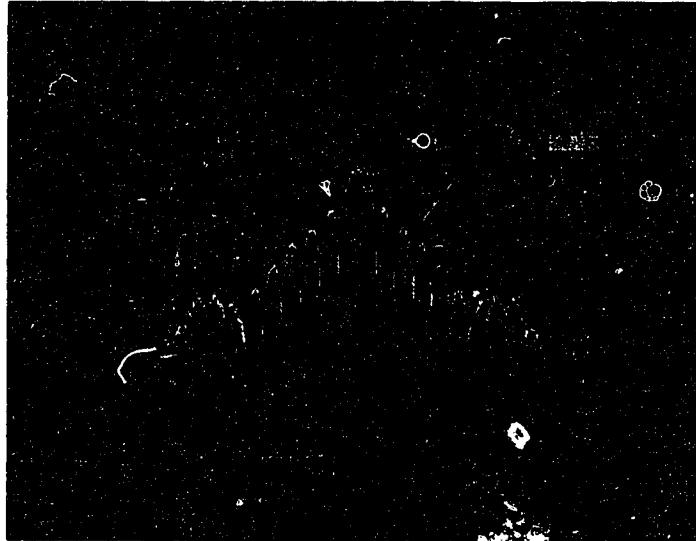


Figure 4.24 Spectrum of the PRBS data pattern of length 2^9-1 at 50 Mbits/s

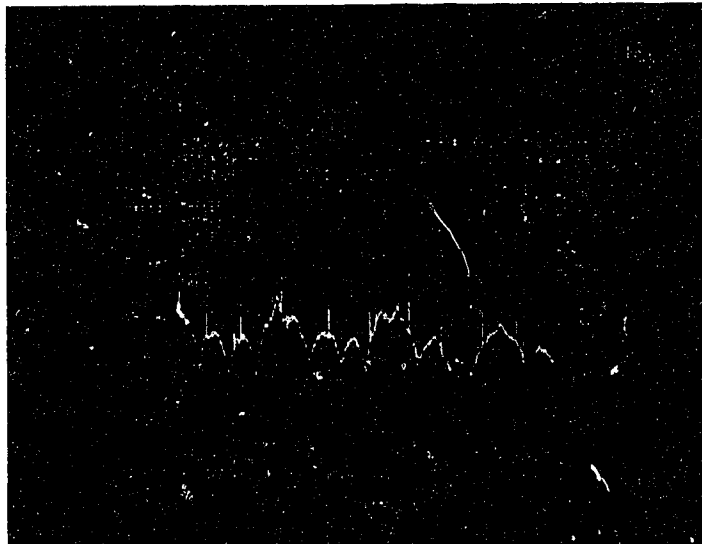


Figure 4.25 Spectrum of the encoded data at the output of the passive electrical encoder circuit. Only one half of the spectrum is shown

Figure 4.26 shows the spectrum of the signal at the output of the complementary correlator detector. The 'despread' auto-correlation signal is clearly evident.

Figure 4.27 shows the spectrum of the recovered and regenerated PRBS pattern of length 2^9-1 at the output of the receiver. Comparing Figure 4.24 and 4.27, it can be seen that the spectrum of the recovered data is similar to that of the transmitted data pattern, as expected.

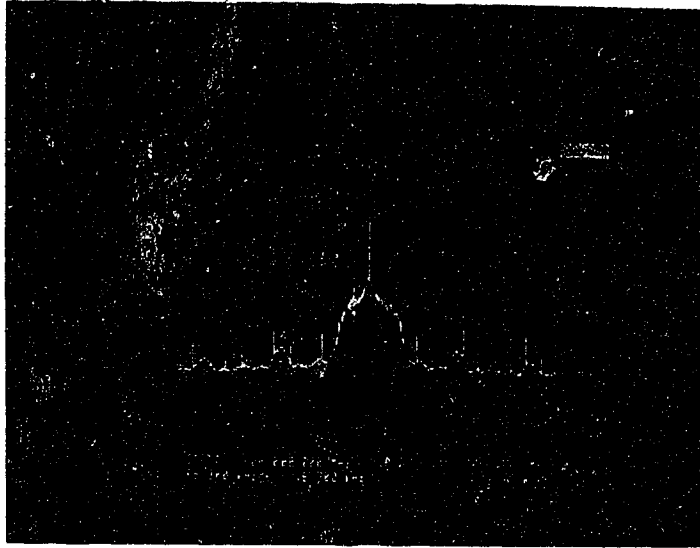


Figure 4.26 Spectrum of the signal at the output of the complementary correlator detector



Figure 4.27 Spectrum of the regenerated data at the output of the receiver

4.6 SUMMARY

A FO-CDMA system using Alberta codes and complementary correlation detection has been demonstrated at a channel rate of 800 MChips/s. The individual data rate is 50 Mbits/s. The performance of the individual blocks making up the system were discussed and results presented.

Bit Error Rate measurements were carried out with and without the presence of an interfering transmitter. BER performance values of the order of 10^{-7} were achieved. Due to the absence of a trend in the BER curves indicating the possibility of an error floor, it is anticipated that bit error rates of the order of 10^{-9} can be achieved if either (i) higher power lasers or (ii) photodetectors with improved responsivities are used. The lack of degradation in the BER performance of the system in the presence of an interfering user indicates that the BER performance of the system is independent of the number of interfering users. The consistent improvement in the BER performance observed at higher optical power levels however indicates that the BER performance improves slightly in the presence of interfering transmitters. This peculiarity is worthy of further investigation.

Measurements of the power spectrum at several points in the experimental system indicate that the spreading and despreading of the spectrum takes place as would be expected in a spread spectrum system.

CHAPTER 5

DISCUSSION AND CONCLUSION

Due to their large bandwidth requirement, spread spectrum systems are not widely used in conventional communication systems. With the large bandwidth capability of optical fibre, FO-CDMA becomes an attractive alternative to conventional modulation schemes.

In this thesis a new set of codes (namely Alberta codes) and a novel complementary correlation scheme have been investigated and demonstrated. Numerous coding schemes exist for spread spectrum communications, but most have been designed for electrical systems. Such codes do not work well when applied to optical systems. Codes designed specifically for optical systems exist but they tend to have a number of limitations which include high bandwidth expansion factors and significant cross-talk levels. This is due to the uni-polar nature of light which, together with conventional correlation methods make the generation of truly orthogonal codes impossible. These problems are overcome, to a large extent, by the use of the novel technique of complementary correlation detection which, when taken together with the Alberta codes, makes the codes truly orthogonal. True orthogonality also means that the performance of a FO-CDMA system using Alberta codes and complementary correlation detection is independent of the number of interfering transmitters in the system. As a result, nominally zero cross-talk is achieved. In addition, Alberta codes are considerably more bandwidth efficient than other optical CDMA codes.

A number of FO-CDMA systems have been demonstrated using either electrical[9] or optical [12, 16][41-46] correlation techniques. The limitation with electrical correlation is the requirement for wideband high speed circuitry at the

receiver. Thus, as transmission speeds increase, the complexity of the receiver also increases significantly. With the use of the optoelectronic correlator, the correlation takes place within the photodetector array. Thus the need for wideband high speed circuitry at the receiver is eliminated. Also, the design of the receiver is greatly simplified as demonstrated in this thesis. Therefore, with the correct choice of photodetectors, extremely high speeds can be achieved. Photodetectors with bandwidths in the order of 105 GHz have been reported [50]. Another advantage of the complementary correlator detector is that it can be operated completely asynchronously, although it has been demonstrated synchronously in this thesis. Thus the need for any form of transmitter - receiver synchronisation is avoided making such a system ideal for broadcast applications where no network control is needed.

The primary objective of this thesis was to demonstrate a synchronous FO-CDMA system using Alberta codes and complementary correlation detection. A mathematical analysis was also performed to investigate the possibility of using Alberta codes and complementary correlation in an asynchronous environment. As a result of this analysis it was found that the Alberta codes and complementary correlation detection exhibit the property that the performance of the system improves as the number of interfering users increases. This is in contrast to the behaviour of conventional systems where the system performance degrades as the number of interfering users increases. Since this analysis was performed in order to determine the possibility of asynchronous operation, an upper bound was determined on the probability of error performance. A more rigorous analysis would be required in order to determine the precise performance of such a system. On the basis of the results obtained, it would appear that the asynchronous use of Alberta codes and complementary

correlation detection is an attractive possibility. This could be useful in Asynchronous Transfer Mode (ATM) [47], where Alberta codes could be used for addressing purposes.

An experimental FO-CDMA system using Alberta codes and complementary correlation detection has been demonstrated. The system consists of two transmitters and a receiver, the receiver being switched to receive transmissions from either transmitter. A 3X1 optical power combiner and 50/125 m fibre complete the experimental setup. A data rate of 50 Mbits/s and a channel rate of 800 Mchips/s was achieved. It appears that this is the fastest direct detection FO-CDMA system demonstrated at the present time.

Bit Error Rate measurements were made with and without the presence of the interfering transmitter. BER's of the order of 10^{-7} were achieved in both cases. The results obtained were consistent with the expected BER performance due to (i) high system losses (21 dB) and (ii) poor MSM photodetector responsivity (0.07 A/W). Since MSM photodetectors with responsivities of the order of 0.2 - 0.3 A/W have been reported [40], the poor responsivity obtained with the devices used in this demonstration was a major factor limiting the BER performance achieved. A factor of 4 improvement in the responsivity corresponds to an increase of 6 dB in optical power. Since no error floors were observed and the trend in the BER performance curves give no indication of one, it is anticipated that, with a 6 dB improvement, BER performance better than 10^{-9} could be achieved. The results of the BER tests performed with and without the presence of an interfering transmitter confirm that the BER performance of a FO-CDMA system using Alberta codes and complementary correlation detection is nominally independent of the number of interfering users. This property comes about due to the truly orthogonal nature of Alberta

codes. As discussed in the previous chapter, there would be some degradation due to increased detector noise due to the interfering transmitters and increased noise in the clipping circuit. Based on the results obtained with one interfering transmitter this degradation is expected to be minimal. On the other hand, there is a consistent improvement in the BER performance of system when the interfering transmitter is present and transmitting at almost equal power as the main transmitter. It is thus possible that the gain provided by the Alberta code - complementary correlation method is greater than the degradation due to increased noise in the system.

On the other hand, this improvement in the BER performance may be due to some slight asynchronicity between the two transmitters. This result would then tie in with the results of the theoretical analysis of the asynchronous system given in Chapter 2 which shows that the BER performance of an asynchronous system using Alberta codes and complementary correlation improves in the presence of interfering transmitters. This feature would have to be confirmed by the addition of more transmitters to the system and is worthy of further investigation at some future date. It was not possible to test the system for more than one interfering transmitter due to optical power limitations caused by the poor responsivity of the MSM photodetectors used in this demonstration.

Spectral power measurements carried out at different points in the experimental system indicate that the spreading and despreading of the spectrum observed is as expected. The 50 Mbits/s data was found to be spread to a bandwidth of 2.8 GHz by the Alberta codes.

The maximum chip rate achieved in this demonstration (800 MChips/s) was limited only by the switching time of the semiconductor lasers. Mode-locked

Lasers that can produce 100 ps wide optical pulses exist commercially [48]. Also, photodetectors with bandwidths of 105 GHz have been reported [50]. Thus with the correct choice of lasers and photodetectors, chip rates in excess of 10 GChips/s could be achieved with relative ease.

With the move to higher speeds it is essential that the optical delay lines in the receiver be implemented with integrated waveguides. The delay lengths would be much more precise than that achieved presently with optical fibre. Also if large code word lengths and therefore larger arrays of photodetectors are used, then the distribution of the optical signals to the individual detectors in the array and the uniformity that can be achieved becomes a significant problem. A possible solution to this problem would be to integrate the waveguides with the photodetectors. The full potential of the complementary correlator receiver can be achieved with such a step. It is believed that a hybrid combination of integrated optical and electronic elements would be the most promising path for the fabrication of complementary correlation receivers for long code lengths. Some research has already been done on the use of waveguides to distribute the optical signals to the photodetectors and the integration of the two [49].

With the use of long codes supporting a large number of users, there will be significant losses incurred at the receiver due to the large optical power splits that will be required. Therefore, an optical amplifier would be required before the optical power splitter in order to compensate for the power loss.

In conclusion, a synchronous FO-CDMA system using Alberta codes and complementary correlation detection has been successfully demonstrated at 800 MChips/s. Bit Error rates of 10^{-7} have been achieved. Improved performance could be achieved by the use of photodetectors with better responsivities.

Results indicate that the BER performance of a FO-CDMA system using Alberta codes and complementary correlation detection is independent of the number of interfering transmitters. This also implies that zero cross-talk is nominally achieved with such a system. It is anticipated that the Alberta codes and complementary correlation detection could form the basis for the distribution of wideband digital signals as in high definition television and high speed high capacity trunk multiplexing systems.

REFERENCES

1. H.J Kochevar, "Spread Spectrum Multiple Access communications experiment through a satellite", *IEEE Trans. Commun.*, vol. 27, pp. 853-856, August 1979.
2. C.R Cooper and R. W Nettleton, " A Spread Spectrum technique for high capacity mobile communications", *IEEE Trans. Vehicu. Technol.*, vol. 27, pp. 264-275, Nov 1978.
3. C.E Shannon, " A Mathematical theory of Communication", *Dell Syst. Tech. J.*, vol. 27, pp. 623 - 656, 1948.
4. R.C Dixon, " Spread Spectrum Systems", New York, Wiley, 1984.
5. W. F. Utlaut, " Spread Spectrum: Principles and possible applications to spectrum utilisation and allocation", *Tutorials in Modern Communications*, Computer Science Press, pp. 323 - 333, 1983.
6. D.V Sarwate and M.B Pursley, " Cross-correlation properties of pseudo-random and related sequences", *Proc. IEEE*, vol. 68, pp. 593-619, 1980.
7. P.S Moharir, " Optical Barker sequences and self - orthogonal Convolutional Codes", *Electron. Lett.*, vol. 11, pp. 124, 1975.
8. R. Gold, " Study of Correlation Properties of Binary Sequences", *Magnavox Research Laboratories Report*, AFAL TR-66-234, August 1966.
9. S. Tamura, S. Nakano and K. Akazaki, "Optical Code-Multiplex transmission by Gold sequences", *J. Lightwave Technol.*, vol. 3, pp. 121 - 127, February 1985.
10. K. P. Jackson, S. A. Newton, B. Moslehi, M. C. Chapin Cutler, J. W. Goodman and H. J. Shaw, "Optical Fibre Delay line Signal Processing", *IEEE Trans. Microwave Theory Tech*, vol 33, pp 193 - 209, March 1985.

11. A. A. Sharr and P. A. Davis, "Prime sequences; Quasi-optimal sequences for Orthogonal Channel Code Division Multiplexing", *Electron. Lett.*, vol. 19, pp. 888 - 889, 1983.
12. P.R.Prucnal, M.A Santoro and S.K Seghal, " Ultra-fast All-optical Synchronous Multiple Access Fibre Networks", *J. Select Areas Commun.*, vol. SAC - 4, No. 9, pp. 1484 - 1493, December 1986.
13. P.R Prucnal, M.A Santoro, T.R Fan, "Spread spectrum Fibre-optic local area network using Optical Processing", *IEEE J.Lightwave Technol*, vol. LT-4, No. 5, pp. 547-554, May 1986.
14. F.R.K Chang, J.A Salehi and V.K Wei, "Optical Orthogonal Codes: Design, Analysis and Applications", *IEEE Symposium on Information Theory*, 1986.
15. J.A Salehi and C.A Brackett, " Code Division Multiple Access techniques in Optical Fibre Networks", *IEEE Trans. Comm.*, vol 37, no 8, pp 824 - 842, August 1989.
16. J.A Salehi and C.A Brackett, " Fundamental Principles of Fibre-optic Code Division Multiple Access (FO-CDMA)", *Proc. of the IEEE Int. Conf. Comm.*, IEEE, New York, pp 1601-1609, 1987.
17. R.I. MacDonald, "Fully Orthogonal optical-code multiplex for broadcasting", *Optics Letters*, vol. 13, pp. 539-541, June 1988.
18. T. Sugeta, T. Urisu, S. Sakata and Y. Mizushima, " Metal-Semiconductor-Metal Photodetector for high speed Optoelectronic circuits", *Proc. 1979 Int. Conf. Solid State Dev.*, August 1979.
19. P. Healy, " Optical Orthogonal Pulse Compression Codes by Hopping", *Electron. Lett.*, vol 17, no 25/26, pp 570 - 571, December 1981.
20. R. I. MacDonald and D. K. W. Lam, " Broadband Matrix Switching : Electro-Optic or Optoelectronic ? ", *Opt. and Quant. Electron.*, vol 18, pp 273 - 277, 1986.

21. G. L. Tangonan, V. Jones, J. Pikulski, D. Jackson and D. Persechini, D. G. Thorneboone and S. R. Forrest, "8X8 Optoelectronic Crossbar Switch", *Electron. Lett.*, vol 24, p 275, 1988.
22. D.K.W Lam, R.I MacDonald, J.P Noad and B.A Syrett, "Surface-Depleted Photoconductors", *IEEE Trans. Electron. Dev.*, vol. ED-34, no 5, pp1057 - 1060, May 1987.
23. R.I MacDonald, M. Veilleux, J.P Noad and F. Gouin, "CRC/ATRC Joint Optoelectronic Switching Project, First Progress Report", *CRC/ATRC Internal Report*, February 1989.
24. Mitsubishi Optical Semiconductor Manual, 1986.
25. Pulse and Waveform Generation with Step Recovery Diodes, *Applications Note 918*, Hewlett - Packard, October 1967.
26. NEC Microwave and RF Semiconductor Guide, 1989-1990.
27. ICAPS/2 Manual, Intusoft, 1989.
28. Precision Tube Company, Semi-Rigid Co-Axial Cable catalogue, 1988.
29. J.Senior, "Optical Fibre Communication Principles and Practice", Prentice-Hall International Series in Optoelectronics, 1985.
30. J. C. Gammel, G. M. Metze, J. M. Ballantyne, "An Epitaxial Photoconductive Detector for high speed optical detection", *IEDM Tech. Digest*, pp 634,1970.
31. C. Y. Chen, Y. M. Pang, K. Alavi, A. Y. Cho and P. A. Gorbinski, "Interdigitated AlInAs/GalnAs photoconductive detectors", *Appl. Phys. Lett.*, vol 44, pp 99-101, January 1984.
32. M. Ito, O. Wada, "Low dark current GaAs Metal-Semiconductor-Metal photodiodes using WSix contacts", *IEEE J. Quant. Electron.*, vol QE-22, no 7, July 1986.

33. M. Veilleux, "Construction of a 10x10 Optoelectronic Switching Matrix", MSc Thesis, Fall 1990.
34. R. I MacDonald, E. H. Hara and R. H. Hum, "Fast Photoconductive Optoelectronic Broadband Switch with Low Control Voltage", *Electron. Lett*, vol 17, pp 611-612, 1981.
35. R. J. Seymour, B. K. Garside, "Intrinsic and Extrinsic factors limiting the time response of interdigitated photodetectors", to be published, 1989.
36. W. C. Koscielniak, J. Pelouard and M. A. Littlejohn, "Intrinsic and Extrinsic response of GaAs Metal-Semiconductor-Metal photodetectors", *IEEE Photonics Tech. Lett*, vol 2, no 2, February 1990.
37. J. Millman and C. C. Halkias, *Intergrated Electronics: Analogue and Digital Circuits and Systems*, MacGraw-Hill International Book Company, 1982.
38. *The TTL Data Book*, vol 2, Texas Instruments, 1985.
39. *Motorola MECL Intergrated Circuits Data Book*, Motorola Inc, 1987.
40. S. R. Forrest, G. L. Tangonan and V. Jones, "A Simple 8X8 Optoelectronic Crossbar Switch", *J. Lightwave Technol.*, vol 7, no 4, pp 607-614, April 1989.
41. P. R. Prucnal and M. A. Santoro, "Spread Spectrum fibre-optic local area network using optical processing", *J. Lightwave Technol.*, vol LT-4, no 5, pp 547-554, May 1987.
42. P. R. Prucnal, "Ultrafast fibre optic networks using all-optical processing", *Proc. ICC '88*, pp 1485-89, 1988.
43. M. A. Santoro and P. R. Prucnal, "Asynchronous fibre optic local area network using CDMA and optical correlation", *Proc IEEE*, vol 75, no 9, pp 1336-38, Sept 1987.

44. R. I. MacDonald and G. D. Fraser, " Optical Code-Division Multiplex for High Speed Transmission", *Proc. 14th Biennial Symp. on Commun.*, Kingston, pp A.4.1-4.3, May 1988.
45. A. D. German et al, " A fibre optic CDMA network for real time communication", *IEEE INFOCOM '88*, New Orleans, pp 62-69, May 1988.
46. J. A. Salehi, " Emerging Optical Code Division Multiple Access Communication Systems", *IEEE Networks*, pp 31-39, March 1988.
47. K. Hgishiman and Y. Doi, " An Optical Self Routing Switch using Multi-Wavelength matching", *IEEE ICC '89*, Boston, pp 23.5.1-5.4, 1989.
48. 1989 Catalogue, Opto-Electronics Inc.
49. J. B. D. Soole, H. Schumacher, R. Esagui, M. A. Koza and R. Bhat, " Waveguide Intergrated MSM photodetector On InP", *Electron. Lett.*, vol 24, no 24, pp 1487-1480, November 1988.
50. B., J., Van Zeghbroeck, W. Patrick, J. M. Halbout and P. Vettiger, *IEEE Electron. Dev. Lett.*, vol 9, p 527, 1988.
51. Avantek Microwave Semiconductor Data Book, Avantek Inc, 1989.

APPENDIX A

This appendix contains the SPICE simulation programs for the following circuits:

1. The Modulator
2. The Encoder
3. The Laser driver

(i) **The Modulator Circuit**

This program simulates the operation of the modulator circuit. The circuit modulates the data pattern (NRZ, 50 Mbits/s) with a pulse stream (500 ps wide) at 50 MHz.

```

TRANS1
*SPICE_NET
*INCLUDE DEVICE.LIB
.SUBCKT GAS#0 1 2 3
RG 2 4 575.00M
RD 1 5 2.0000
DGS 4 3 DGAS
*THE GATE DRAIN DIODE IS NOT MODELED SINCE IT IS ALWAYS REVERSE BIASED
* THIS IS AN ESTIMATE OF A GAS JFET, SET N=1 FOR A MESFET
* FOR MORE DETAIL, SEE THE CHAPTER ON DIODE MODELS
.MODEL DGAS D(N=2)
RGG 4 6 1E10
J1 5 4 3 JFET
J2 5 6 3 JFET AREA=.33
*THE ABOVE AREA PARAMETER MUST BE DETERMINED EXPERIMENTALLY
*TO MATCH THE DEVICE SATURATION SLOPES AT HIGH FREQUENCY
.MODEL JFET NJF(BETA=15.000M LAMBDA=.02 IS=1E-30 CGS=552.00F
+ CGD=552.00F VTO=-2.0000 )
.ENDS
.TRAN 32P 16N
.OPTIONS LIMPTS=501
*ALIAS V(1)=VIN
*ALIAS I(V3)=IDS
*ALIAS V(3)=VTEST
*ALIAS V(10)=VOUT
.PRINT AC V(1) VP(1) I(V3) IP(V3)
.PRINT AC V(3) VP(3) V(10) VP(10)
.PRINT DC V(1) I(V3) V(3) V(10)
.PRINT TRAN V(1) I(V3) V(3) V(10)
V1 1 0 DC=0V AC=1 PULSE 0 -3 4N 0.4N 0.4N 0.1N 16N
V2 2 0 DC=0V AC=1 PULSE 0V 3V 0N 2N 2N 12N 32N
V3 3 10 DC=0
R3 2 3 25
R6 10 0 10MEG
X1 3 1 0 GAS#0
*{VT=-2V L=1 W=100 KP=37.5E-6 DC=1.38E-15 RHOG=0.023
* RHOD=0.08 N=4} {VT=xxx L=xxx W=xxx KP=xxx DC=xxx RHOG=xxx RHOD=xxx
* N=xxx )
.END

```

(ii) The Encoder Circuit

This program simulates the encoder circuit that codes the data with the 16 chip address of the transmitter in question. Lossless transmission lines are used to model the co-axial delay lines. T networks are used to represent the losses introduced by the co-axial delay lines.

```

TRANS2
*SPICE NBT
*INCLUDE DEVICE.LIB
.SUBCKT GAS#0 1 2 3
RG 2 4 575.00M
RD 1 5 2.0000
DGS 4 3 DGAS
*THE GATE DRAIN DIODE IS NOT MODELED SINCE IT IS ALWAYS REVERSE BIASED
* THIS IS AN ESTIMATE OF A GAS JFET, SET N=1 FOR A MESFET
* FOR MORE DETAIL, SEE THE CHAPTER ON DIODE MODELS
.MODEL DGAS D(N=2)
RGG 4 6 1E10
J1 5 4 3 JFET
J2 5 6 3 JFET AREA=.33
*THE ABOVE AREA PARAMETER MUST BE DETERMINED EXPERIMENTALLY
*TO MATCH THE DEVICE SATURATION SLOPES AT HIGH FREQUENCY
.MODEL JFET NJF(BETA=15.000M LAMBDA=.02 IS=1E-30 CGS=552.00F
+ CGD=552.00F VTO=-2.0000 )
.ENDS
.TRAN 32P 16N
.OPTIONS LIMPTS=501
*ALIAS V(12)=VOUT
*ALIAS V(1)=VIN
.PRINT AC V(12) VP(12) V(1) VP(1)
.PRINT DC V(12) V(1)
.PRINT TRAN V(12) V(1)
R1 2 26 50
V2 2 0 DC=6V AC=1
T1 0 18 7 0 ZO=50 TD=0.5N
T2 0 20 6 0 ZO=50 TD=2.5N
T3 0 19 5 0 ZO=50 TD=5.5N
T4 0 27 4 0 ZO=50 TD=7.5N
V3 1 0 DC=0V AC=1 PULSE 0V -3V 1N 0.4N 0.4N 0.1N 16N
R3 4 9 33
R4 7 8 33
R5 6 8 33
R6 8 10 33
R7 5 9 33
R8 9 13 33
R9 11 12 33
R10 12 0 50
R11 10 11 33
R12 13 11 33
R13 25 14 1.4
R15 3 15 2.9
R16 17 31 8.5
R17 31 18 8.5
R18 31 0 142
R19 15 20 2.9
R20 15 0 433
R21 14 19 1.4
R22 14 0 868
R27 26 27 33
R28 25 26 33
R29 3 26 33
R30 26 17 33
X1 26 1 0 GAS#0
*(VT=-2V L=1 W=100 KP=37.5E-6 DC=1.38E-15 RHOG=0.023
* RHOD=0.08 N=4) (VT=xxx L=xxx W=xxx KP=xxx DC=xxx RHOG=xxx RHOD=xxx
* N=xxx )
.END

```

(iii) The Laser Driver circuit

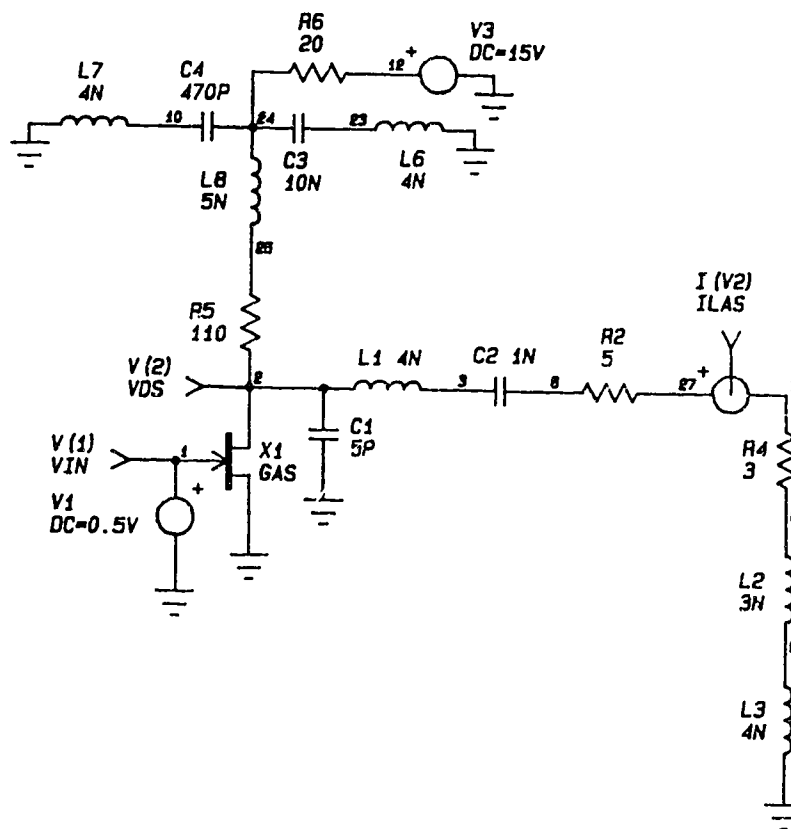
This program simulates the laser driver circuit. The parasitics of the various components have been added to determine their effects on the pulse response of the laser (Mitsubishi ML6411C). The circuit assumes that the laser is biased above threshold. The laser is thus represented by a series RL circuit. Capacitors are represented by their RLC equivalents taking into account packaging effects. C1 represents the drain to source parasitic capacitance of the MESFET. It also takes into account the capacitance of the track. The schematic is also attached.


```

tx2
*SPICE NET
*INCLUDE DEVICE.LIB
.TRAN 50P 20N
.OPTIONS LYMPTS=1001
*ALIAS I(V2)=ILAS
*ALIAS V(2)=VDS
*ALIAS V(1)=VIN
.PRINT AC I(V2) IP(V2) V(2) VP(2)
.PRINT AC V(1) VP(1)
.PRINT DC I(V2) V(2) V(1)
.PRINT TRAN I(V2) V(2) V(1)
V1 1 0 DC=0.5V AC=1 PULSE 0V -4V 2N 0.2N 0.2N 0.1N 20N
C1 2 0 5P
L1 2 3 4N
C2 3 6 1N
R2 6 27 5
V2 27 7
R4 7 8 2
L2 8 9 3N
L3 9 0 4N
R1 2 25 110
C3 24 23 10N
C4 24 10 470P
R6 24 12 20
V3 12 0 DC=-15V AC=0
L6 23 0 4N
L7 0 10 4N
L8 24 25 5N
X1 2 1 0 GAS (VT=-2V L=1 W=100 KP=37.5E-6 DC=1.375E-15 RHOG=0.023
+ RHOD=0.08 N=4) (VT=xxx L=xxx W=xxx KP=xxx DC=xxx RHOG=xxx RHOD=xxx
+ N=xxx )
.END

```

Laser driver circuit showing the parasitic components:



APPENDIX B

This appendix contains the simulation program for the complementary correlator detector. The complementary correlator detector is represented by an array of 16 photodetectors. The schematic diagram of the complementary correlator detector is attached.

```

REC2
*SPICE_NET
*INCLUDE CUSTOM.LIB
*INCLUDE SIGNAL.LIB
*INCLUDE DEVICE.LIB
.TRAN 0.1N 47.5N
* This circuit simulates the complementary correlation/detection using
* photodetectors which have been equalised to 1.2GHz. The data pattern
* used is :ch1 010 ,ch2 111 and ch3 111(reading the data from right to
* left).
.OPTIONS LIMPTS=2001
*ALIAS I(V1)-IIN1
*ALIAS I(V9)-IIN9
*ALIAS I(V16)-IIN16
*ALIAS V(33)-VOUT
*ALIAS V(51)-VOUT2
.PRINT TRAN I(V1) I(V9) I(V16)
.PRINT TRAN V(33) V(51)
V1 1 15
R1 15 35 200
L1 35 0 50N
I1 0 1 PWL ON OV 5N OV 5.4N 0.2MV 6N OV 6.25N OV 6.65N 0.1MV 7.25N OV 7.5N OV
+ 7.9N 0.1MV 8.5N OV 8.75N OV 9.15N 0.1MV 9.75N OV 10N OV 10.4N 0.1MV 11N OV
+ 11.25N OV 11.65N 0.1MV 12.25N OV 12.5N OV 12.9N 0.2MV 13.5N OV 25N OV
+ 25.4N 0.3MV 26N OV 26.25N OV 26.65N 0.1MV 27.25N OV 27.5N OV 27.9N 0.2MV
+ 28.5N OV 28.75N OV 29.15N 0.2MV 29.75N OV 30N OV 30.4N 0.1MV 31N OV 31.25N
+ OV 31.65N 0.1MV 32.25N OV 32.5N OV 32.9N 0.2MV 33.5N OV 45N OV 45.4N 0.2MV
+ 46N OV 46.25N OV 46.65N 0.1MV 47.25N OV 47.5N OV
X2 2 33 0 PHOTOC {RD=xxx CPD=xxx RF=xxx LF=xxx CFG=xxx CPG=xxx }
R2 2 36 200
L2 36 0 50N
I2 0 2 PWL ON OV 3.75N OV 4.15N 0.2MV 4.75N OV 5N OV 5.4N 0.1MV 6N OV 6.25N OV
+ 6.65N 0.1MV 7.25N OV 7.5N OV 7.9N 0.1MV 8.5N OV 8.75N OV 9.15N 0.1MV
+ 9.75N OV 10N OV 10.4N 0.1MV 11N OV 11.25N OV 11.65N 0.2MV 12.25N OV 23.75N OV
+ 24.15N 0.3MV 24.75N OV 25N OV 25.4N 0.1MV 26N OV 26.25N OV 26.65N 0.2MV
+ 27.25N OV 27.5N OV 27.9N 0.2MV 28.5N OV 28.75N OV 29.15N 0.1MV 29.75N OV
+ 30N OV 30.4N 0.1MV 31N OV 31.25N OV 31.65N 0.2MV 32.25N OV 43.75N OV
+ 44.15N 0.2MV 44.75N OV 45N OV 45.4N 0.1MV 46N OV 46.25N OV 46.65N 0.1MV
+ 47.25N OV 47.5N OV
X3 14 33 0 PHOTOC {RD=xxx CPD=xxx RF=xxx LF=xxx CFG=xxx CPG=xxx }
R3 14 37 200
L3 37 0 50N
I3 0 14 PWL ON OV 2.5N OV 2.9N 0.2MV 3.5N OV 3.75N OV 4.15N 0.1MV 4.75N OV
+ 5N OV 5.4N 0.1MV 6N OV 6.25N OV 6.65N 0.1MV 7.25N OV 7.5N OV 7.9N 0.1MV 8.5N OV
+ 8.75N OV 9.15N 0.1MV 9.75N OV 10N OV 10.4N 0.2MV 11N OV 22.5N OV 22.9N 0.3MV
+ 23.5N OV 23.75N OV 24.15N 0.1MV 24.75N OV 25N OV 25.4N 0.2MV 26N OV 26.25N
+ OV 26.65N 0.2MV 27.25N OV 27.5N OV 27.9N 0.1MV 28.5N OV 28.75N OV 29.15N
+ 0.1MV 29.75N OV 30N OV 30.4N 0.2MV 31N OV 42.5N OV 42.9N 0.2MV 43.5N
+ OV 43.75N OV 44.15N 0.1MV 44.75N OV 45N OV 45.4N 0.1MV 46N OV 46.25N OV
+ 46.65N 0.1MV 47.25N OV 47.5N OV
X4 4 33 0 PHOTOC {RD=xxx CPD=xxx RF=xxx LF=xxx CFG=xxx CPG=xxx }
R4 4 38 200
L4 38 0 50N
I4 0 4 PWL ON OV 1.25N OV 1.65N 0.2MV 2.25N OV 2.5N OV 2.9N 0.1MV 3.5N OV
+ 3.75N OV 4.15N 0.1MV 4.75N OV 5N OV 5.4N 0.1MV 6N OV 6.25N OV 6.65N 0.1MV
+ 7.25N OV 7.5N OV 7.9N 0.1MV 8.5N OV 8.75N OV 9.15N 0.2MV 9.75N OV 21.25N OV
+ 21.65N 0.3MV 22.25N OV 22.5N OV 22.9N 0.1MV 23.5N OV 23.75N OV 24.15N 0.2MV
+ 24.75N OV 25N OV 25.4N 0.2MV 26N OV 26.25N OV 26.65N 0.1MV 27.25N OV
+ 27.5N OV 27.9N 0.1MV 28.5N OV 28.75N OV 29.15N 0.2MV 29.75N OV 41.25N OV
+ 41.65N 0.2MV 42.25N OV 42.5N OV 42.9N 0.1MV 43.5N OV 43.75N OV 44.15N 0.1MV

```

```

+ 44.75N OV 45N OV 45.4N 0.1MV 46N OV 46.25N OV 46.65N 0.1MV 47.25N OV 47.5N OV
X5 5 33 0 PHOTOC (RD=xxx CPD=xxx RF=xxx LF=xxx CFG=xxx CPG=xxx )
R5 5 39 200
L5 39 0 50N
I5 0 5 PWL ON OV 0.4N -0.2MV 1N OV 1.25N OV 1.65N -0.1MV 2.25N OV 2.5N OV
+ 2.9N -0.1MV 3.5N OV 3.75N OV 4.15N -0.1MV 4.75N OV 5N OV 5.4N -0.1MV 6N OV
+ 6.25N OV 6.65N -0.1MV 7.25N OV 7.5N OV 7.9N -0.2MV 8.5N OV 20N OV 20.4N -0.3MV
+ 21N OV 21.25N OV 21.65N -0.1MV 22.25N OV 22.5N OV 22.9N -0.2MV 23.5N OV
+ 23.75N OV 24.15N -0.2MV 24.75N OV 25N OV 25.4N -0.1MV 26N OV 26.25N OV
+ 26.65N -0.1MV 27.25N OV 27.5N OV 27.9N -0.2MV 28.5N OV 40N OV
+ 40.4N -0.2MV 41N OV 41.25N OV 41.65N -0.1MV 42.25N OV 42.5N OV 42.9N -0.1MV
+ 43.5N OV 43.75N OV 44.15N -0.1MV 44.75N OV 45N OV 45.4N -0.1MV
+ 46N OV 46.25N OV 46.65N -0.1MV 47.25N OV 47.5N OV
X6 6 33 0 PHOTOC (RD=xxx CPD=xxx RF=xxx LF=xxx CFG=xxx CPG=xxx )
R6 6 40 200
L6 40 0 50N
I6 0 6 PWL ON OV 0.4N -0.1MV 1N OV 1.25N OV 1.65N -0.1MV 2.25N OV 2.5N OV
+ 2.9N -0.1MV 3.5N OV 3.75N OV 4.15N -0.1MV 4.75N OV 5N OV 5.4N -0.1MV
+ 6N OV 6.25N OV 6.65N -0.2MV 7.25N OV 18.75N OV 19.15N -0.3MV 19.75N OV
+ 20N OV 20.4N -0.1MV 21N OV 21.25N OV 21.65N -0.2MV 22.25N OV 22.5N OV
+ 22.9N -0.2MV 23.5N OV 23.75N OV 24.15N -0.1MV 24.75N OV 25N OV 25.4N -0.1MV
+ 26N OV 26.25N OV 26.65N -0.2MV 27.25N OV 38.75N OV 39.15N -0.2MV
+ 39.75N OV 40N OV 40.4N -0.1MV 41N OV 41.25N OV 41.65N -0.1MV 42.25N OV
+ 42.9N -0.1MV 43.5N OV 43.75N OV 44.15N -0.1MV 44.75N OV 45N OV 45.4N
+ -0.1MV 46N OV 46.25N OV 46.65N -0.2MV 47.25N OV 47.5N OV
X7 8 33 0 PHOTOC (RD=xxx CPD=xxx RF=xxx LF=xxx CFG=xxx CPG=xxx )
R7 8 41 200
L7 41 0 50N
I7 0 8 PWL ON OV 0.4N -0.1MV 1N OV 1.25N OV 1.65N -0.1MV 2.25N OV 2.5N OV
+ 2.9N -0.1MV 3.5N OV 3.75N OV 4.15N -0.1MV 4.75N OV 5N OV 5.4N -0.2MV
+ 6N OV 17.5N OV 17.9N -0.3MV 18.5N OV 18.75N OV 19.15N -0.1MV 19.75N OV
+ 20N OV 20.4N -0.2MV 21N OV 21.25N OV 21.65N -0.2MV 22.25N OV 22.5N OV
+ 22.9N -0.1MV 23.5N OV 23.75N OV 24.15N -0.1MV 24.75N OV 25N OV 25.4N -0.2MV
+ 26N OV 37.5N OV 37.9N -0.2MV 38.5N OV 38.75N OV 39.15N -0.1MV 39.75N OV
+ 40N OV 40.4N -0.1MV 41N OV 41.25N OV 41.65N -0.1MV 42.25N OV 42.5N OV
+ 42.9N -0.1MV 43.5N OV 43.75N OV 44.15N -0.1MV 44.75N OV 45N OV
+ 45.4N -0.2MV 46N OV 47.5N OV
X8 10 33 0 PHOTOC (RD=xxx CPD=xxx RF=xxx LF=xxx CFG=xxx CPG=xxx )
R8 10 42 200
L8 42 0 50N
I8 0 10 PWL ON OV 0.4N -0.1MV 1N OV 1.25N OV 1.65N -0.1MV 2.25N OV 2.5N OV
+ 2.9N -0.1MV 3.5N OV 3.75N OV 4.15N -0.2MV 4.75N OV 5N OV 16.25N OV 16.65N -0.3MV
+ 17.25N OV 17.5N OV 17.9N -0.1MV 18.5N OV 18.75N OV 19.15N -0.2MV 19.75N OV
+ 20N OV 20.4N -0.2MV 21N OV 21.25N OV 21.65N -0.1MV 22.25N OV 22.5N OV
+ 22.9N -0.1MV 23.5N OV 23.75N OV 24.15N -0.2MV 24.75N OV 36.25N OV 36.65N
+ -0.2MV 37.25N OV 37.5N OV 37.9N -0.1MV 38.5N OV 38.75N OV 39.15N -0.1MV
+ 39.75N OV 40N OV 40.4N -0.1MV 41N OV 41.25N OV 41.65N -0.1MV 42.25N OV
+ 42.5N OV 42.9N -0.1MV 43.5N OV 43.75N OV 44.15N -0.2MV 44.75N OV
+ 47.5N OV
X9 17 33 0 PHOTOC (RD=xxx CPD=xxx RF=xxx LF=xxx CFG=xxx CPG=xxx )
R9 17 43 200
L9 43 0 50N
I9 0 18 PWL ON OV 0.4N 0.1MV 1N OV 1.25N OV 1.65N 0.1MV 2.25N OV 2.5N OV
+ 2.9N 0.2MV 3.5N OV 15N OV 15.4N 0.3MV 16N OV 16.25N OV 16.65N 0.1MV 17.25N
+ OV 17.5N OV 17.9N 0.2MV 18.5N OV 18.75N OV 19.15N 0.2MV 19.75N OV 20N OV
+ 20.4N 0.1MV 21N OV 21.25N OV 21.65N 0.1MV 22.25N OV 22.5N OV 22.9N 0.2MV
+ 23.5N OV 35N OV 35.4N 0.2MV 36N OV 36.25N OV 36.65N 0.1MV 37.25N OV 37.5N
+ OV 37.9N 0.1MV 38.5N OV 38.75N OV 39.15N 0.1MV 39.75N OV 40N OV 40.4N
+ 0.1MV 41N OV 41.25N OV 41.65N 0.1MV 42.25N OV 42.5N OV 42.9N 0.2MV 43.5N OV

```

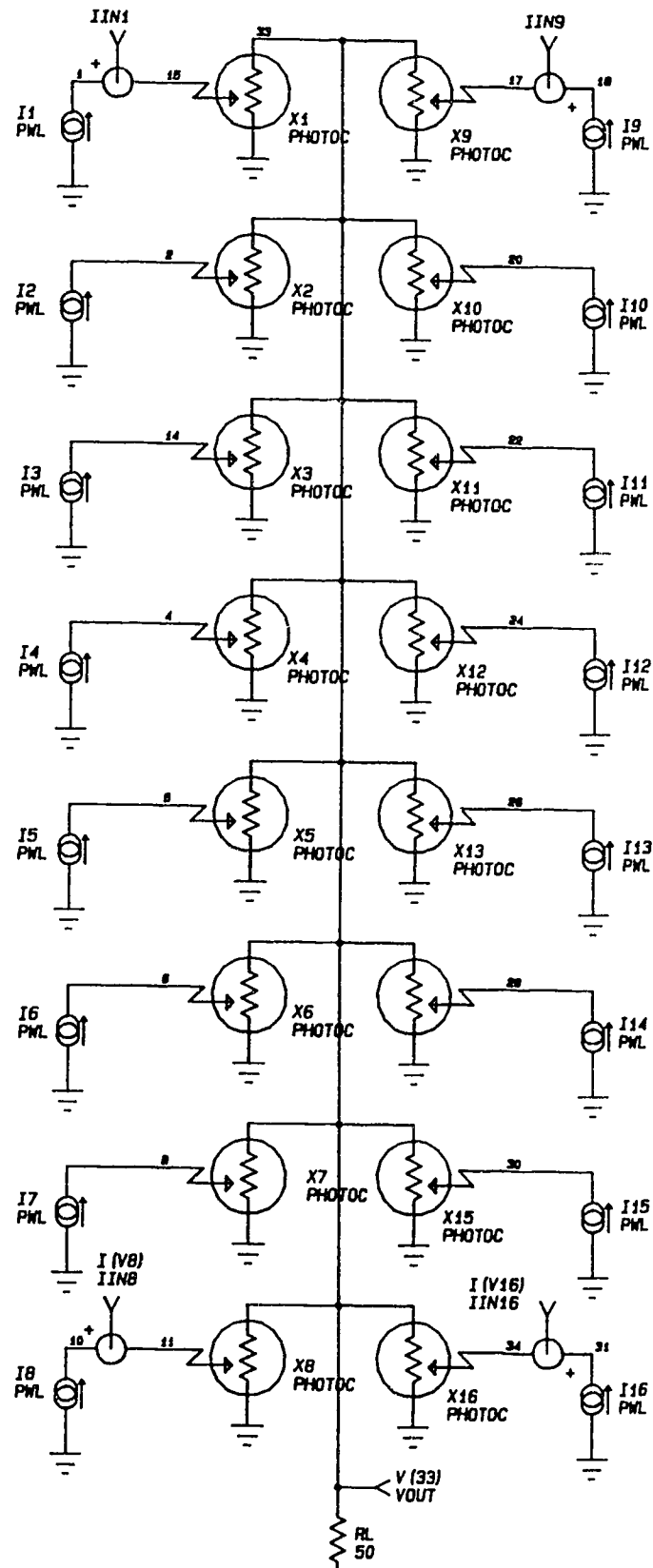
```

+ 47.5N OV
X10 20 33 0 PHOTOC (RD=xxx CPD=xxx RF=xxx LF=xxx CFG=xxx CPG=xxx )
R10 20 44 200
L10 44 0 50N
I10 0 20 PWL ON OV 0.4N 0.1MV 1N OV 1.25N OV 1.65N 0.2MV 2.25N OV 2.5N OV
+ 13.75N OV 14.15N 0.3MV 14.75N OV 15N OV 15.4N 0.1MV 16N OV 16.25N OV
+ 16.65N 0.2MV 17.25N OV 17.5N OV 17.9N 0.2MV 18.5N OV 18.75N OV 19.15N 0.1MV
+ 19.75N OV 20N OV 20.4N 0.1MV 21N OV 21.25N OV 21.65N 0.2MV 22.25N OV 33.75N
+ 0V 34.15N 0.2MV 34.75N OV 35N OV 35.4N 0.1MV 36N OV 36.25N OV 36.65N 0.1MV
+ 37.25N OV 37.5N OV 37.9N 0.1MV 38.5N OV 38.75N OV 39.15N 0.1MV 39.75N OV
+ 40N OV 40.4N 0.1MV 41N OV 41.25N OV 41.65N 0.2MV 42.25N OV 47.5N OV
X11 22 33 0 PHOTOC (RD=xxx CPD=xxx RF=xxx LF=xxx CFG=xxx CPG=xxx )
R11 22 45 200
L11 45 0 50N
I11 0 22 PWL ON OV 0.4N 0.2MV 1N OV 12.5N OV 12.9N 0.3MV 13.5N OV 13.75N OV
+ 14.15N 0.1MV 14.75N OV 15N OV 15.4N 0.2MV 16N OV 16.25N OV 16.65N 0.2MV
+ 17.25N OV 17.5N OV 17.9N 0.1MV 18.5N OV 18.75N OV 19.15N 0.1MV 19.75N OV
+ 20N OV 20.4N 0.2MV 21N OV 32.5N OV 32.9N 0.2MV 33.5N OV 33.75N OV 34.15N
+ 0.1MV 34.75N OV 35N OV 35.4N 0.1MV 36N OV 36.25N OV 36.65N 0.1MV
+ 37.25N OV 37.5N OV 37.9N 0.1MV 38.5N OV 38.75N OV 39.15N 0.1MV 39.75N
+ 0V 40N OV 40.4N 0.2MV 41N OV 47.5N OV
X12 24 33 0 PHOTOC (RD=xxx CPD=xxx RF=xxx LF=xxx CFG=xxx CPG=xxx )
R12 24 46 200
L12 46 0 50N
I12 0 24 PWL ON OV 11.25N OV 11.65N 0.3MV 12.25N OV 12.5N OV 12.9N 0.1MV
+ 13.5N OV 13.75N OV 14.15N 0.2MV 14.75N OV 15N OV 15.4N 0.2MV 16N OV
+ 16.25N OV 16.65N 0.1MV 17.25N OV 17.5N OV 17.9N 0.1MV 18.5N OV 18.75N OV
+ 19.15N 0.2MV 19.75N OV 31.25N OV 31.65N 0.2MV 32.25N OV 32.5N OV 32.9N 0.1MV
+ 33.5N OV 33.75N OV 34.15N 0.1MV 34.75N OV 35N OV 35.4N 0.1MV 36N
+ 0V 36.25N OV 36.65N 0.1MV 37.25N OV 37.5N OV 37.9N 0.1MV 38.5N OV 38.75N OV
+ 39.15N 0.2MV 39.75N OV 47.5N OV
X13 26 33 0 PHOTOC (RD=xxx CPD=xxx RF=xxx LF=xxx CFG=xxx CPG=xxx )
R13 26 47 200
L13 47 0 50N
I13 0 26 PWL ON OV 10N OV 10.4N 0.3MV 11N OV 11.25N OV 11.65N 0.1MV 12.25N OV
+ 12.5N OV 12.9N 0.2MV 13.5N OV 13.75N OV 14.15N 0.2MV 14.75N OV 15N OV 15.4N
+ 0.1MV 16N OV 16.25N OV 16.65N 0.1MV 17.25N OV 17.5N OV 17.9N 0.2MV 18.5N
+ 0V 30N OV 30.4N 0.2MV 31N OV 31.25N OV 31.65N 0.1MV 32.25N OV 32.5N OV
+ 32.9N 0.1MV 33.5N OV 33.75N OV 34.15N 0.1MV 34.75N OV 35N OV 35.4N 0.1MV
+ 36N OV 36.25N OV 36.65N 0.1MV 37.25N OV 37.5N OV 37.9N 0.2MV 38.5N OV 47.5N OV
X14 28 33 0 PHOTOC (RD=xxx CPD=xxx RF=xxx LF=xxx CFG=xxx CPG=xxx )
R14 28 48 200
L14 48 0 50N
I14 0 28 PWL ON OV 8.75N OV 9.15N 0.3MV 9.75N OV 10N OV 10.4N 0.1MV 11N OV
+ 11.25N OV 11.65N 0.2MV 12.25N OV 12.5N OV 12.9N 0.2MV 13.5N OV 13.75N OV
+ 14.15N 0.1MV 14.75N OV 15N OV 15.4N 0.1MV 16N OV 16.25N OV 16.65N 0.2MV
+ 17.25N OV 28.75N OV 29.15N 0.2MV 29.75N OV 30N OV 30.4N 0.1MV 31N
+ 0V 31.25N OV 31.65N 0.1MV 32.25N OV 32.5N OV 32.9N 0.1MV 33.5N OV 33.75N OV
+ 34.15N 0.1MV 34.75N OV 35N OV 35.4N 0.1MV 36N OV 36.25N OV 36.65N 0.2MV
+ 37.25N OV 47.5N OV
X15 30 33 0 PHOTOC (RD=xxx CPD=xxx RF=xxx LF=xxx CFG=xxx CPG=xxx )
R15 30 49 200
L15 49 0 50N
I15 0 30 PWL ON OV 7.5N OV 7.9N 0.3MV 8.5N OV 8.75N OV 9.15N 0.1MV 9.75N OV
+ 10N OV 10.4N 0.2MV 11N OV 11.25N OV 11.65N 0.2MV 12.25N OV 12.5N OV
+ 12.9N 0.1MV 13.5N OV 13.75N OV 14.15N 0.1MV 14.75N OV 15N OV 15.4N 0.2MV
+ 16N OV 27.5N OV 27.9N 0.2MV 28.5N OV 28.75N OV 29.15N 0.1MV 29.75N OV
+ 30N OV 30.4N 0.1MV 31N OV 31.25N OV 31.65N 0.1MV 32.25N OV 32.5N OV
+ 32.9N 0.1MV 33.5N OV 33.75N OV 34.15N 0.1MV 34.75N OV 35N OV 35.4N 0.2MV
+ 36N OV 46.25N OV 46.65N 0.2MV 47.25N OV 47.5N OV

```

```
X16 34 33 0 PHOTOC (RD=xxx CPD=xxx RF=xxx LF=xxx CFG=xxx CPG=xxx )
V16 31 34
R16 34 50 200
L16 50 0 50N
I16 0 31 PWL ON OV 6.25N OV 6.65N 0.3MV 7.25N OV 7.5N OV 7.9N 0.1MV 8.5N OV
+ 8.75N OV 9.15N 0.2MV 9.75N OV 10N OV 10.4N 0.2MV 11N OV 11.25N OV 11.65N
+ 0.1MV 12.25N OV 12.5N OV 12.9N 0.1MV 13.5N OV 13.75N OV 14.15N 0.2MV 14.75N
+ OV 26.25N OV 26.65N 0.2MV 27.25N OV 27.5N OV 27.9N 0.1MV 28.5N OV 28.75N
+ OV 29.15N 0.1MV
+ 29.75N OV 30N OV 30.4N 0.1MV 31N OV 31.25N OV 31.65N 0.1MV 32.25N OV 32.5N
+ OV 32.9N 0.1MV 33.5N OV 33.75N OV 34.15N 0.2MV 34.75N OV 45N OV
+ 45.4N 0.2MV 46N OV 46.25N OV 46.65N 0.1MV 47.25N OV 47.5N OV
RL 33 0 50
X17 51 33 0 GAS (VT=-2 L=1 W=100 KP=37.5E-6 DC=1.38E-15 RHOG=0.023 RHOD=0.08 N=4)
* (VT=xxx L=xxx W=xxx KP=xxx DC=xxx RHOG=xxx RHOD=xxx N=xxx)
R17 51 52 200
V3 52 0 DC=5V AC=0
X1 15 33 0 PHOTOC (RD=xxx CPD=xxx RF=xxx LF=xxx CFG=xxx CPG=xxx )
.END
```

Configuration of the complementary correlator detector:



APPENDIX C

This appendix contains the data sheets for the following components and devices:

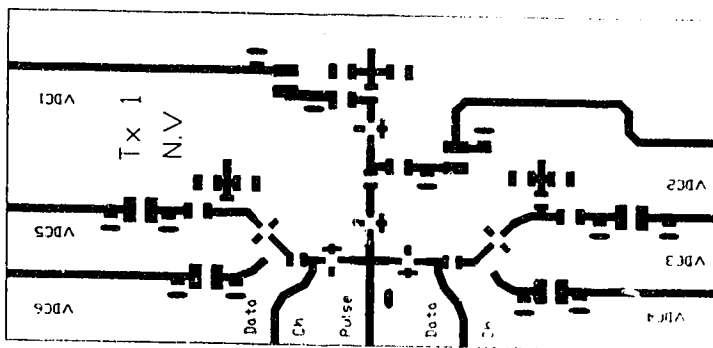
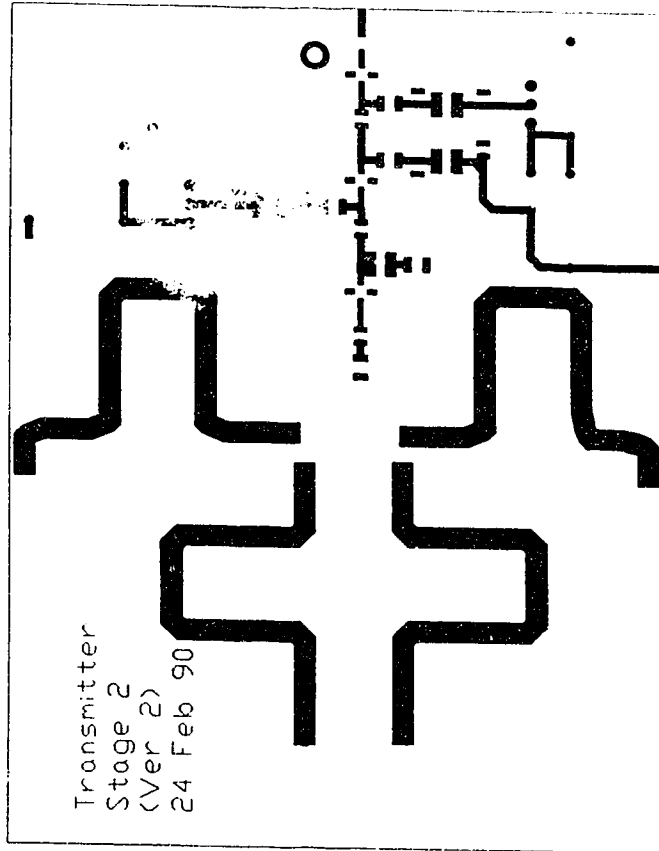
1. Mitsubishi ML6411C laser diode
2. Corning 1x3 Optical Power Splitter/Combiner
3. Canstar 1x16 Optical Power Splitter/Combiner
4. Co-axial cable - 0.034 inch outer diameter

Appendix C has been removed due to the unavailability of copyright permission. Appendix C includes pages 158-174

APPENDIX D

This appendix contains the printed circuit board layouts for the transmitters and the complementary correlator detector module of the receiver.

Transmitter (stages 1 and 2) printed circuit board layout. Actual size



Complementary correlator detector module printed circuit board layout.
Actual size. The MMIC package fits within the rectangular area shown above

